Theses and Dissertations   1. Thesis and Dissertation Collection, all items

AERODYNAMIC VALIDATION OF EMERGING PROJECTILE CONFIGURATIONS

Sor, Wei Lun

Monterey, California. Naval Postgraduate School

https://hdl.handle.net/10945/14852

NAVAL POSTGRADUATE SCHOOL

MONTEREY, CALIFORNIA

THESIS

AERODYNAMIC VALIDATION OF EMERGING PROJECTILE CONFIGURATIONS

by

Sor Wei Lun

December 2011

Thesis Advisor:	Maximilian F. Platzer
Thesis Co-Advisor:	Anthony J. Gannon

THIS PAGE INTENTIONALLY LEFT BLANK

REPORT DOCUMENTATION PAGE		*Form Approved OMB No. 0704-0188*
Public reporting burden for this collection of information is estimated to average 1 hour per response, including the time for reviewing instruction, searching existing data sources, gathering and maintaining the data needed, and completing and reviewing the collection of information. Send comments regarding this burden estimate or any other aspect of this collection of information, including suggestions for reducing this burden, to Washington headquarters Services, Directorate for Information Operations and Reports, 1215 Jefferson Davis Highway, Suite 1204, Arlington, VA 22202-4302, and to the Office of Management and Budget, Paperwork Reduction Project (0704-0188) Washington DC 20503.		

1. AGENCY USE ONLY *(Leave blank)*	**2. REPORT DATE** December 2011	**3. REPORT TYPE AND DATES COVERED** Master's Thesis
4. TITLE AND SUBTITLE Aerodynamic Validation of Emerging Projectile Configurations		**5. FUNDING NUMBERS**
6. AUTHOR(S) Sor Wei Lun		
7. PERFORMING ORGANIZATION NAME(S) AND ADDRESS(ES) Naval Postgraduate School Monterey, CA 93943-5000		**8. PERFORMING ORGANIZATION REPORT NUMBER**
9. SPONSORING /MONITORING AGENCY NAME(S) AND ADDRESS(ES) N/A		**10. SPONSORING/MONITORING AGENCY REPORT NUMBER**

11. SUPPLEMENTARY NOTES The views expressed in this thesis are those of the author and do not reflect the official policy or position of the Department of Defense or the U.S. Government. IRB Protocol number _____N/A_____.

12a. DISTRIBUTION / AVAILABILITY STATEMENT Approved for public release, distribution is unlimited	**12b. DISTRIBUTION CODE**

13. ABSTRACT (maximum 200 words)

Ever-increasing demands for accuracy and range in modern warfare have expedited the optimization of projectile design. The crux of projectile design lies in the understanding of its aerodynamic properties early in the design phase. This research first investigated the aerodynamic properties of a standard M549, 155mm projectile. The transonic speed region was the focus of the research as significant aerodynamic variation occurs within this particular region. Aerodynamic data from wind tunnel and range testing was benchmarked against modern aerodynamic prediction programs like ANSYS CFX and Aero-Prediction 09 (AP09). Next, a comparison was made between two types of angle of attack generation methods in ANSYS CFX. The research then focused on controlled tilting of the projectile's nose to investigate the resulting aerodynamic effects. ANSYS CFX was found to provide better agreement with the experimental data than AP09.

14. SUBJECT TERMS Aerodynamic Coefficients, Normal Force Coefficient, Pitching Moment Coefficient, Total Drag Coefficient, Transonic, Angle of Attack, Re-design, ANSYS CFX, AP09	**15. NUMBER OF PAGES** 103
	16. PRICE CODE

17. SECURITY CLASSIFICATION OF REPORT Unclassified	**18. SECURITY CLASSIFICATION OF THIS PAGE** Unclassified	**19. SECURITY CLASSIFICATION OF ABSTRACT** Unclassified	**20. LIMITATION OF ABSTRACT** UU

i

THIS PAGE INTENTIONALLY LEFT BLANK

**AERODYNAMIC VALIDATION OF EMERGING PROJECTILE
CONFIGURATIONS**

Sor Wei Lun
Captain, Singapore Armed Forces
Bachelor of Engineering
The University of Western Australia, 2007

Submitted in partial fulfillment of the
requirements for the degree of

**MASTER OF SCIENCE IN
ENGINEERING SCIENCE (MECHANICAL ENGINEERING)**

from the

**NAVAL POSTGRADUATE SCHOOL
December 2011**

Author: Sor Wei Lun

Approved by: Maximilian F. Platzer
                     Thesis Advisor

                     Anthony J. Gannon
                     Thesis Co-Advisor

                     Knox T. Millsaps
                     Chair, Department of Mechanical Engineering and Aerospace
                     Engineering

THIS PAGE INTENTIONALLY LEFT BLANK

ABSTRACT

Ever-increasing demands for accuracy and range in modern warfare have expedited the optimization of projectile design. The crux of projectile design lies in the understanding of its aerodynamic properties early in the design phase. This research first investigated the aerodynamic properties of a standard M549, 155mm projectile. The transonic speed region was the focus of the research as significant aerodynamic variation occurs within this particular region. Aerodynamic data from wind tunnel and range testing was benchmarked against modern aerodynamic prediction programs like ANSYS CFX and Aero-Prediction 09 (AP09). Next, a comparison was made between two types of angle of attack generation methods in ANSYS CFX. The research then focused on controlled tilting of the projectile's nose to investigate the resulting aerodynamic effects. ANSYS CFX was found to provide better agreement with the experimental data than AP09.

THIS PAGE INTENTIONALLY LEFT BLANK

TABLE OF CONTENTS

LIST OF FIGURES

LIST OF TABLES

THIS PAGE INTENTIONALLY LEFT BLANK

LIST OF ACRONYMS AND ABBREVIATIONS

A_{ref} = Reference Area [m^2]

AOA = Angle of Attack [°]

C_{DO} = Total Drag Coefficient

c = Chord [m]

C_L = Lift Coefficient

C_N = Normal Coefficient

C_P = Pressure Coefficient

$C_{N\alpha}$ = Normal Force Coefficient Slope

$C_{M\alpha}$ = Pitching Moment Coefficient Slope

D = Drag Force [N]

F_A = Axial Force [N]

F_N = Normal Force [N]

L = Lift Force [N]

L_{ref} = Reference Length [m]

M = Pitching Moment [N]

N = Normal Force [N]

y = Distance between the first and second grid points off the wall.

ρ = Free-stream Density [kg/m^3]

u = Velocity in "X" direction [m/s]

v = Velocity in "Y" direction [m/s]

w = Velocity in "Z" direction [m/s]

V_∞ = Free-stream Velocity [m/s]

V = Constant Velocity [m/s]

Y+ = Dimensionless Distance from Wall

τ_ω = Wall shear stress [N/m^2]

u* = Friction Velocity [m/s]

v = Kinematic Viscosity [m^2/s]

THIS PAGE INTENTIONALLY LEFT BLANK

ACKNOWLEDGMENTS

THIS PAGE INTENTIONALLY LEFT BLANK

I.   INTRODUCTION

A.   MOTIVATION

The start of the fourteenth century marked the end of hand-to-hand combat and ushered in a new martial law, with the introduction of the cannon proper on the battlefield [1]. By the seventeenth century, artillery was employed with great effect against enemy troops in the open [1].

Since then, man has been trying to improve the precision and range of artillery. Modern warfare, characterized by urban close fire support and larger areas of operation, has further escalated the demands for precision and range [2]. In the current context, a precision guided missile presents itself as an effective but costly option [3]. A more economical option is to explore ways to improve the existing projectile stockpile's precision and range by redesign.

B.   TRADITIONAL PROJECTILE DESIGN

A conventional 155mm projectile consists of a hollow steel shell filled with high explosive [4]. The projectile's body generally begins with a streamlined nose and terminates using a boat tail base for aerodynamic efficiency. Prior to firing, a fuze is placed into the fuze adapter located at the projectile nose.

Conventional 155mm projectile design was popularized during the World War II era. Since then, modifications to the projectile design have been minimal. The projectile is "dumb" and employed in an open loop manner. Once in flight, the dumb round does not have any means to guide itself to the target. Therefore in a typical engagement scenario, several iterative adjustments are made before the projectile is able to land near the intended target. This inevitably drives up the mission cost, lengthens the mission duration and increases the possibility of enemy counter-fire. This is even more unacceptable in urbanized combat zones, where collateral damage is less tolerable.

C.   DESIGN CONSIDERATIONS

The flight of a projectile is complex in nature. The projectile is subjected to a wide range of Mach numbers during its flight. This complexity is further compounded by the fact that the projectile is subjected to varying atmospheric conditions as it cuts through various altitudes.

Therefore, an understanding of the aerodynamic characteristics of a projectile is critical in the design of new projectile configurations to achieve improved performance [5]. From studies, the critical aerodynamic behavior occurs in the transonic speed range from Mach 0.9 to 1.2 [5]. An in-depth understanding of the aerodynamic behavior in this region is crucial in the development of a projectile [5]. Aerodynamic properties of a projectile have been found to vary drastically within the transonic speed region [6]. With current advancements in simulation technologies and perhaps a more in depth understanding of the subject, it may be possible to make a minor modification to a traditional projectile to improve its performance, using existing artillery howitzers.

D.   PREVIOUS WORK

This thesis continued the aerodynamic studies of the M549 projectile started by [5], [6] and [7]. Past studies focused on finding the aerodynamic properties of the projectile using dated modeling simulation and modeling tools. Current advancement in simulation and modeling justified a reinvestigation.

Recent work of [7] focused solely on the drag prediction for the M549 projectile. A more in-depth understanding of other important aerodynamic coefficients like pitching moment and normal force is required. In addition, the simulation and modeling tools used by [5] and [6] have been superseded by newer versions. These observations justify further investigation.

E.   SCOPE AND ORGANIZATION

1.   Scope

The scope of this thesis aims to get a better understanding of an M549 projectile's stability derivatives. The modeling program SolidWorks is used to model the projectile. The simulation program ANSYS CFX is employed to determine the stability derivatives of the projectile at various conditions. AP09 and live firing data are used as benchmarks for the simulation results.

Comparison studies are conducted between two angle of attack (AOA) generation methodologies in ANSYS CFX. Finally, an investigation is conducted to explore the effect of nose modification on the M549 155mm projectile's lift coefficient. The redesigned projectile's aerodynamic data is compared against the baseline projectile's data.

2.   Organization

Chapter II: The separation of the aerodynamic forces into lift and drag is presented. This is followed by an explanation of the aerodynamic moment. Equations relevant to both aerodynamic force and moment are described.

Chapter III: The use of the simulation program, ANSYS CFX in the aerodynamic prediction of the projectile is described. Advice that is helpful in resolving some of the common simulation issues is documented. In addition, optimization and tuning techniques to improve the accuracy of the simulation is discussed. Finally, an introduction of two types of AOA generation techniques is presented.

Chapter IV: The use of the simulation program AP09 in the aerodynamic prediction of the projectile is described.

Chapter V: The results and analysis for both the standard and modified projectile configuration are discussed. Results from the two different methods of AOA generation techniques are evaluated. The accuracy of the simulation results is validated by comparing the results with published experimental results.

Chapter VI: The conclusions drawn from this research and recommendations for follow-on research are discussed.

II.   DEVELOPMENT OF AERODYNAMICS

Aerodynamics, a branch of theoretical physics, has progressed greatly since Leonardo da Vinci speculated on the possibility of human flight [8]. Aerodynamics is concerned with the interaction between a moving object and the surrounding air. Aerodynamics can be further divided into two main areas, external and internal aerodynamics. Internal aerodynamics focuses on the study of flow though passages within an object. In this thesis, the concern is the external aerodynamic flow around a projectile.

Nature can only transmit a force to a moving body through the pressure and shear stress distributions on the body surface. Regardless of the complexity of a body shape, aerodynamic forces and moments on the body are due to pressure and shear stress distributions over the body surface. [9]

A.   AERODYNAMIC FORCE

An aerodynamic force is the result of the integrated pressure and shear stress distribution over the entire body surface. The aerodynamic force can be divided into lift and drag as shown in Figure 1[9].
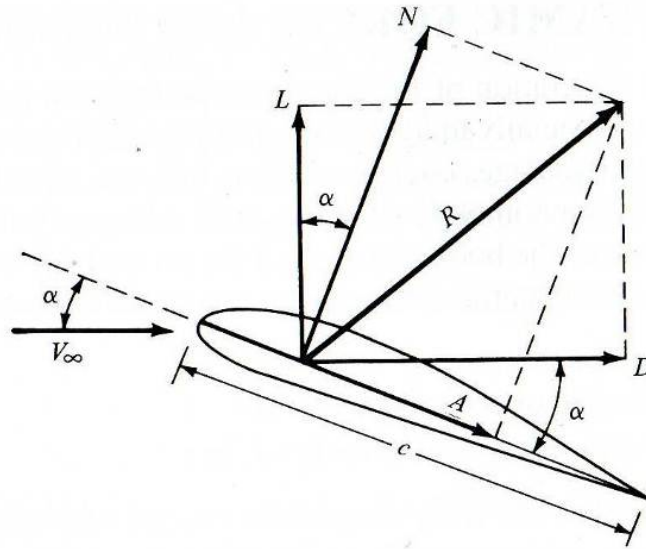
Figure 1.   Aerodynamic Forces. From [9]

5

1. Lift

Lift is defined as the force component which acts on a body in a direction perpendicular to the free-stream velocity vector. Regardless of the variation in AOA, lift always maintains this orientation to the velocity vector [9]. The lift coefficient, C_L is a dimensionless coefficient that relates lift generated by a body highlighted in Equation 2.1.

$$C_L = \frac{L}{0.5 \rho V_\infty^2 A_{ref}} \qquad (2.1)$$

2. Drag

In a real viscous flow, total drag consists of friction and pressure drag force [10]. Pressure drag is created by normal force perpendicular to the boundary surface [8]. Friction drag is created by tangential forces parallel to the boundary surface [8]. In a viscous flow, particles come to a stop at the body surface. The sum of this effect generates the skin friction drag. At certain conditions, the flow is separated from the body surface creating a pressure difference which causes the pressure drag [10]. It is important to highlight that even when the flow is not detached from the body surface, shear forces can still alter the pressure difference and create pressure drag [10]. Drag is defined as the force component which acts on a body in a direction parallel to the free-stream velocity vector [9]. Similar to lift force, regardless of the variation in AOA, drag always maintains this orientation to the velocity vector.

$$C_D = \frac{D}{0.5 \rho V_\infty^2 A_{ref}} \qquad (2.2)$$

3. Normal and Axial Force

Normal force can be defined as the force component which acts on a body in a direction perpendicular to the body axis. Axial force is defined as the force component which acts on a body in a direction parallel to the axis line. Regardless of the variation in AOA, both normal and axial force always maintains this orientation to the axis line. The following equations relate the lift and drag force to the normal and axial force.

$$\text{Lift} = F_N \cos(\alpha) - F_A \sin(\alpha) \qquad (2.3)$$

$$\text{Drag} = F_N \sin(\alpha) + F_A \cos(\alpha) \tag{2.4}$$

B.   SLENDER BODY THEORY

For slender bodies of revolution flying at small AOA, the lift can be estimated by considering only the flow in a plane perpendicular to the flight direction, the cross flow plane [10]. This reduces the problem to finding the solution for incompressible flow over a cylinder. Using slender body theory in Figure 2, the lift coefficient is found to be linearly proportional to the AOA [10].

d(x)

R(x)

Cross Flow Plane

Cross Sectional
View of d(x)
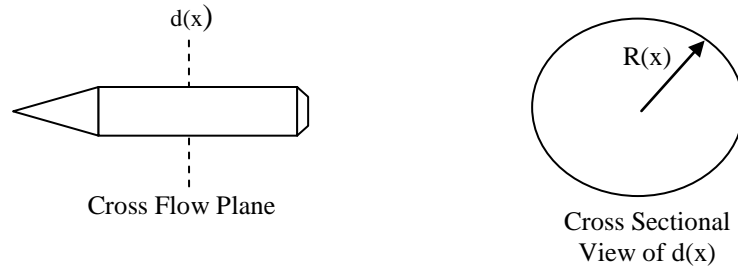
Figure 2.   Slender Body.

From [10], the derivation of lift coefficient is given by:

Local lift is defined as $L' = \dfrac{\partial L(x)}{\partial x}$, $\qquad$ (2.5)

$$= \int_0^{2\pi} pR(x)\cos\theta\, d\theta$$

$$= \int_0^{2\pi} (p - p_\infty)R(x)\cos\theta\, d\theta \tag{2.6}$$

Since, $C_p = \dfrac{p - p_\infty}{\dfrac{1}{2}\rho V_\infty^2}$ $\qquad$ (2.7)

$$L' = \int_0^{2\pi} (C_p \frac{\rho V_\infty^2}{2})R(x)\cos\theta\, d\theta$$

$$= \frac{\rho V_\infty^2}{2}\int_0^{2\pi} (C_p)R(x)\cos\theta\, d\theta \tag{2.8}$$

7

From the incompressible flow over a cylinder, one finds that,

$$C_p(r = R(x)) = \frac{2\cos\theta}{V_\infty R(x)}\frac{\partial}{\partial x}(R^2(x)w_a(x)) \tag{2.9}$$

$$L'(x) = \frac{\rho V_\infty^2}{2}\int_0^{2\pi}\left[\frac{2\cos\theta}{V_\infty R(x)}\frac{\partial}{\partial x}(R^2(x)w_a(x))\right]R(x)\cos\theta d\theta \tag{2.10}$$

$$= \rho V_\infty\int_0^{2\pi}\left[\cos^2\theta d\theta\frac{\partial}{\partial x}R^2(x)w_a(x))\right]$$

$$= \rho V_\infty\pi\frac{\partial}{\partial x}R^2(x)w_a(x) \tag{2.11}$$

where for flight at a steady AOA, $w_a = V_\infty\alpha$,

$$L = \int_{Nose}^{Tail}\frac{\partial L}{\partial x}\partial x$$

$$= \rho V_\infty\pi\int_{Nose}^{Tail}\frac{\partial}{\partial x}R^2(x)V_\infty\alpha\partial x \tag{2.12}$$

For a body with a pointed nose and a finite base radius R$_B$,

$$L = \rho V_\infty^2\pi R_B^2\alpha \tag{2.13}$$

$$C_L = \frac{L}{\frac{1}{2}\rho V_\infty^2\pi R_B^2} \tag{2.14}$$

$$= \frac{\rho V_\infty^2\pi R_B^2\alpha}{\frac{1}{2}\rho V_\infty^2\pi R_B^2}$$

$$C_L = 2\alpha \tag{2.15}$$

Equation 2.15 provides a quick estimate of the lift at small AOA [9, 10]. However, it predicts no effect of Mach number and Reynolds number on the body geometry. Therefore, more accurate theories are needed to account for these effects.

C.   AERODYNAMIC MOMENT

A force has both direction and magnitude. The product of force and perpendicular distance from the center of gravity is known as moment or torque. The aerodynamic moment which act to change the AOA is called a pitching moment [9]. Positive pitching moment occurs when a body is pitched in a nose up direction. The pitching moment coefficient then is:

$$C_M = \frac{M}{0.5 \rho V_\infty^2 A_{ref} L_{ref}}$$

(2.16)

D.   COMPRESSIBILITY EFFECT

The disturbances emitted by a disturbance source travel at the speed of sound, as illustrated in Figure 3 [11, 12]. The generated wave patterns are strongly dependent on the ratio of the speed of the disturbance source to the speed of sound. With that, it is important to introduce the definition of Mach number. It is named after Ernst Mach and is defined as the ratio between the velocity of a body moving through the air and the velocity of sound in the air [8].

$$M = \frac{V}{a}$$

(2.17)

As depicted in Figure 3, if M<1 or V<a, the disturbances can propagate ahead of the moving body whereas at M=1 the body moves as fast as the disturbance fronts. If M>1 or V>a, the disturbances can only propagate downstream of the body within the so-called Mach cone. It is obvious that fundamentally different flow phenomena occur depending on the value of the Mach number, requiring more accurate analyses than slender body theory. Such analyses have been developed in recent years which can not only predict the Mach number effects but also viscous flow effects. They are based on the numerical solution of the Navier-Stokes equations for compressible viscous flows [10]. To this end, a system of six equations consisting of the continuity equations, the three momentum equations, the energy equations and the equation of state for air needs to be solved [10].

Continuity Equation:

$$\frac{\partial \rho}{\partial t}+\frac{\partial(\rho u)}{\partial x}+\frac{\partial(\rho v)}{\partial y}+\frac{\partial(\rho w)}{\partial z}=0 \tag{2.18}$$

Momentum Equation:

$$\rho\frac{\partial u}{\partial t}+\rho u\frac{\partial u}{\partial x}+\rho v\frac{\partial u}{\partial y}+\rho w\frac{\partial u}{\partial z}=-\frac{\partial P}{\partial x}$$

$$+\frac{\partial}{\partial x}\left\{2\mu\frac{\partial u}{\partial x}-\left(\frac{2}{3}\right)\mu\left(\frac{\partial u}{\partial x}+\frac{\partial v}{\partial y}+\frac{\partial w}{\partial z}\right)\right\}$$

$$+\frac{\partial}{\partial y}\left\{\mu\left(\frac{\partial u}{\partial y}+\frac{\partial v}{\partial x}\right)\right\}+\frac{\partial}{\partial z}\left\{\mu\left(\frac{\partial w}{\partial x}+\frac{\partial u}{\partial z}\right)\right\}$$

$$\rho\frac{\partial v}{\partial t}+\rho u\frac{\partial v}{\partial x}+\rho v\frac{\partial v}{\partial y}+\rho w\frac{\partial v}{\partial z}=-\frac{\partial P}{\partial y}$$

$$+\frac{\partial}{\partial y}\left\{2\mu\frac{\partial v}{\partial y}-\left(\frac{2}{3}\right)\mu\left(\frac{\partial u}{\partial x}+\frac{\partial v}{\partial y}+\frac{\partial w}{\partial z}\right)\right\}$$

$$+\frac{\partial}{\partial x}\left\{\mu\left(\frac{\partial u}{\partial y}+\frac{\partial v}{\partial x}\right)\right\}+\frac{\partial}{\partial z}\left\{\mu\left(\frac{\partial w}{\partial y}+\frac{\partial v}{\partial z}\right)\right\}$$

$$\rho\frac{\partial w}{\partial t}+\rho u\frac{\partial w}{\partial x}+\rho v\frac{\partial w}{\partial y}+\rho w\frac{\partial w}{\partial z}=-\frac{\partial P}{\partial z}$$

$$+\frac{\partial}{\partial z}\left\{2\mu\frac{\partial w}{\partial z}-\left(\frac{2}{3}\right)\mu\left(\frac{\partial u}{\partial x}+\frac{\partial v}{\partial y}+\frac{\partial w}{\partial z}\right)\right\}$$

$$+\frac{\partial}{\partial x}\left\{\mu\left(\frac{\partial w}{\partial x}+\frac{\partial u}{\partial z}\right)\right\}+\frac{\partial}{\partial y}\left\{\mu\left(\frac{\partial v}{\partial z}+\frac{\partial w}{\partial y}\right)\right\}$$

$$\tag{2.19}$$

Energy Equation:

$$\rho \frac{D}{Dt}\left(e + \frac{V^2}{2}\right) = \frac{\partial}{\partial x}\left(k_e \frac{\partial T}{\partial x}\right) + \frac{\partial}{\partial y}\left(k_e \frac{\partial T}{\partial y}\right) + \frac{\partial}{\partial z}\left(k_e \frac{\partial T}{\partial z}\right)$$

$$-\frac{\partial}{\partial x}(Pu) - \frac{\partial}{\partial y}(Pv) - \frac{\partial}{\partial z}(Pw)$$

$$+\frac{\partial}{\partial x}\{u\tau_{xx}\} + \frac{\partial}{\partial y}\{u\tau_{yx}\} + \frac{\partial}{\partial z}\{u\tau_{zx}\}$$

$$+\frac{\partial}{\partial x}\{v\tau_{xy}\} + \frac{\partial}{\partial y}\{v\tau_{yy}\} + \frac{\partial}{\partial z}\{v\tau_{zy}\}$$

$$+\frac{\partial}{\partial x}\{w\tau_{xz}\} + \frac{\partial}{\partial y}\{w\tau_{yz}\} + \frac{\partial}{\partial z}\{w\tau_{zz}\}$$

$$\frac{D}{Dt} = \frac{\partial}{\partial t} + u\frac{\partial}{\partial x} + v\frac{\partial}{\partial y} + w\frac{\partial}{\partial z}$$

$$e = c_v T$$

$$\tau_{xy} = \tau_{yx} = \mu\left(\frac{\partial v}{\partial x} + \frac{\partial u}{\partial y}\right)$$

$$\tau_{yz} = \tau_{zy} = \mu\left(\frac{\partial w}{\partial y} + \frac{\partial v}{\partial z}\right)$$

$$\tau_{zx} = \tau_{xz} = \mu\left(\frac{\partial u}{\partial z} + \frac{\partial w}{\partial x}\right)$$

$$\tau_{xx} = -\frac{2}{3}\mu\left(\frac{\partial u}{\partial x} + \frac{\partial v}{\partial y} + \frac{\partial w}{\partial z}\right) + 2\mu\frac{\partial u}{\partial x}$$

$$\tau_{yy} = -\frac{2}{3}\mu\left(\frac{\partial u}{\partial x} + \frac{\partial v}{\partial y} + \frac{\partial w}{\partial z}\right) + 2\mu\frac{\partial v}{\partial y}$$

$$\tau_{zz} = -\frac{2}{3}\mu\left(\frac{\partial u}{\partial x} + \frac{\partial v}{\partial y} + \frac{\partial w}{\partial z}\right) + 2\mu\frac{\partial w}{\partial z} \tag{2.20}$$

Equation of State:

$$P = R\rho T \tag{2.21}$$

M<1

M=1

M>1
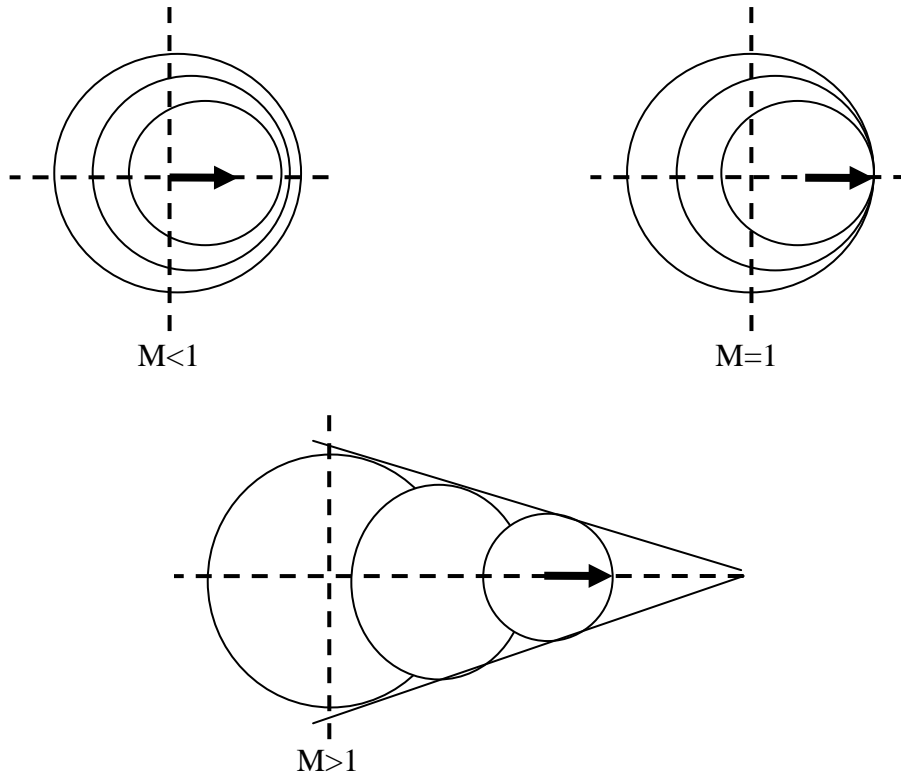
Figure 3.   Subsonic, Sonic and Supersonic Motions. From [11]

III.   ANSYS CFX

One of the commercially available codes for the numerical solution of the system of six equations is the ANSYS CFX code.

Modern Computational Fluid Dynamics (CFD) can be regarded as equal partner with pure theory and pure experiment in the analysis of aerodynamic flows. As illustrated in Figure 4, they do not stand alone but help each other to understand aerodynamic flows [9].

Pure
Experiment

Pure
Theory

CFD
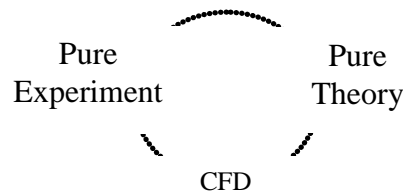
Figure 4.   Aerodynamic Partnership. From [9]

A.   WORK FLOW

ANSYS CFX is a CFD solver program that utilizes the finite volume technique [13], [14]. In this technique, the area of interest is subdivided into smaller regions. Each region is discretized and iteratively solved. In this manner, an approximation of the value of each variable at a specific point within the domain can be determined. One can then develop a full understanding of the flow behavior. While the system of Equations 2.18-2.21 completely describes laminar flows, the analysis of turbulent flow requires an averaging process known as Reynolds averaging, which introduces the need for turbulence modeling [15]. The work process flow of ANSYS CFX is depicted in Figure 5.
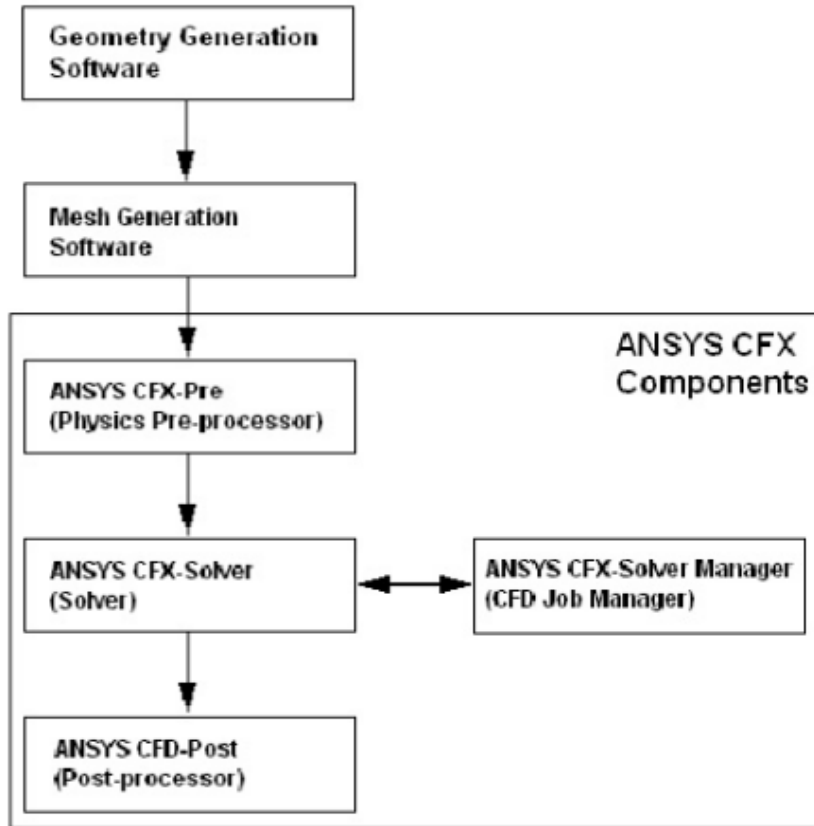
Figure 5.　　　ANSYS CFX Work Process Flow. From [14]

1.   Model Generation

In this thesis, the body of interest is a modified M549 155mm projectile with a power series blunt nose and removed rotating band [16]. The power series blunt nose profile provides an accurate description of the discontinuities between fuze and projectile. The entire projectile has a length of 874.975mm and a diameter of 155mm. The reference area is defined as the circular cross sectional area of the projectile. The center of gravity (CG) of the projectile is 542.5mm from the projectile nose. A diagram of the actual M549 projectile is depicted in Figure 6.
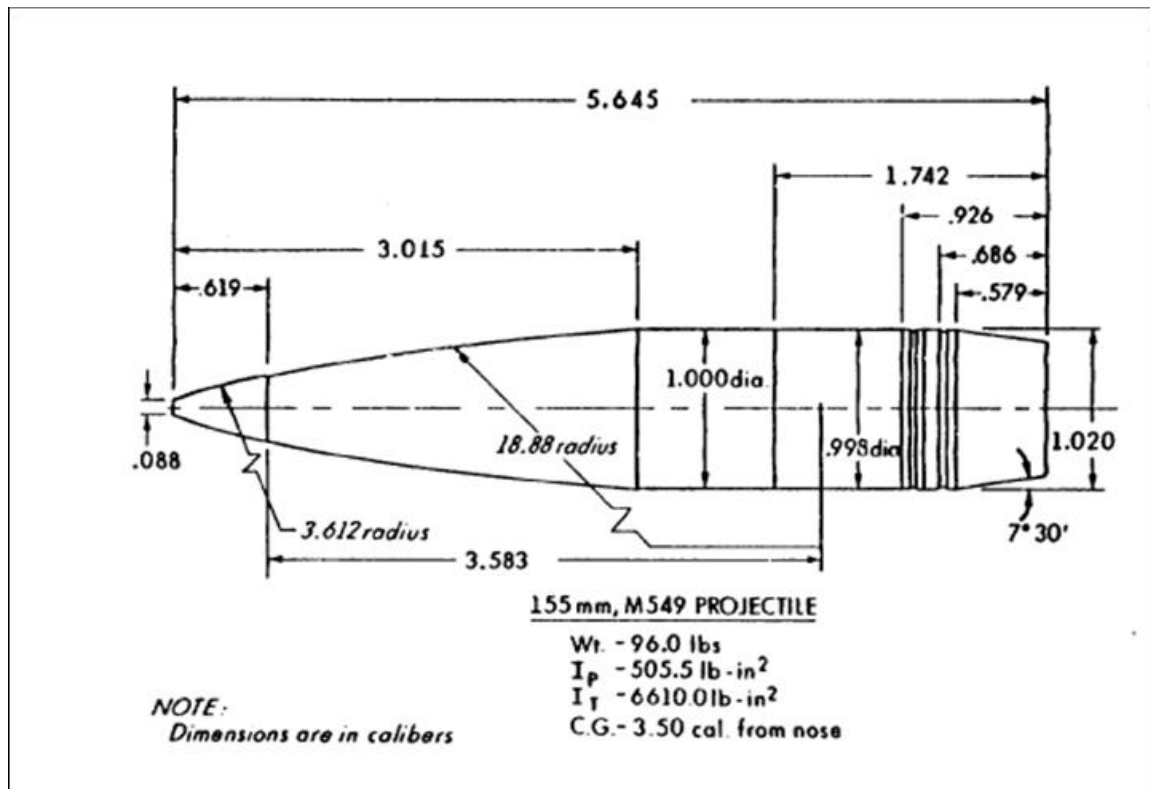
Figure 6.   Geometry Profile of M549 Projectile. From [16]

The body of interest is modeled using the modeling tool SolidWorks before it is imported to ANSYS CFX Geometry for further processing. SolidWorks is a widely used modeler program that applies a parametric feature-based approach in models and assemblies creation [17], [18]. The model's center of origin is centered at the CG of the projectile. The constructed model in SolidWorks is depicted in Figure 7.

15
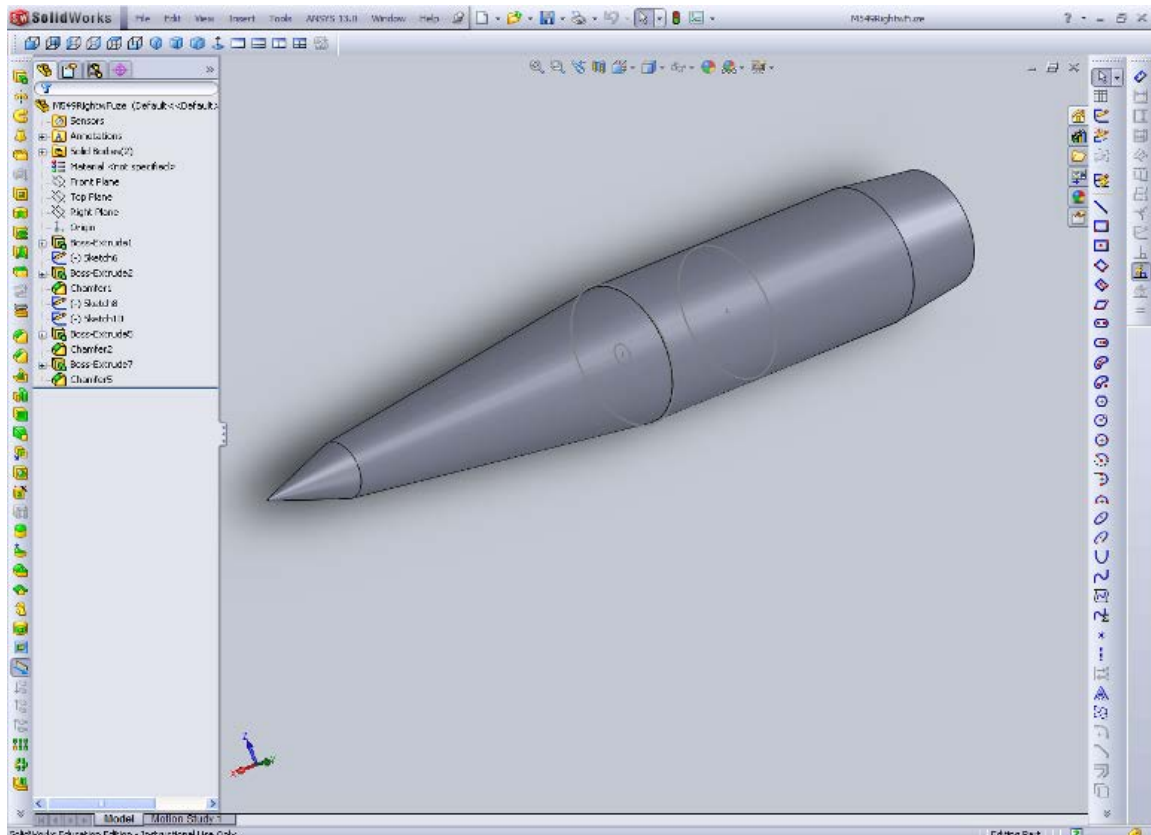
Figure 7.   Constructed Model of Standard M549 Projectile in SolidWorks.

The constructed model is saved and imported into ANSYS CFX Geometry. It is recommended to save the model as "Parasolid (*.x_t)" file type to prevent compatibility issues during the transfer from SolidWorks to ANSYS CFX.

A control volume for the projectile is also created using SolidWorks. A control volume is fixed in space with air moving through it [9]. The fundamental physical principles and required flow directions are applied to the air crossing the control surface. It is recommended to have a large control volume to effectively capture the shock wave phenomena. The control volume is modeled to be approximately twenty times the size of the projectile. Likewise, the model is saved as "Parasolid (*.x_t)" file type and imported into ANSYS CFX Geometry. Both projectile and control volume are then merged and cut in the ANSYS CFX Geometry. This effectively creates a 2D slice through the combined model to reduce computational time. However, this imposes a need to multiply result

values by a factor of two to properly account for full size model. The "sliced" projectile within the control volume is depicted in Figure 8.
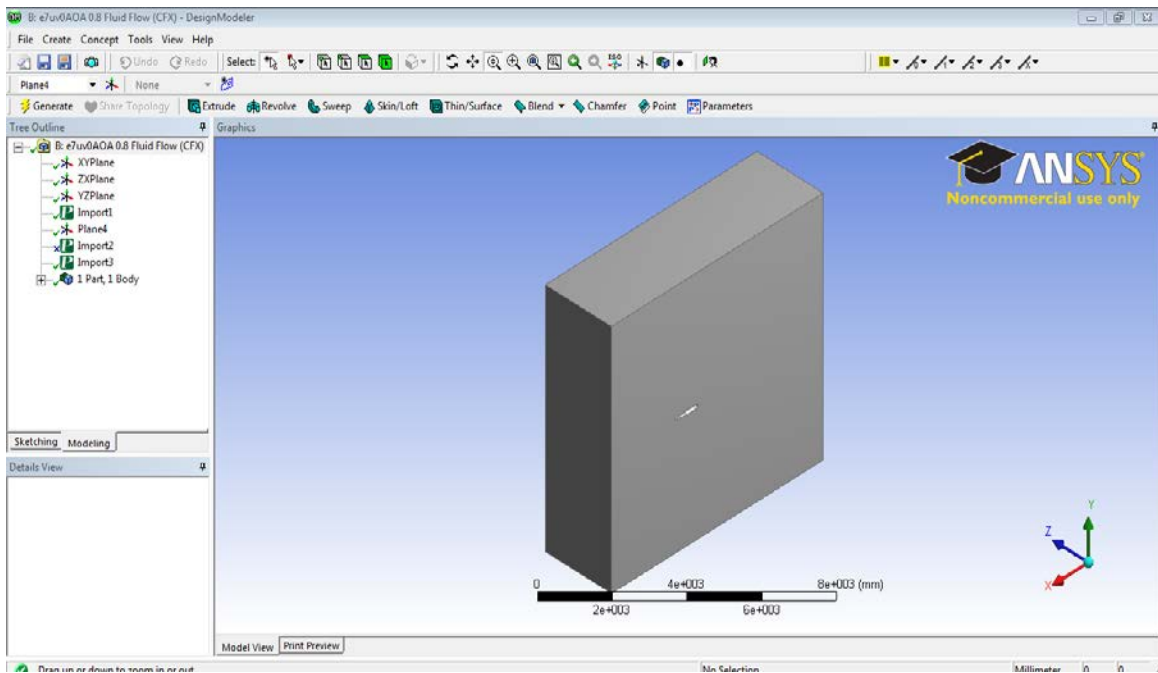
Figure 8.   Control Volume with "Sliced" Projectile in ANSYS CFX Geometry.

2.   Mesh Generation

Mesh generation of the combined model was performed using ANSYS CFX Mesh. A mesh is a generated collection of edges, vertices and faces that define the shape and size of the model. A more detailed mesh of the model allows a more accurate representation of the model in simulation. A poor mesh often results in abrupt simulation termination and poor convergence. The average generated mesh consists of approximately 950,000 nodes and 5,300,000 elements to achieve an average Y+ of 1.

Additional refinement settings like Inflation and Vertex sizing were applied to specific areas on the projectile to improve the number of mesh elements and nodes in that particular area of interest. The meshed profile of the combined model is depicted in Figure 9.

17
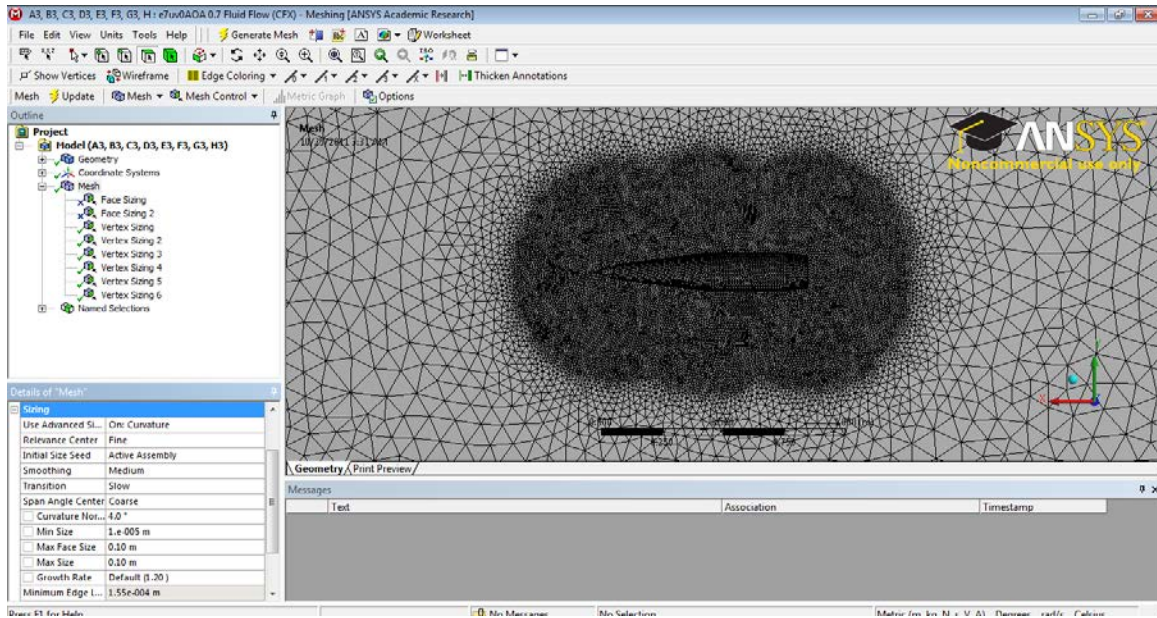
Figure 9.   Generated Mesh Profile of Combined Model in ANSYS CFX Mesh.

3.   Pre-Processor Setup

A simulation profile is created by specifying the required boundary conditions, flow physics, initial values and solver parameter in ANSYS CFX Pre. In the Domain Setup under Basic Settings tab, Material is set to Air Ideal Gas. Reference Pressure is set to 1 atm. In the Fluid Models tab, Heat Transfer Option is set to Total Energy for compressible simulations. Viscous Work Term is enabled to include viscous heating effects. High Speed Models is activated in Expert parameter with a maximum continuity loop of value 3, Turbulence Option is set to Shear Stress Transport (SST). The SST model is known for robust simulation of aerodynamic flows. It works especially well to predict separated flow behavior. The SST model effectively integrates the accurate formulation of k-ω model in the near wall region with the free stream independence of the k-e model in the far field [19]. This blending ensures that the model equations behave appropriately in both the near wall and far field regions [20]. With the SST turbulence model, the simulation can handle any sensible value of Y+ and automatically transition from integration to the wall to wall functions. Y+ is easily extended to include curvature effects, transition and several effects if required [14].

18

In order to specify the flow direction and AOA, boundary conditions were created under Fluid setting. Under the Boundary Details tab, Mass and Momentum option was changed to Cart. Vel Components to simulate flow in u, v and w directions were set as illustrated in Figure 10. Static temperature was set at 288.15k.
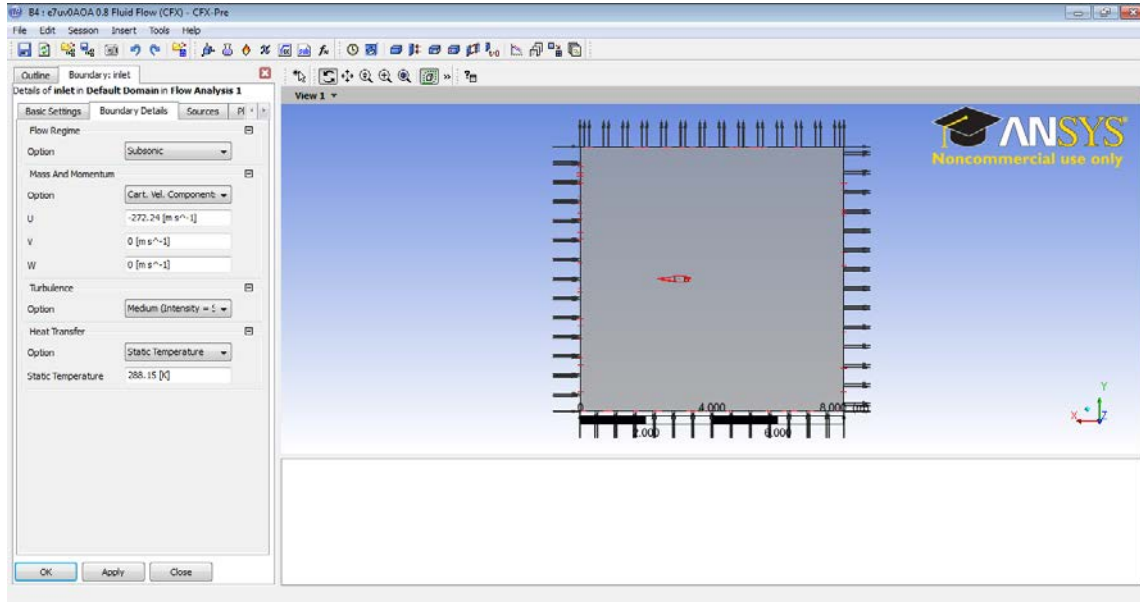
Figure 10.   Boundary Condition Setting in ANSYS CFX Pre.

4.   Solver Control

Upon completion of the pre-processing setup, solver control settings are initiated in ANSYS CFX Pre for the simulation runs. The solver resolves the Navier-Stokes equations using the created finite volume and algebraic multi-grid approach [14]. It applies the law of conservation of mass, momentum and energy to the created control volume [14]. Partial differential equations are integrated over the control volumes. These equations are translated to algebraic equations by approximations. These equations are then iteratively solved. The solver will end the simulation and generate results when residuals converge to a steady state. Convergence occurs when the residuals have been reduced by at least three orders of magnitude [14]. The maximum iteration is set to 100 to ensure convergence. The timescale factor is increased from 1 to 10 to accelerate convergence to steady state as fast as possible. Residual target is set to 1e-7 to ensure

solution converged well. Often, one has to strike a balance between iteration counts, residual target and timescale factor for solution optimization.

5.   Solver Manager

The flow computation is controlled in ANSYS CFX Solver Manager. The Solver Manager will attempt to resolve all the solution variables for the problem specified in the Solver Control. In Solver Manager, users can choose either "Initial Conditions" or "Current Solution Data" under the Initialization Option. "Current Solution Data" option is recommended if a previous run of the same profile was conducted. The solver will make use of the past generated data to kick-start the new simulation. "Double Precision" is chosen to maintain simulation accuracy.

Run mode is dependent on the number of processors. One can select parallel processing if more than one processor is available [14]. Increasing the number of processors and Random Access Memory (RAM) capacity will drastically reduce the required computational time. The recommended computer hardware is at least 8GB RAM and four core processors. During the simulation, it is recommended to open the Display Monitor to monitor the progress of the runs and detect any abnormal report. A snapshot of ANSYS CFX Solver Manager is depicted in Figure 11. Upon the completion of the simulation, the results files are generated.
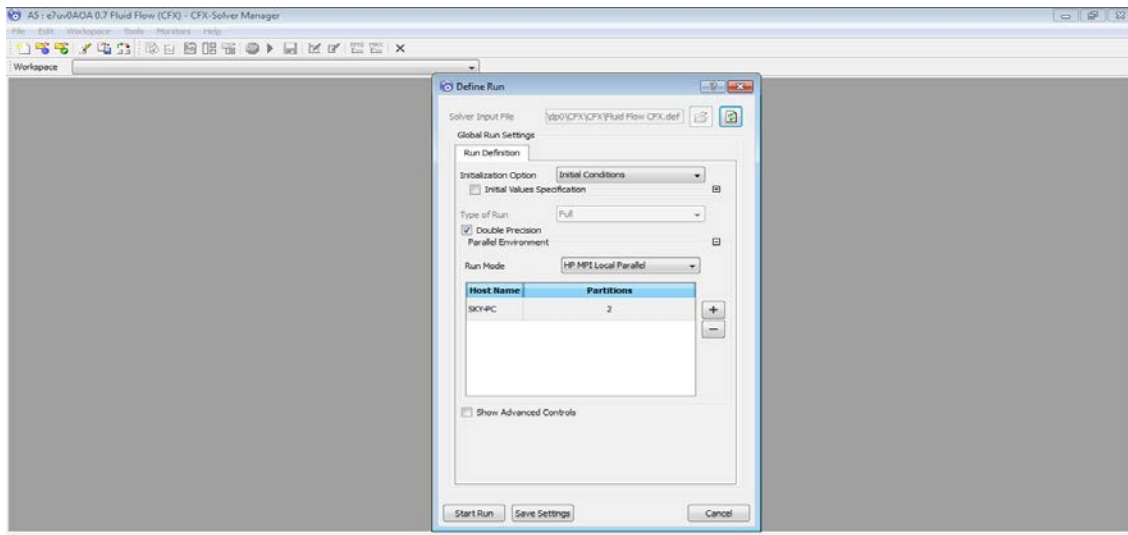
Figure 11.   "Run Define" in ANSYS CFX Solver Manager.

20

6.   Post Processing

Upon the successful completion of the simulation run, output results and plots can be seen from ANSYS CFX Post. ANSYS CFX Post is an interactive post processing tool that allows the visualization of the output results. Scalar variables like pressure, velocity, Mach numbers and Y+ value can be checked. A quantitative numerical calculator known as Function Calculator is used to calculate the various flow parameters. Interactive view of the shockwave phenomena can be called up. The post processing tools in ANSYS CFX Post are depicted in Figure 12.
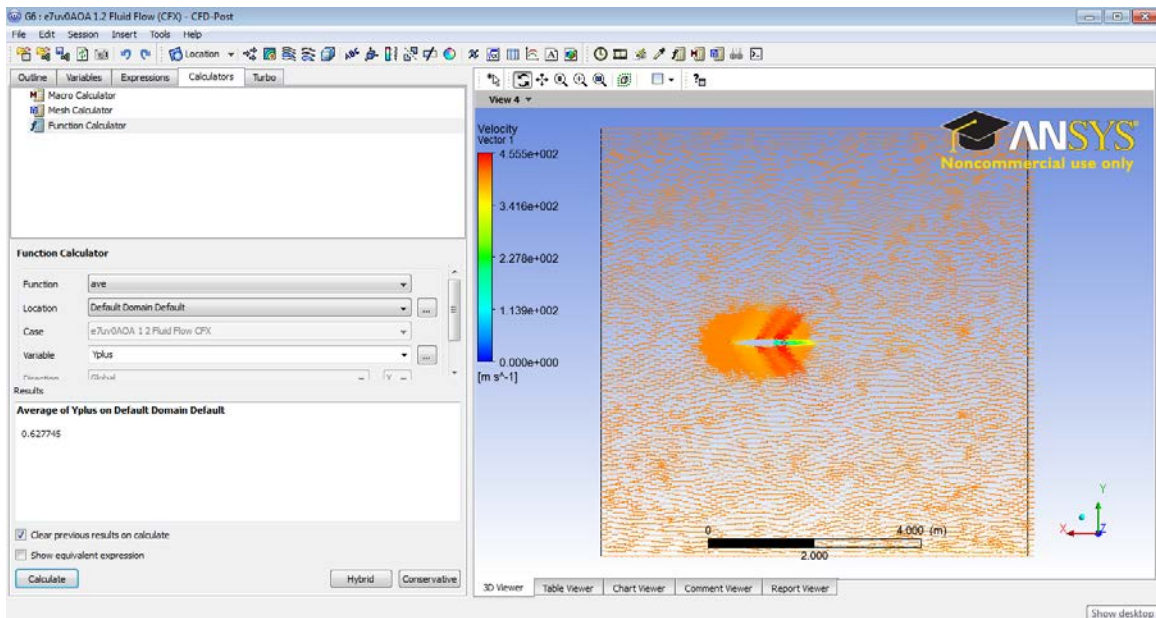
Figure 12.   Post Processing Tools in ANSYS CFX Post.

7. Coordinate Axis Definition

Similar coordinate axes illustrated in Figure 13, are defined for both SolidWorks and ANSYS CFX. The center of gravity is defined at the center of origin. The simulated free-stream flow is running from left to right for AOA of 0°. Drag force or force component in -X direction can be extracted using "force_x" in the Function Calculator. Lift force or force component in Y direction can be extracted using "force_y" in the Function Calculator. Torque about Z axis (into the diagram) can be extracted using "torque_z" in the Function Calculator.

Figure 13.   Coordinate System.

B.   OPTIMIZATION AND TUNING TECHNIQUES

The state of a model mesh has a direct effect on the generated results. A high resolution mesh is critical to the integrity of the generated output. In order to improve the accuracy, one should aim to enhance meshing within computational and resource constraint. However, a general enhancement of mesh will vastly increase computational load. 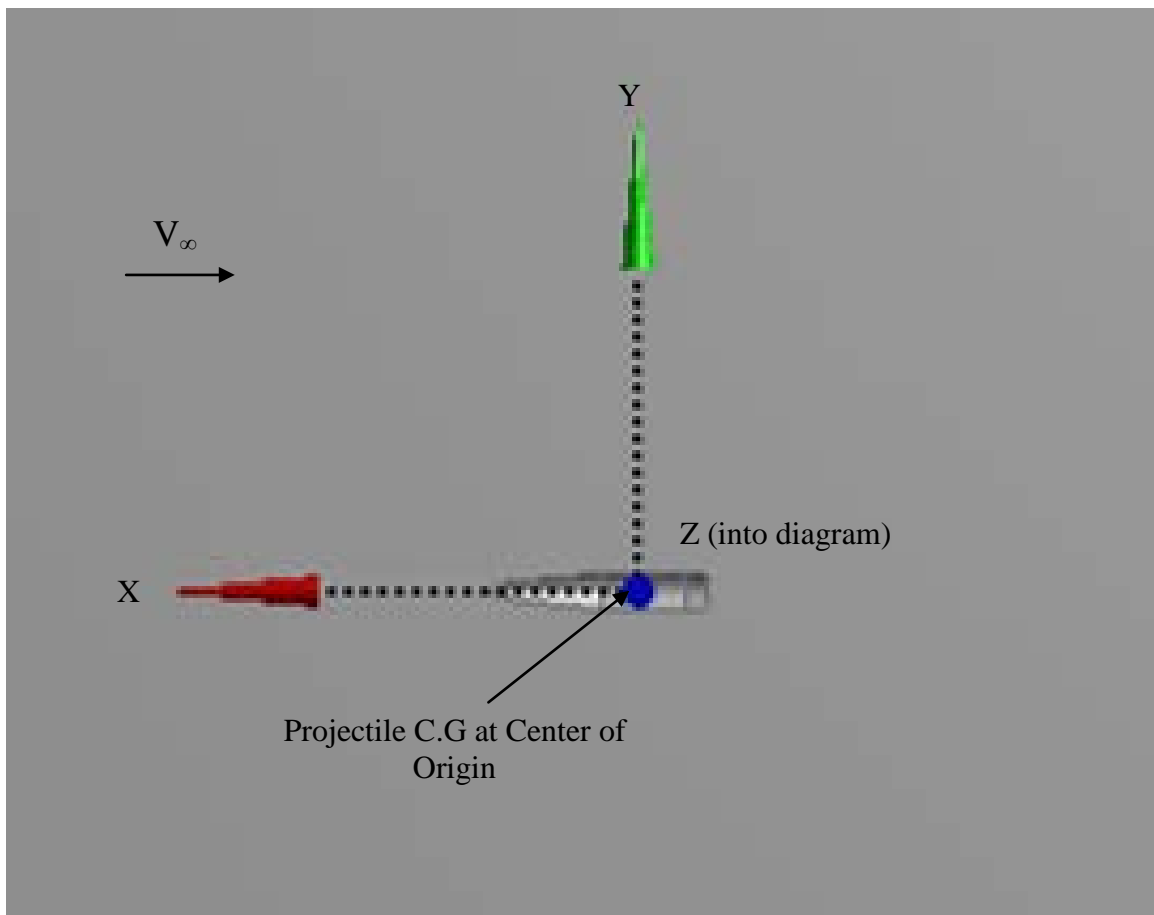Therefore it is advisable to enhance meshing at selected areas of interest that might experience drastic variations in pressure or velocity. A coarser mesh may be employed on other non-critical areas to reduce computational time. Several mesh refinement techniques were tested and two techniques stood out in terms of performance and ease of employment.

1.   Inflation

Inflation is a useful mesh enhancement technique for improving boundary layer resolution [14]. Inflation improves the mesh of the boundary layer by further refining the mesh normal to the wall. Inflation can be employed after the initial meshing of the model is completed. It is especially useful in reducing the Y+ value to an acceptable level in order to resolve the viscous sub-layer. Y+ is the dimensionless distance from the wall and it is an indicator of how well the boundary layer is being modeled. Y+ should be approximately 1 or below to capture laminar and transitional boundary layers correctly [14]. It is also necessary for flow characterized by separation and reattachment. From Equation 3.1, Y+ is dependent on friction velocity [14]. An increase in Mach number will lead to an increase in friction velocity. It is recommended to lower Y+ from onstart with a good mesh of the model with sufficient inflation layers.

$$Y+ = \frac{u^{*}y}{\upsilon} \qquad (3.1)$$

It is recommended to slowly increase the inflation level from default number. An abrupt jump in the inflation layer number will drastically increase computational time. A close up view of the generated inflation layers at boundary is depicted in Figure 14.
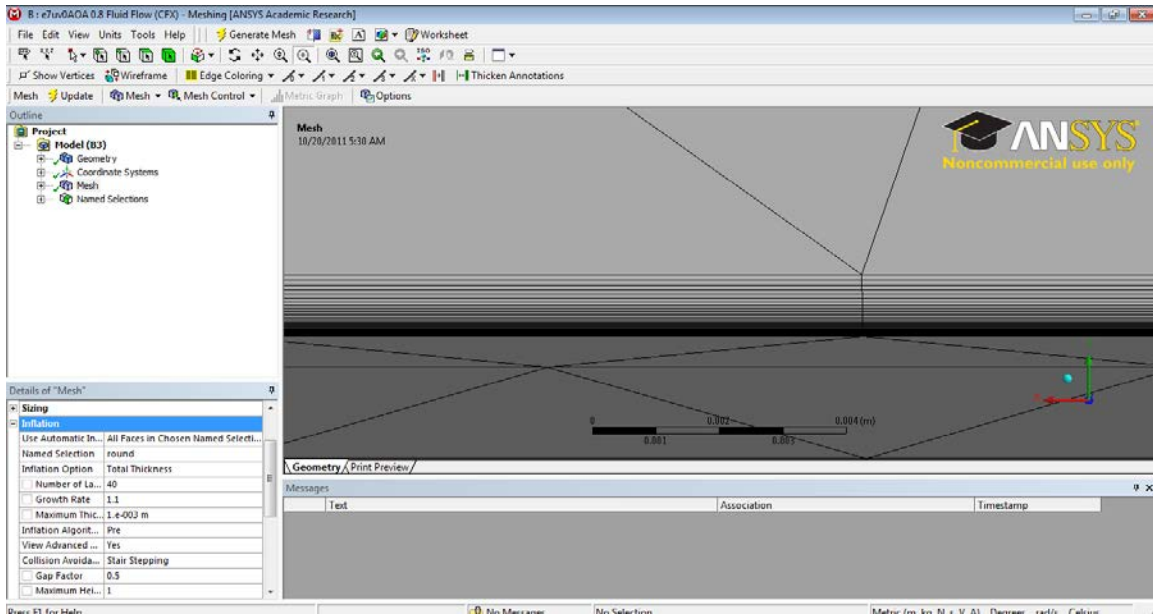
Figure 14.   Inflation Layers at Boundary.

2.   Sizing

ANSYS CFX Meshing allows two types of size functions to provide appropriate mesh sizing for different physics [14]. The default size function is designed to accurately capture the geometry while minimizing the number of elements in the model [14]. User invoked advanced size function is similar except that a smooth growth rate is maintained between the regions of curvature [14]. Region of interest is determined by user and the mesh in the region can be further enhanced with detailed meshing. An illustration of vertex sizing is depicted in Figure 15 and enhanced meshing in area of interest is depicted in Figure 16.

Figure 15.   Vertex Sizing
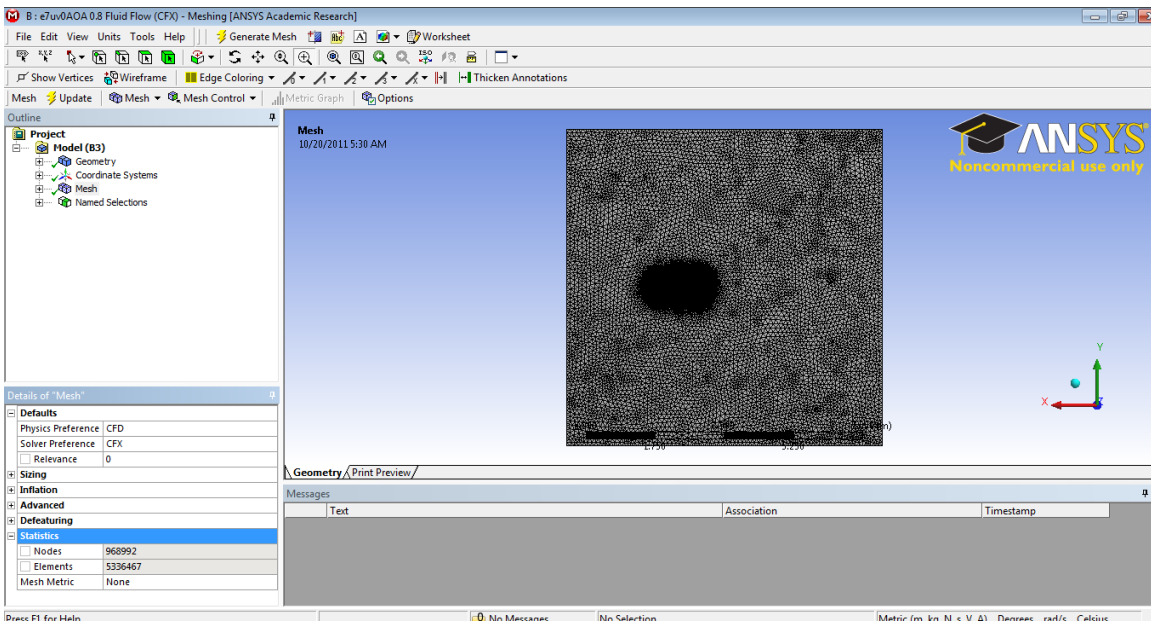
Figure 16.   Enhanced Mesh at Area of Interest.

C.   ANGLE OF ATTACK GENERATION METHODOLOGIES

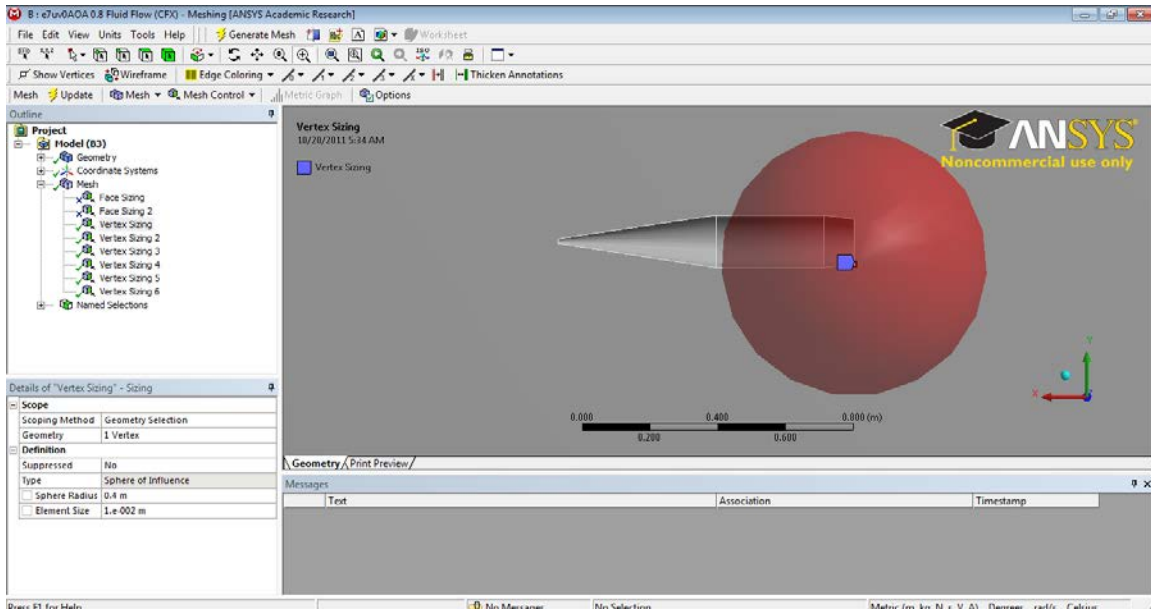Generally, the body of interest can be made to experience an AOA by two methods in ANSYS CFX. The first method is to rotate the body of interest about a particular axis. The other method is to modify the inlet velocity components.

1.   Body of Interest Rotation

Using this method, the free-stream flow direction is maintained at X axis direction. The body of interest is made to rotate to the desired AOA. Under ANSYS CFX Geometry, user can insert a plane and indicate an axis of interest for rotation. The degree of rotation is the desired degree of AOA. This is relatively easy to implement. However, each modification of the rotation will require a new mesh. An illustration of body rotation is depicted in Figure 17.

Figure 17.   Body of Interest at 10° Rotation.

2. Inlet Velocity Modification

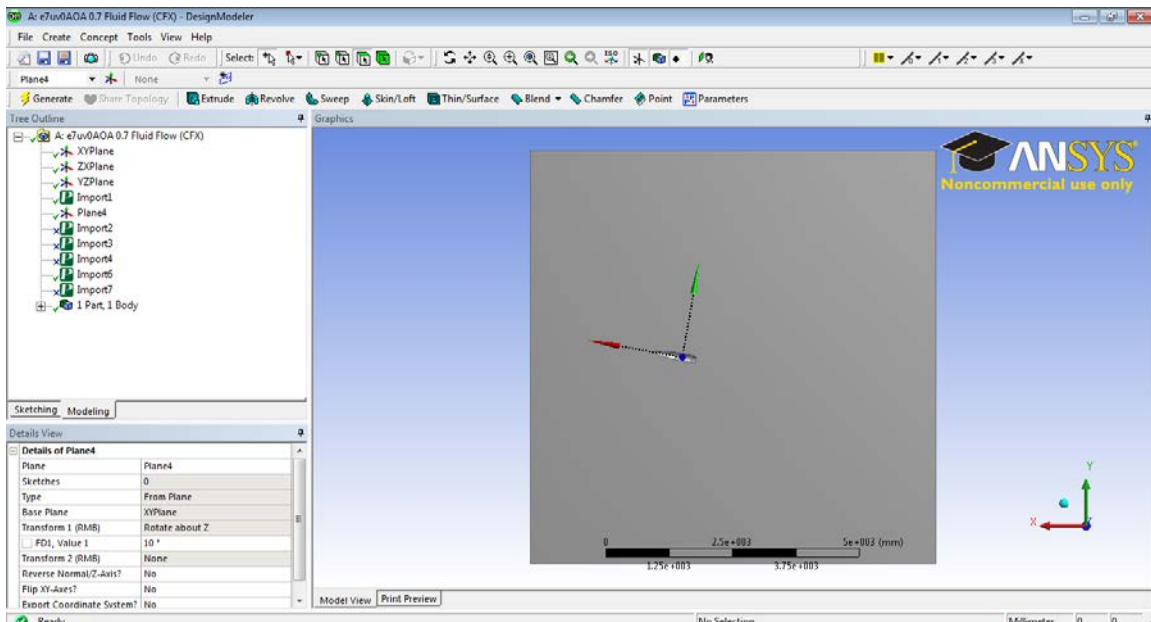Using this method, the free-stream flow is deliberately offset from the X axis direction to simulate the AOA. User will not be required to make any changes to the existing generated geometry and mesh of the body of interest. The only required change is made in ANSYS CFX Setup. Under all inlet and initialization details, the user is required to insert both u and v velocity components. For a certain AOA profile, one can make use of the following equations to determine the required u and v velocity components.

$$U = V_\infty \cos{(\alpha)} \qquad (3.2)$$

$$V = V_\infty \sin{(\alpha)} \qquad (3.3)$$

The corresponding creation of inlet is required to match with an outlet. Therefore with two inlets, one will expect two outlets to be created. The u and v inlets and outlets are illustrated in Figure 18.
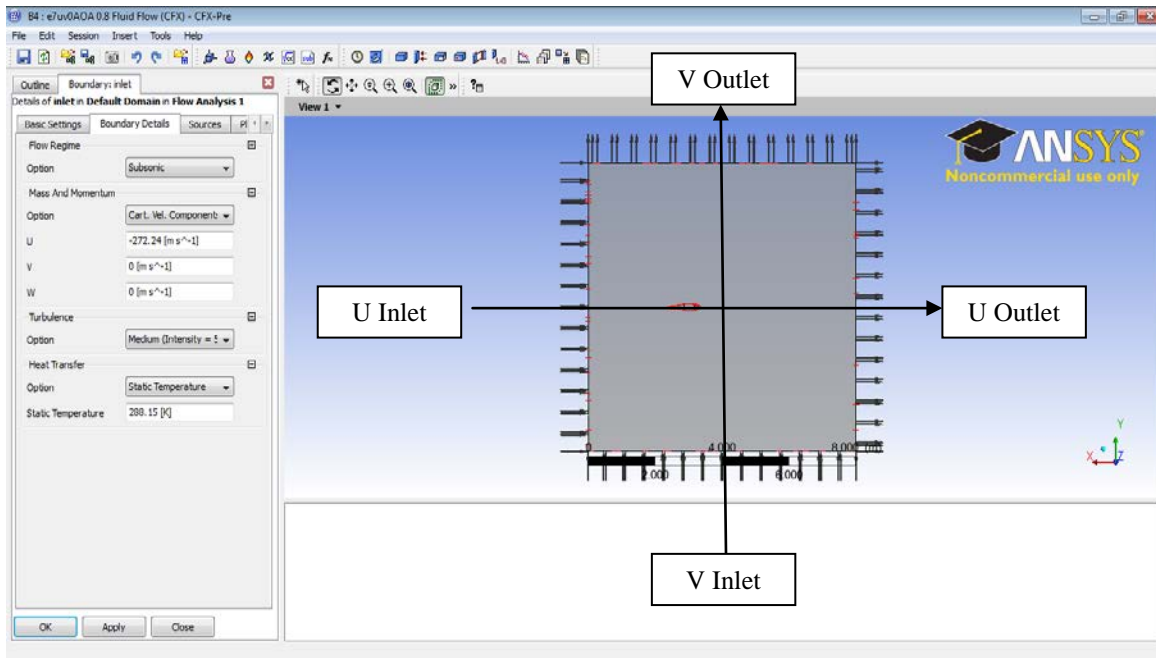

Figure 18.   U and V Inlets and Outlets.

THIS PAGE INTENTIONALLY LEFT BLANK

IV. AERO-PREDICTION (AP) 09 CODE

The Aero-Prediction (AP) code is used for the aerodynamic prediction of mortars, low drag bombs, projectile and missile bodies [21]. The AP code has undergone several iterations of improvement and the thesis will make use of the latest version known as AP09 [21]. It employs semi-empirical techniques based on both experimental results and theoretical methods to predict the aerodynamic coefficients [21]. The greatest advantage offered by the AP09 code is rapid result generation. After the geometry and essential simulation conditions are entered into the program, the result is generated instantly.

A. LOGIC FLOW

The AP09 code consists of the pre-processor, the post-processor, the aerodynamic module, trim aerodynamics module, a ballistic trajectory module and a three degrees of freedom trim performance module [22]. The geometry and simulation conditions are keyed into the pre-processor. The pre-processor consists of geometry, free-stream, option and trajectory inputs [22]. After the results generation is completed, the user can access the results in the post-processor. The post-processor consists of output data which can be in the form of tables of data or plots of aerodynamic data or trajectory information [22]. The aerodynamics module contains all aerodynamic computations and is used in a stand-alone mode or to provide inputs to the trajectory modules [22]. User is required to generate a feasible geometry prior to result generation. The geometry inputs are required for all aerodynamic computations in the code. AP09 followed its predecessor, AP05's logic flow [21]. The AP code's logic flow is depicted in Figure 19.

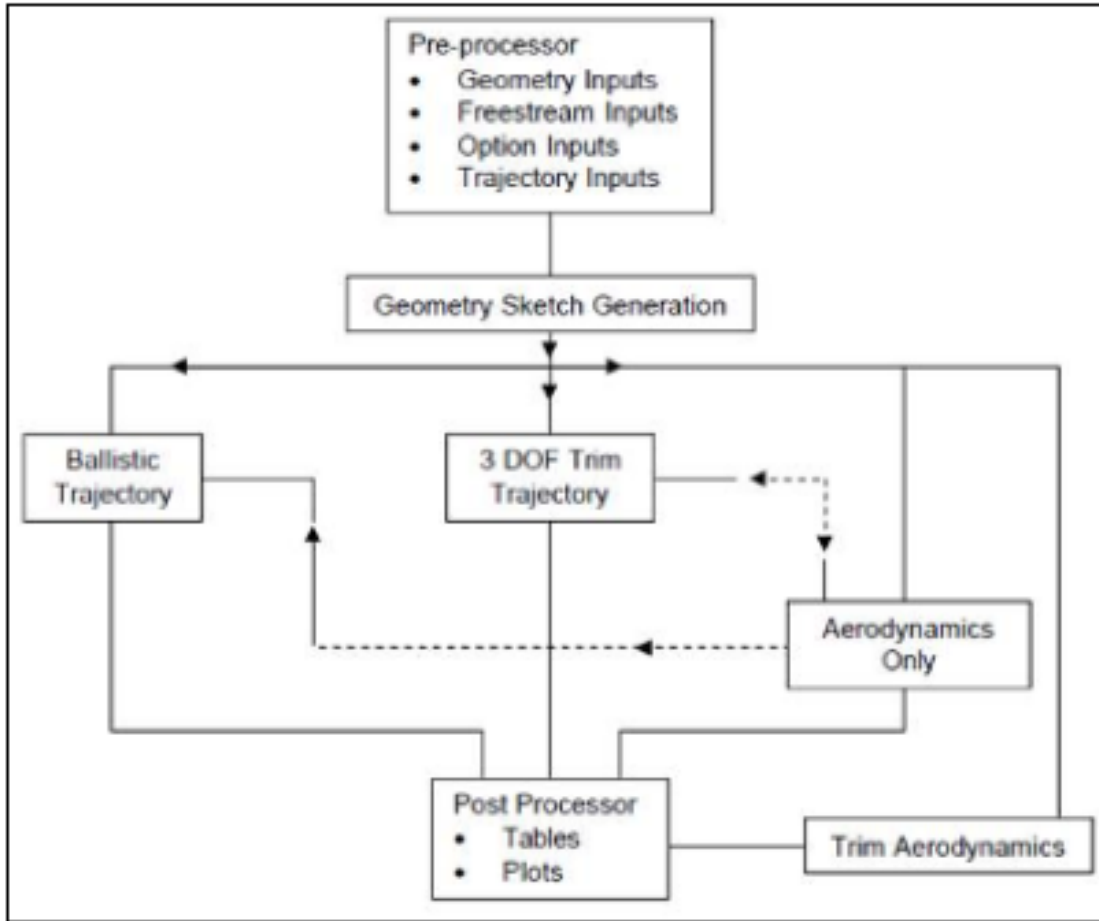Figure 19.   AP Code Logic Flow. From [22]

B.   PRE PROCESSOR

Prior to the creation of a M549 projectile geometry model, the global configuration is determined in AP09 Pre Processor. Under Configuration tab on the AP09's interface, "Body-Alone" is selected for M549 geometry modeling. In the Input tab, "Geometry (Millimeters)" format was selected as default unit for the subsequent data inputs.

1. Geometry Creation

The projectile dimension highlighted in Figure 3 is entered into the Body-Alone Geometry Tab. The interface of Body-Alone Geometry Tab is illustrated in Figure 20. With the dimension, AP09 creates a geometry model of the projectile which can be viewed under Generation Tab.
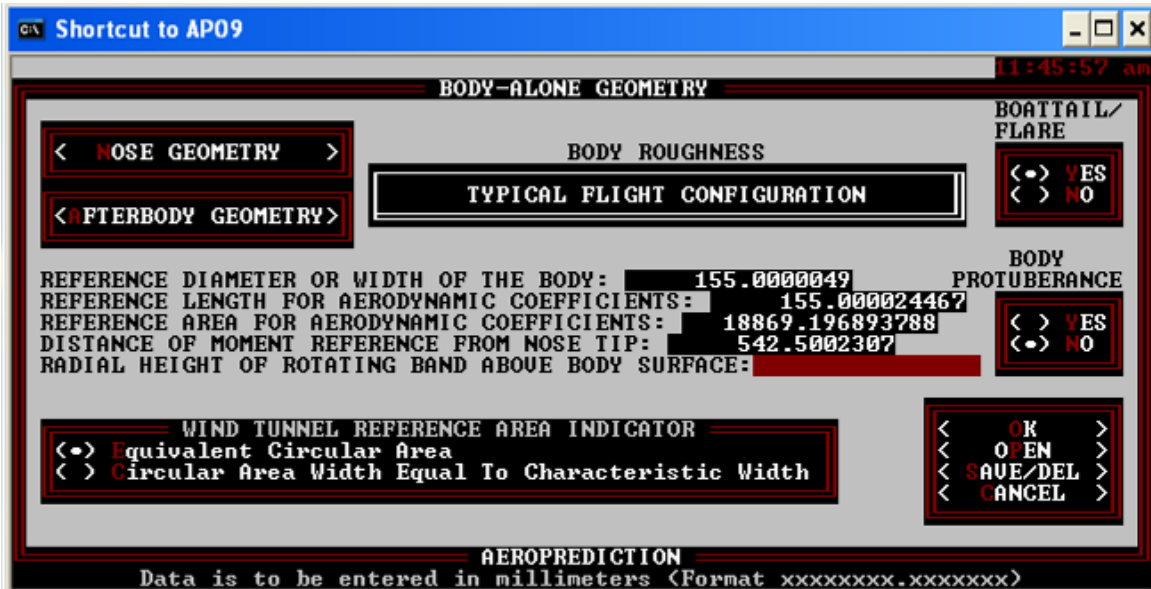
Figure 20.   Body-Alone Geometry Tab.

Upon completion of Body-Alone Geometry Tab's entries, the Nose Geometry's entries are required for the creation of the projectile's nose profile. Circular shape and power series blunt was selected for the nose profile. The circular radius of the nose end is 79mm, half of the projectile's diameter. The interface of Nose Geometry is illustrated in Figure 21.
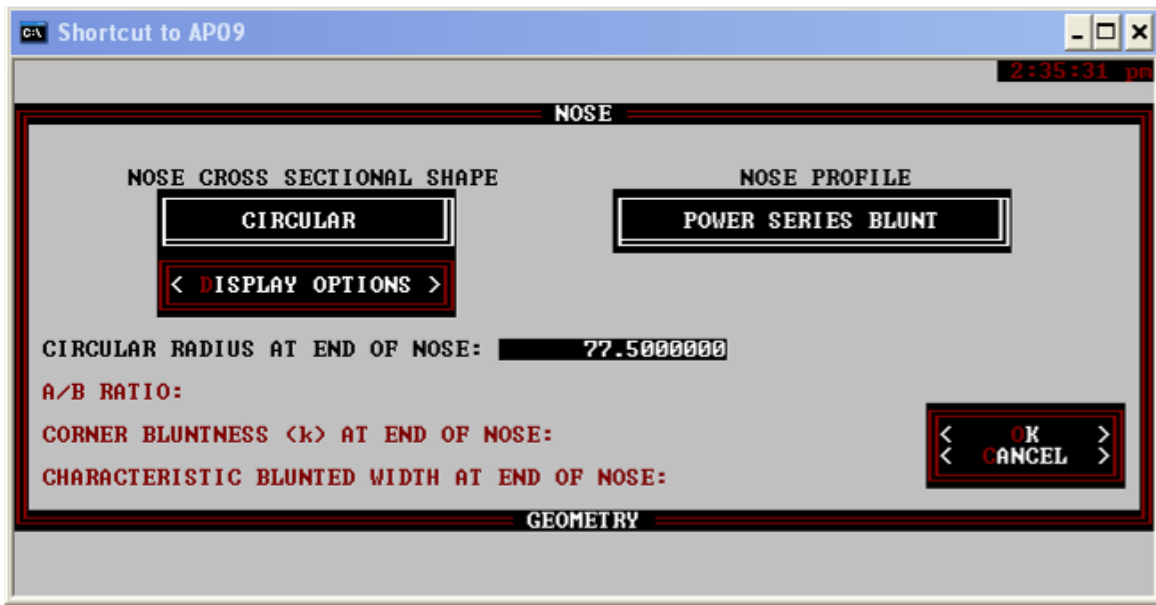
Figure 21.   Nose Geometry.

Within the nose profile, the power series exponent, truncation tip radius and length of nose is specified. This is illustrated in Figure 22.
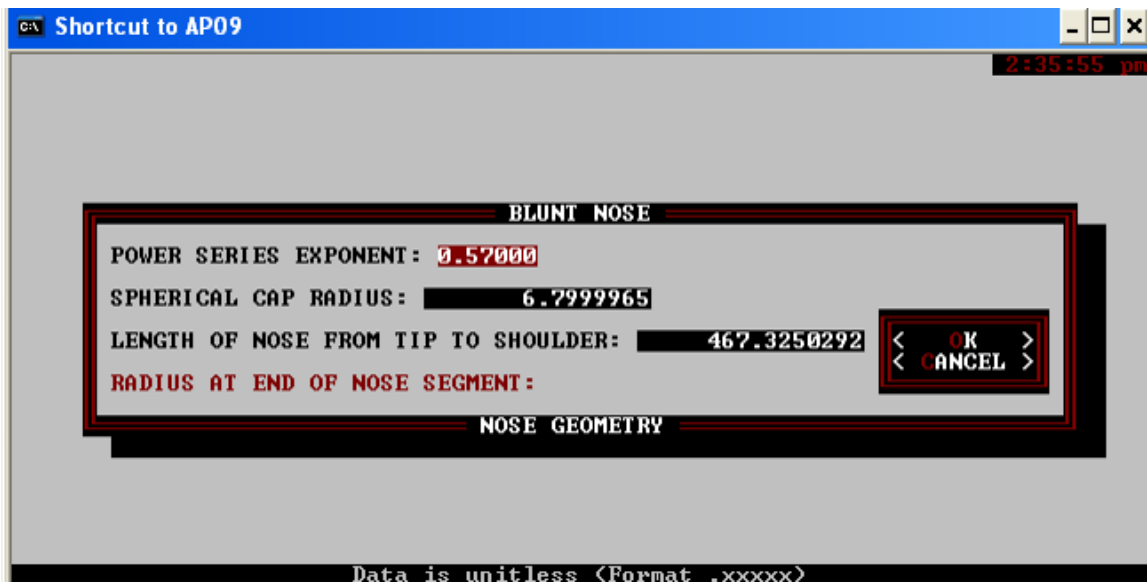
Figure 22.   Nose Profile.

Upon the completion of Nose Geometry's entries, circular cross section and standard profile was selected for the model as illustrated in Figure 23.
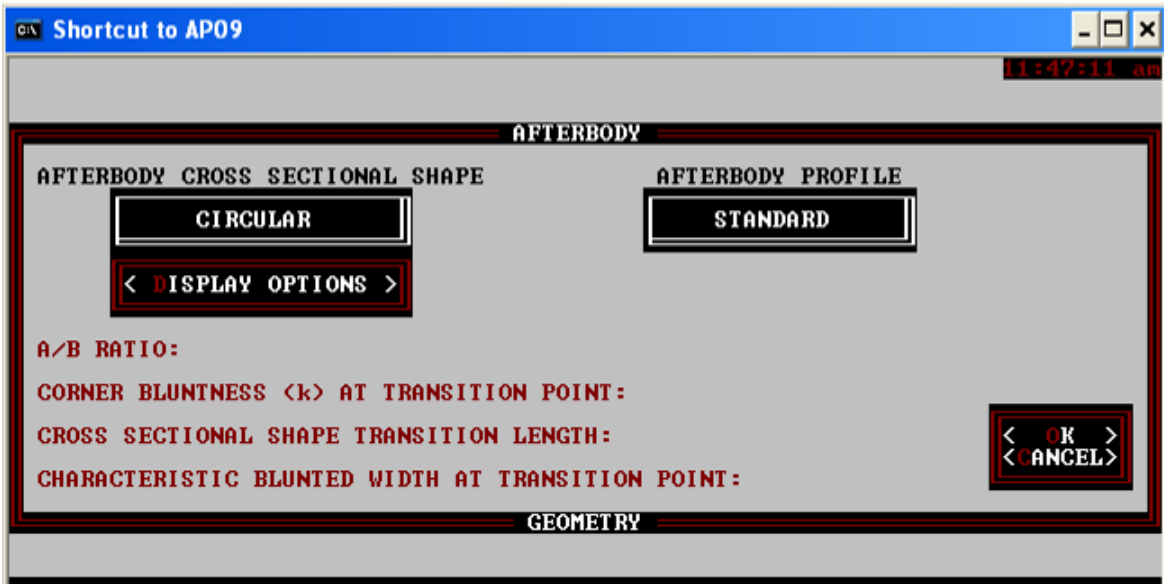
Figure 23.   Afterbody Geometry.

Under the Standard Tab in the Afterbody Geometry Tab, the longitudinal Afterbody coordinate from nose tip or entire length of the projectile nose and Afterbody only was indicated as illustrated in Figure 24.
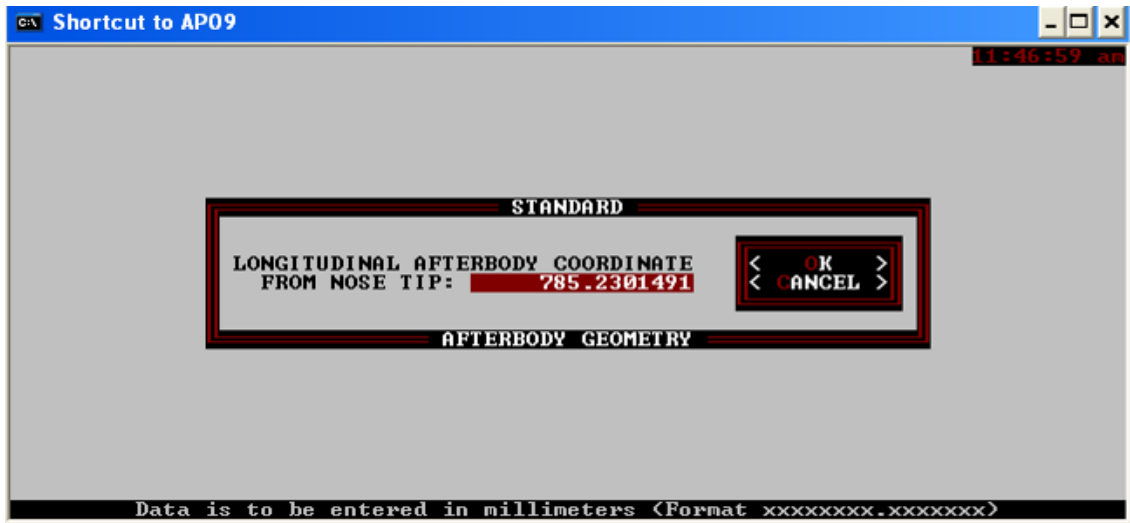
Figure 24.   Afterbody Standard Tab.

Finally, the longitudinal boattail/flare coordinate from nose tip or entire length of projectile is indicated. The boattail/flare half width or radius is required too. This is illustrated in Figure 25.
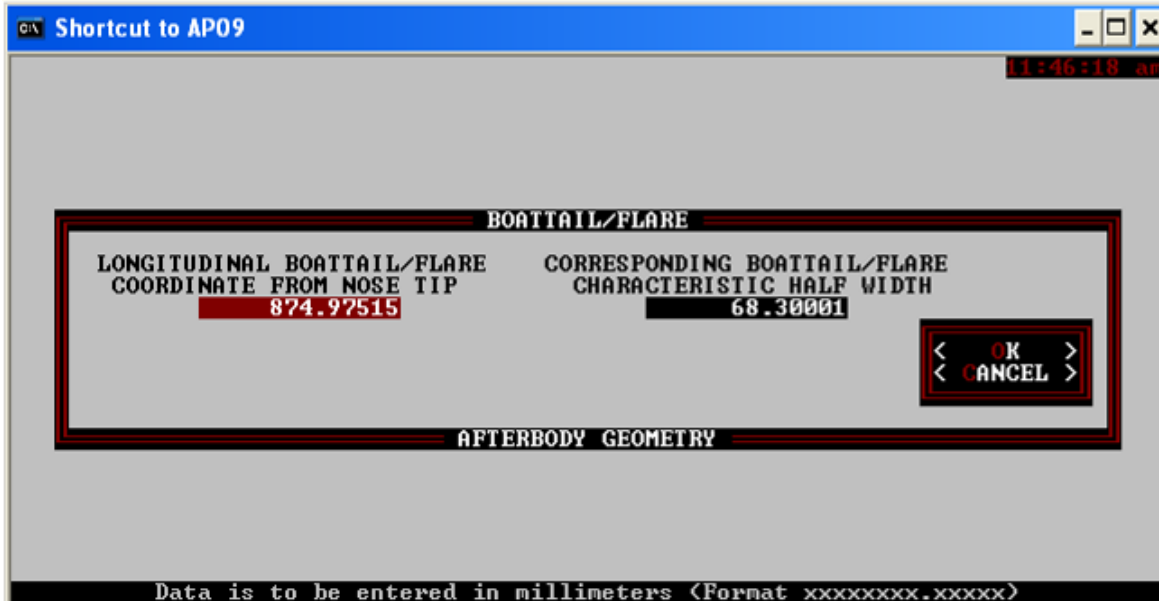
Figure 25.   Boattail/Flare Tab.

The essential dimensions of the projectile highlighted in Figure 3 were keyed into the body alone geometry tab. Using the dimensions given, AP09 will generate a geometry model which can be viewed under Generation Tab.

2.   Free Stream Condition and Option Setup

Upon verification of the geometry model, the free stream condition for type of simulation is specified. In this thesis, Mach Sweep is initialized for a sweep from Mach 0.7 to Mach 1.4 at various AOA at an altitude of 20000 feet. The simulation option is the last step before simulation generation. These are illustrated in Figure 26.

Figure 26.   Simulation Option.

C.   POST PROCESSOR

Upon the completion of the result generation, the relevant result in plot and table format can be called up. The results can be extracted out in text file for plotting in Excel.

THIS PAGE INTENTIONALLY LEFT BLANK

V. RESULTS AND ANALYSIS

The generated results and analysis are categorized into three main segments, Part I for Standard Nose Configuration, Part II for Comparison Studies of the AOA Generation Methodologies and Part III for Modified Nose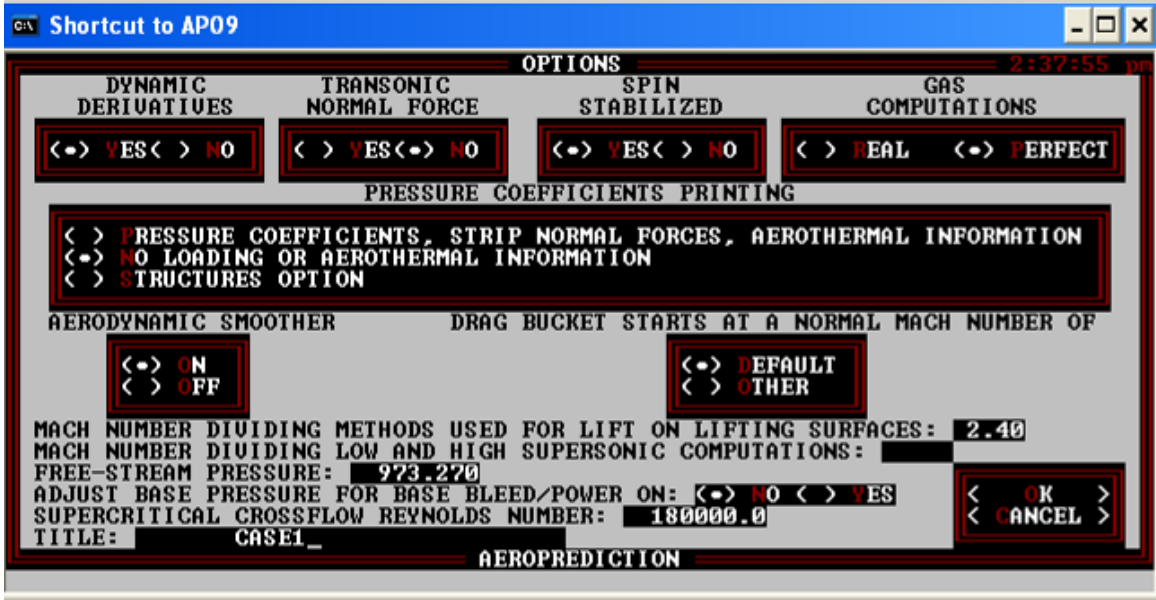 Configuration. Experimental data from [5, 6] are used as the benchmark reference data for the ANSYS CFX and AP09 results.

A. PART I–STANDARD NOSE CONFIGURATION

Under the Standard Nose Configuration, ANSYS CFX and AP09 simulations were performed on a standard M549 projectile model. Total drag coefficient, normal force coefficient and pitching moment coefficient were evaluated for various AOA and Mach numbers. These simulations were performed using IVM method.

1. Total Drag Coefficient versus Mach Number

The generated total drag coefficient versus Mach Numbers at AOA of 0° results are illustrated in Figure 26. The variation of the total drag coefficient was determined using six data points from Mach 0.7 to Mach 1.2 with an interval of 0.1. The generated Y+ ranged from 0.8 to 1.6.
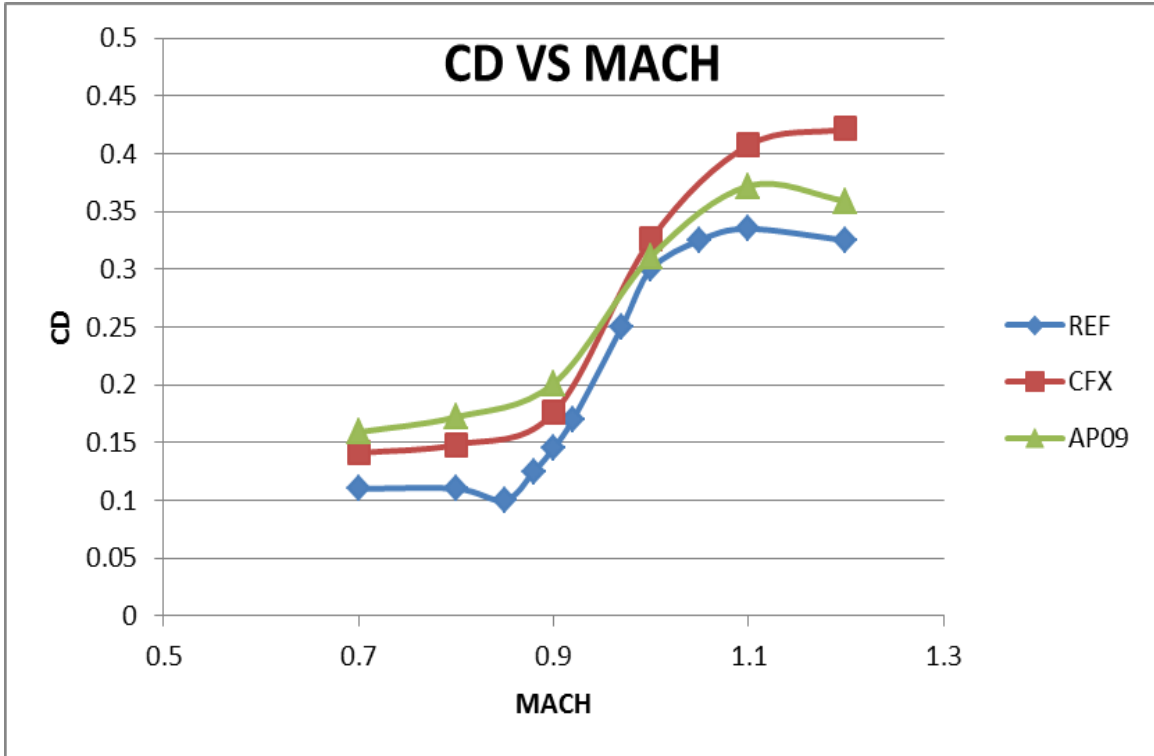
Figure 27.   Total Drag Coefficient versus Mach at AOA of 0°.

From Figure 27, ANSYS CFX and AP09 and reference data from [5] exhibited similar total drag coefficient trends. ANSYS CFX and AP09 correctly predicted the increase in total drag coefficient in transonic region. This increase can be explained by the change in pressure distribution caused by the changes in flow speed. As the Mach number reached transonic and supersonic values, shocks start to form. Thus drag starts to increase at high speed flow. This form of drag is known as wave drag.

Comparing prediction accuracy, ANSYS CFX fared better in the subsonic and transonic region. AP09 was able to give a better prediction in the supersonic region as compared to ANSYS CFX. This could be due to increasing Y+ value illustrated in Figure 28.
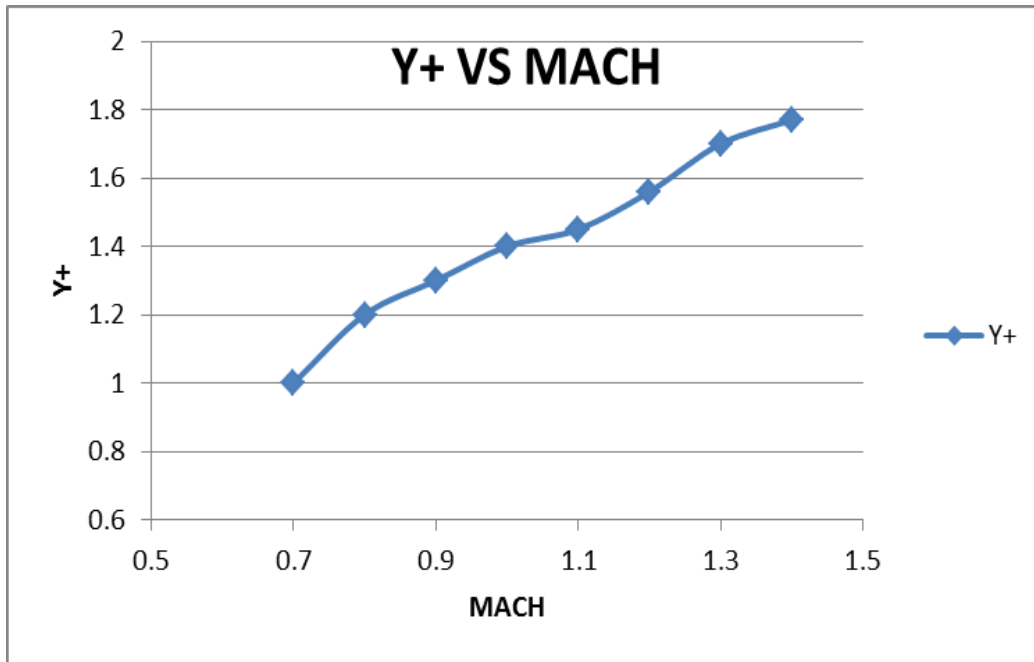
Figure 28.   Simulation Y+ versus Mach at AOA of 0°.

Based on Equation 3.1, Y+ is dependent on friction velocity. Thus, increase in Mach number will lead to an increase in Y+, contributing to simulation error. This may explain the large deviation of the ANSYS CFX prediction from the experiment in low supersonic flow.

In order to investigate whether these observations are still valid at finite AOA, the simulations were repeated for AOA of 2° and 4° as illustrated in Figures 29 and 30. It was observed that the ANSYS CFX and AP09 prediction agree well at subsonic Mach numbers, but deviate in supersonic flow.

Figure 29.   Total Drag Coefficient versus Mach at AOA of 2°.
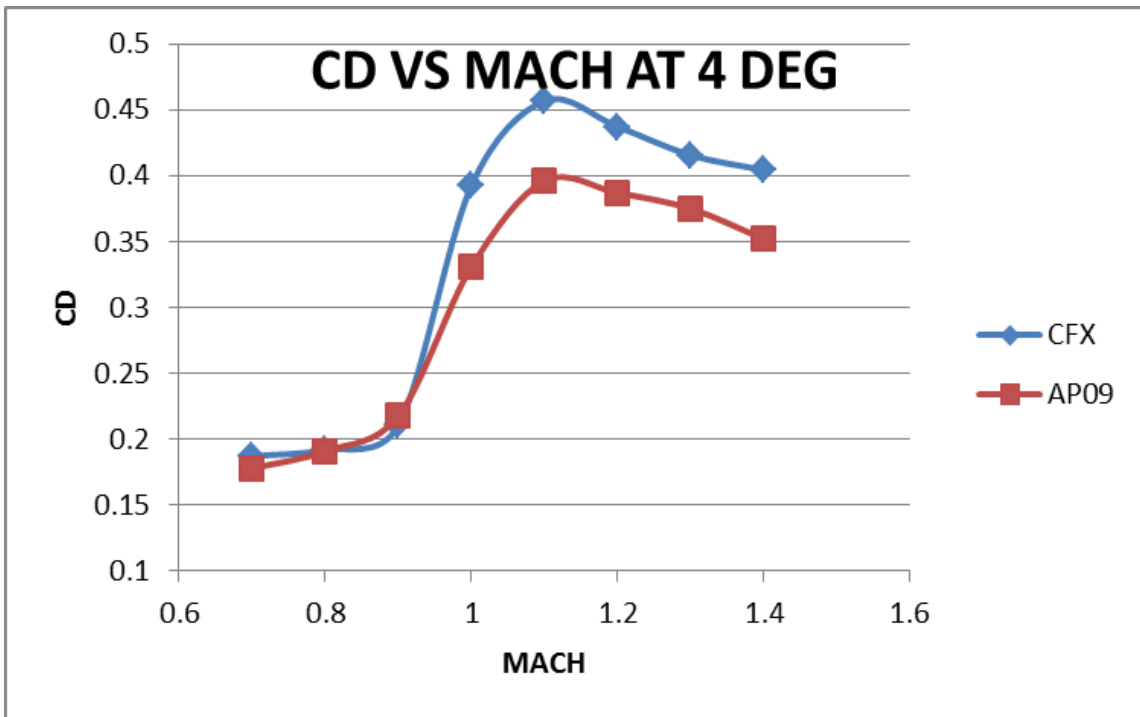
Figure 30.   Total Drag Coefficient versus Mach at AOA of 4°.

2. Normal Force Coefficient Slope versus Mach Number

The normal force coefficient slope versus Mach Number results are illustrated in Figure 31. The normal force coefficient slope was calculated by taking the normal force difference between AOA of 2° and 0°. The variation of the normal fo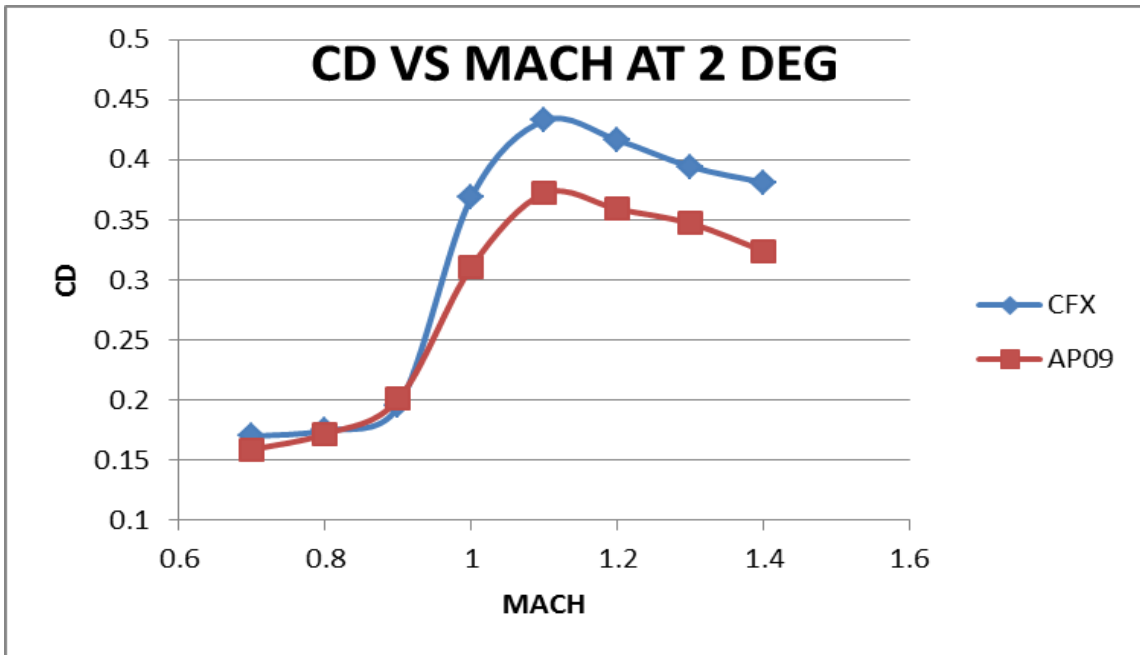rce coefficient slope with Mach number was determined using eight data points from Mach 0.7 to Mach 1.4 with an interval of 0.1. The simulation was conducted using ANSYS CFX and AP09. The generated Y+ ranged from 1 to 1.8.

Figure 31.   Normal Force Coefficient Slope versus Mach Number.

From Figure 31, it is apparent that the ANSYS CFX and AP09 predictions differ quite substantially from the experiment [5]. However, ANSYS CFX correctly predicted the decrease in normal force coefficient in the transonic region found in the experiment. The ANSYS CFX deviation from both AP09 and the experiment at Mach=1.4 may be due to the same reason explained before.

3. Pitching Moment Coefficient Slope versus Mach Number

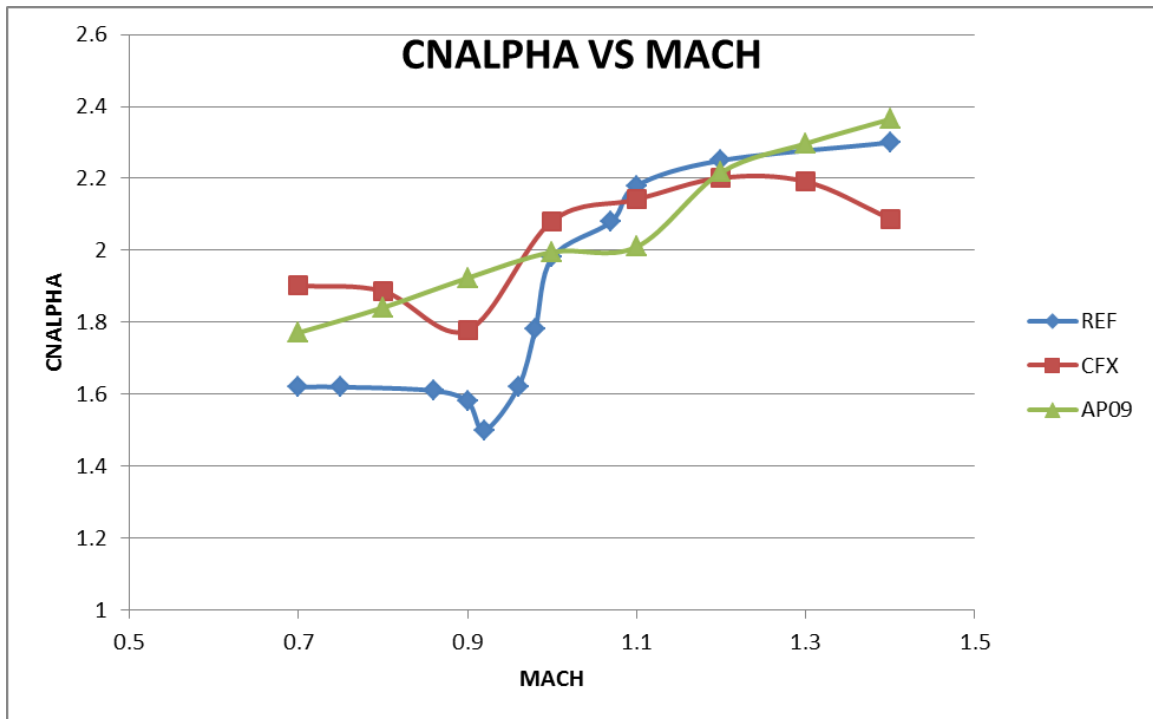The pitching moment coefficient slope versus Mach Number results are illustrated in Figure 32. The pitching moment coefficient slope was calculated by taking the torque (Z axis) difference between AOA of 2° and 0°. The variation of the pitching moment coefficient slope from subsonic to supersonic region was determined using eight data points from Mach 0.7 to Mach 1.4 with an interval of 0.1. The generated Y+ ranged from 1 to 1.8.
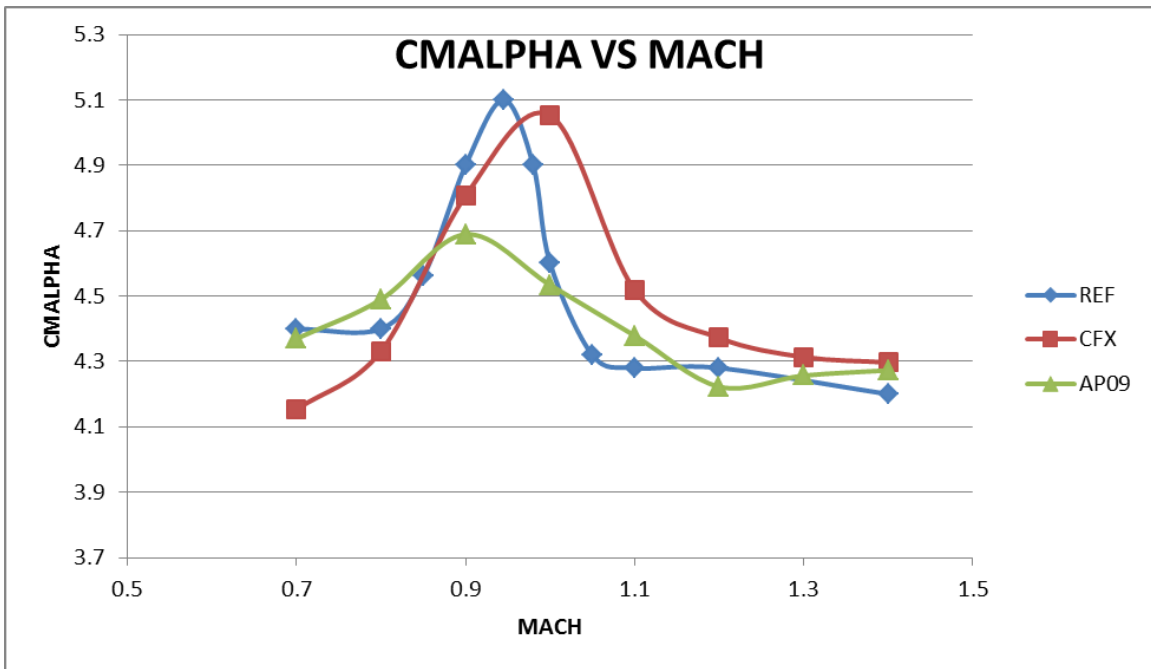
Figure 32.   Pitching Moment Coefficient Slope versus Mach Number.

From Figure 32, it is seen that ANSYS CFX correctly predicted the increase in pitching moment coefficient slope in the transonic region found in the experiment [5, 6], whereas AP09 under-predicts by a significant margin.

4. Lift Coefficient at Different Speed Regimes

The computed lift coefficients at different speed regimes are illustrated in Figure 33, 34 and 35 for AOA of 0°, 2° and 4°. Both ANSYS CFX and AP09 correctly predict the upward trend of Lift Coefficient with increasing AOA.
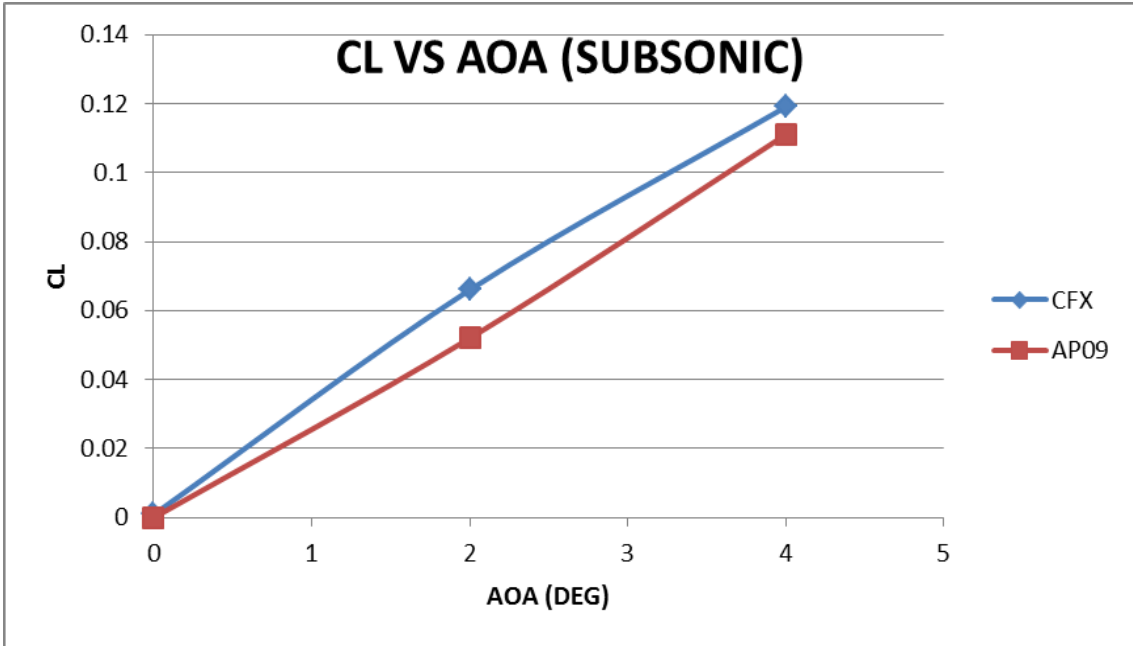
Figure 33.   Lift Coefficient at Subsonic Region.
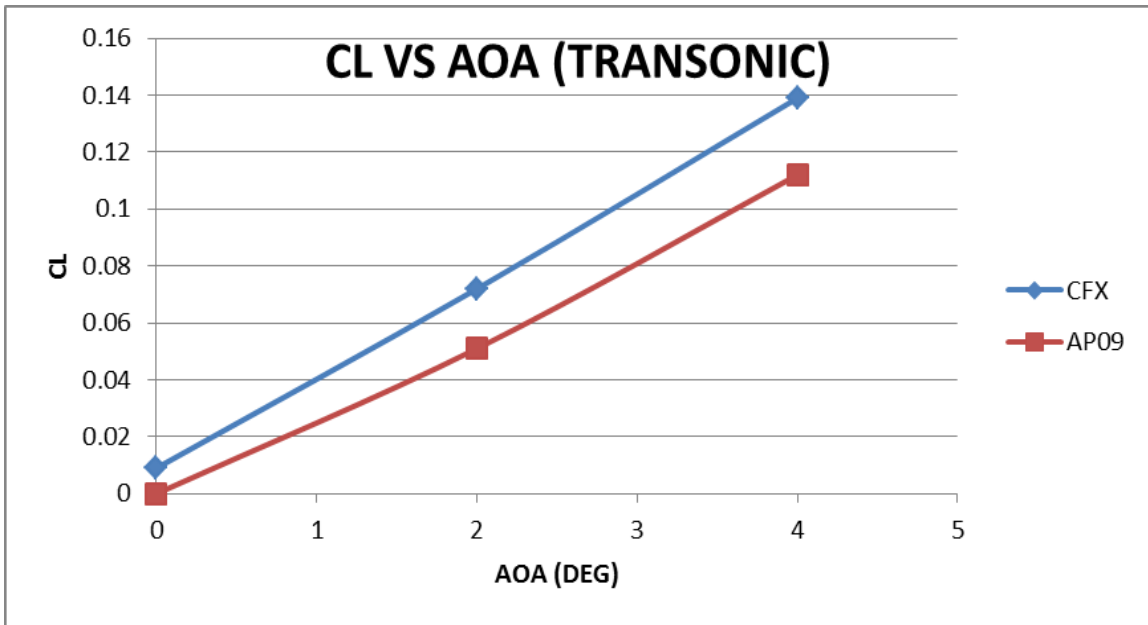
Figure 34.   Lift Coefficient at Transonic Region.
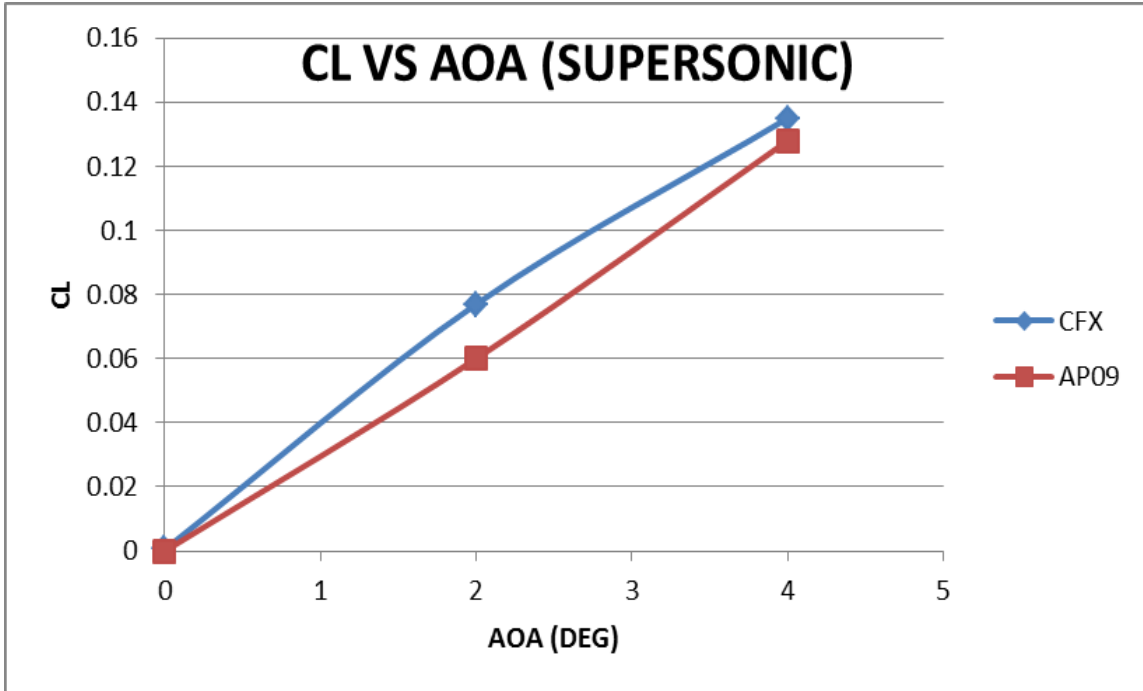
Figure 35.   Lift Coefficient at Supersonic Region.

5.   Flow Visualization

Additional insight can be obtained by visualizing the flow field changes with the Mach number and AOA. Therefore, Mach contour plots in the XZ plane at Mach Numbers of 0.7, 0.9, 1 and 1.4 at AOA of 2° using IVM are presented in Figure 36, 37, 38 and 39. Figure 40, 41, 42 and 43 offer an alternate perspective in the Y-Z plane. From Figures 44 and 45, one can observe the change in the base velocity vectors as the AOA is changed from 0° and 2°.

Figure 36.   Mach Contour at M=0.7, AOA of 2°, IVM.

Figure 37.   Mach Contour at M=0.9, AOA of 2°, IVM.
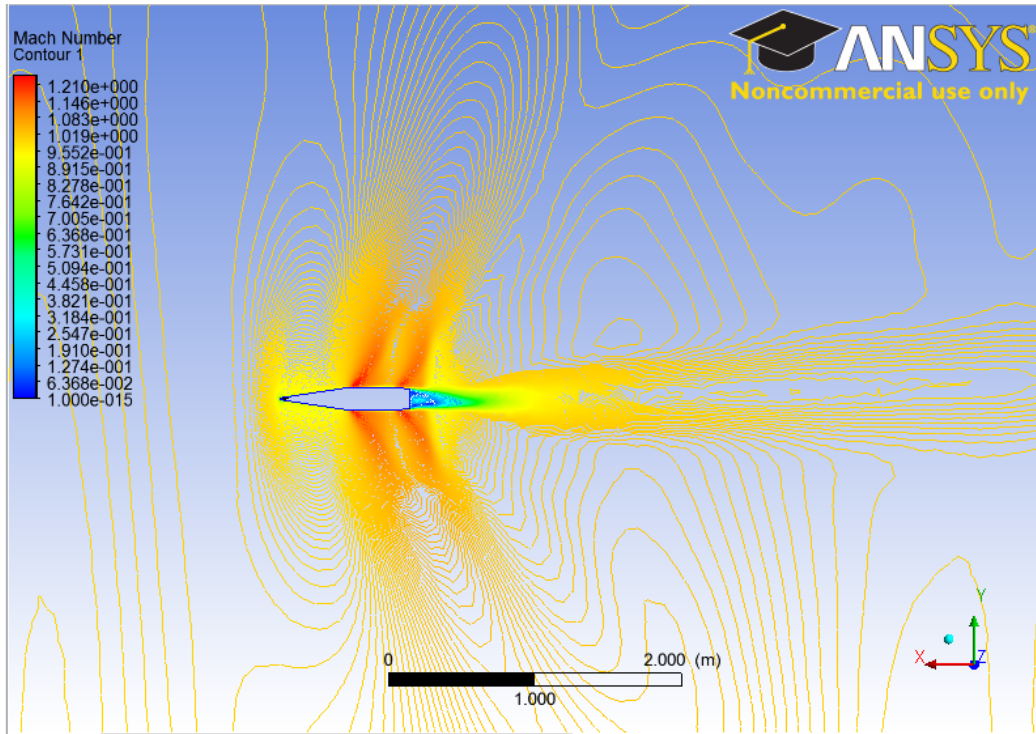
Figure 38.   Mach Contour at M=1, AOA of 2°, IVM.

Figure 39.   Mach Contour at M=1.4, AOA of 2°, IVM.

Figure 40.   Side Profile-Mach Contour at M=0.7,
AOA of 2°, IVM.
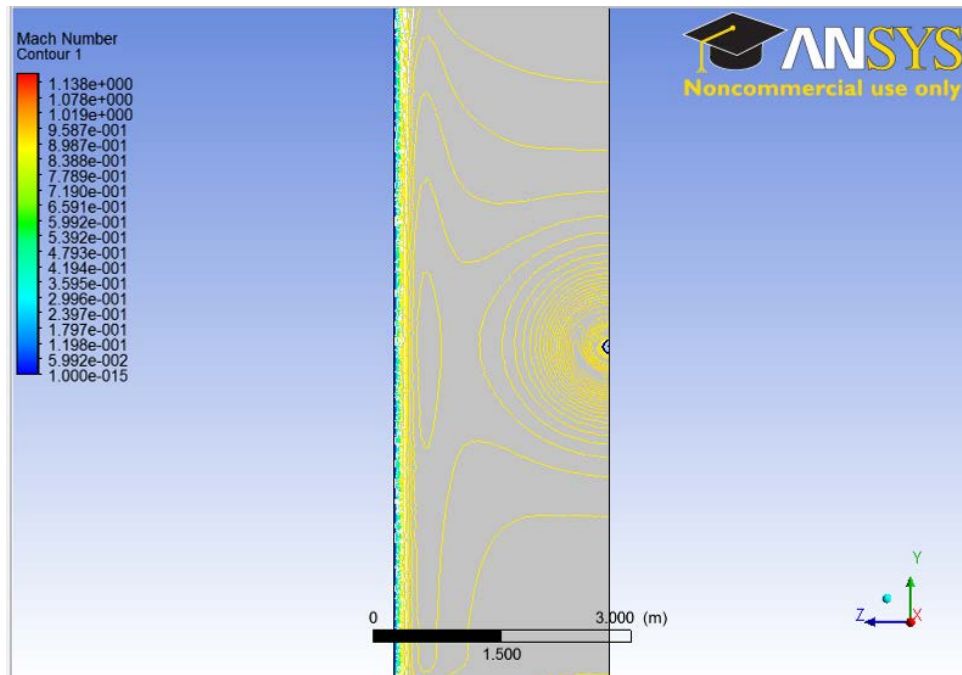
Figure 41.   Side Profile-Mach Contour at M=0.9,
AOA of 2°, IVM.
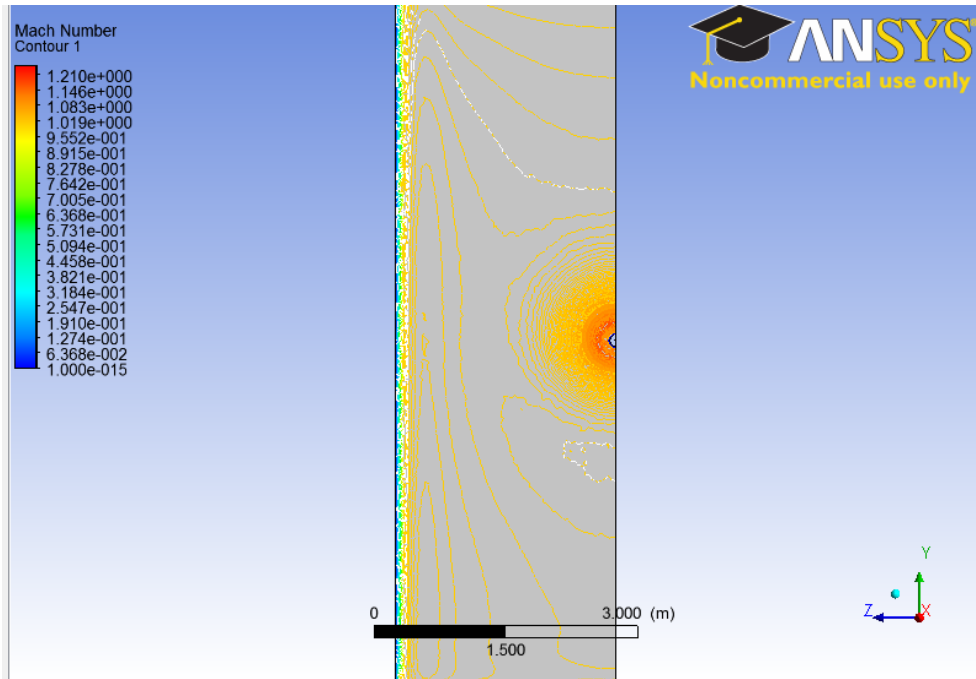
Figure 42.   Side Profile-Mach Contour at M=1,
AOA of 2°, IVM.
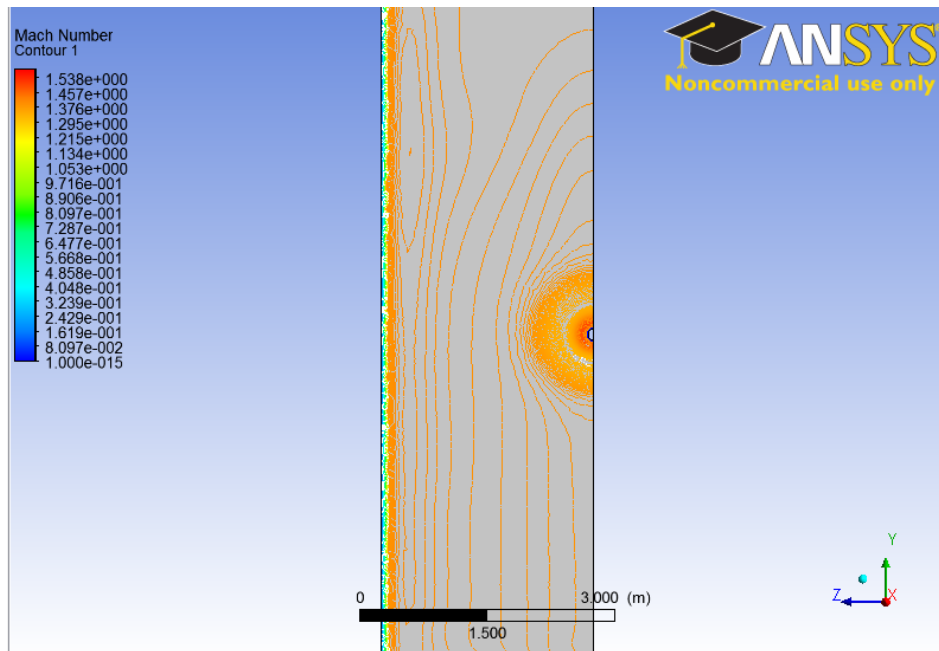
Figure 43.   Side Profile-Mach Contour at M=1.4,
AOA of 2°, IVM.

48
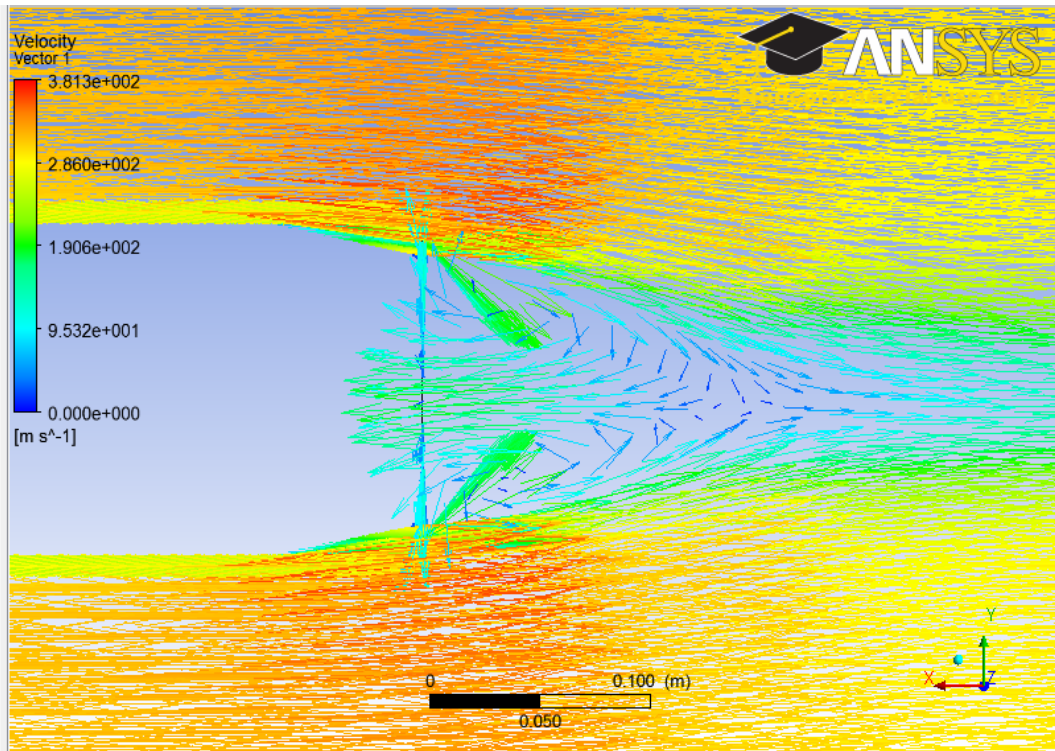
Figure 44.   Base Velocity Vector Flow at AOA of 0°, IVM.
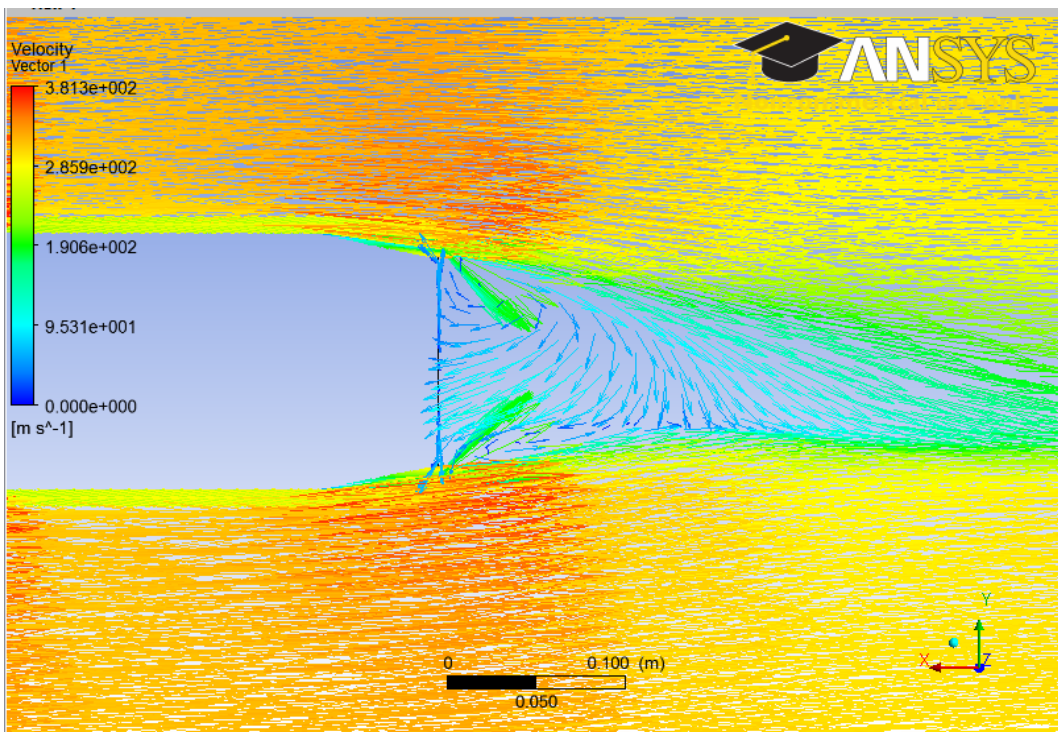
Figure 45.   Base Velocity Vector Flow at AOA of 2°, IVM.

B.   PART II–COMPARISON OF AOA GENERATION METHODS

In Part I, the simulations were performed using the IVM method for AOA Generation. In Part II, additional simulations for the Standard Nose Configuration were performed with the BIR method. Using BIR, the body of interest is rotated to the desired AOA. Results from the two methods are compared in Figure 46, 47 and 48. It is observed from Figure 46 that the two methods produce essentially identical total drag coefficients.
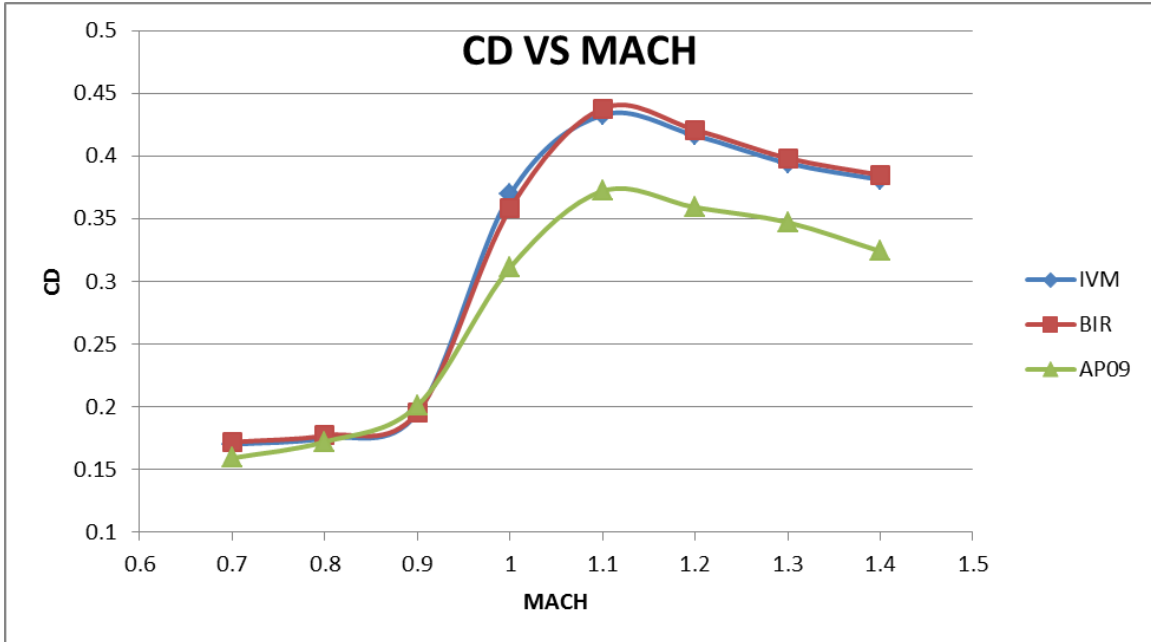
Figure 46.   Comparison of Total Drag Coefficient for IVM and BIR AOA Generation Methods.

The agreement in predicted normal coefficient slope, shown in Figure 47 and in pitching moment coefficient slope, shown in Figure 48, is somewhat less satisfactory.
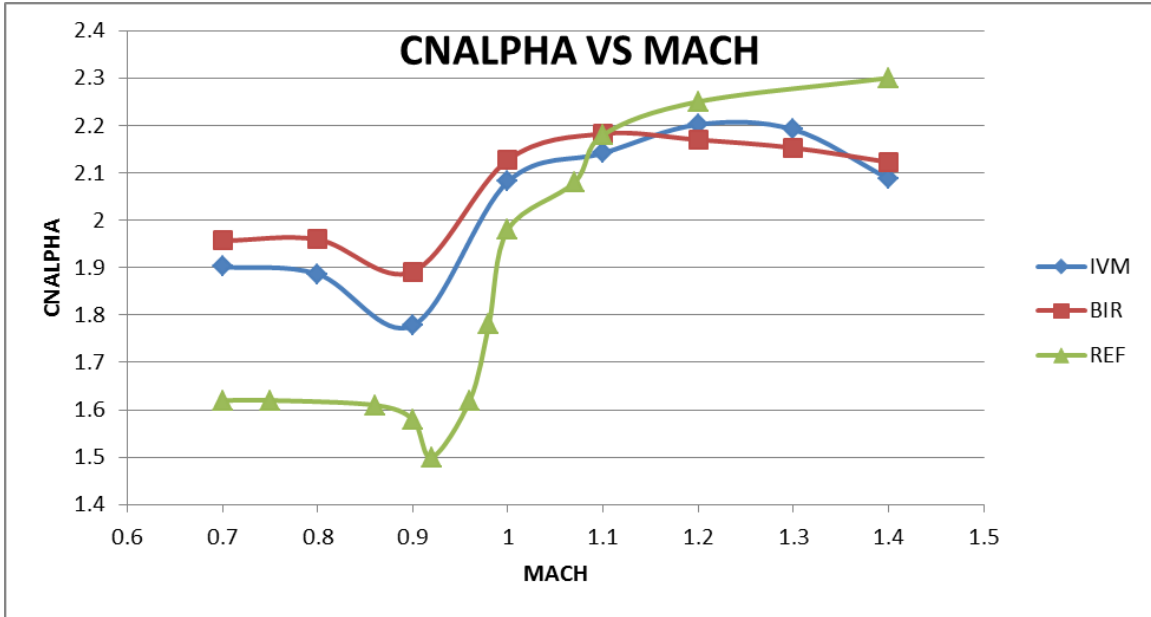
Figure 47.   Comparison of Normal Force Coefficient Slope for IVM and BIR
AOA Methods.
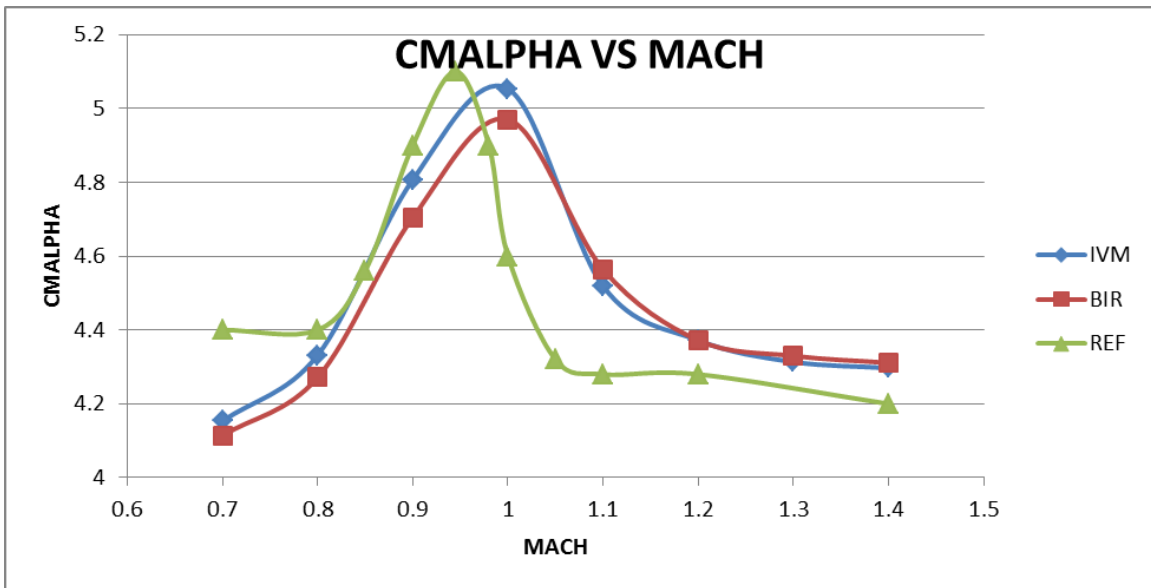
Figure 48.   Comparison of Pitching Moment Coefficient Slope for IVM and BIR
AOA Generation Methods.

Mach contours at Mach Numbers of 0.7, 0.9, 1 and 1.4 at AOA of 2° using BIR are illustrated in Figures 49, 50, 51 and 52. From the plots, it is observed that the Mach contours of BIR are in good agreement with that of IVM.
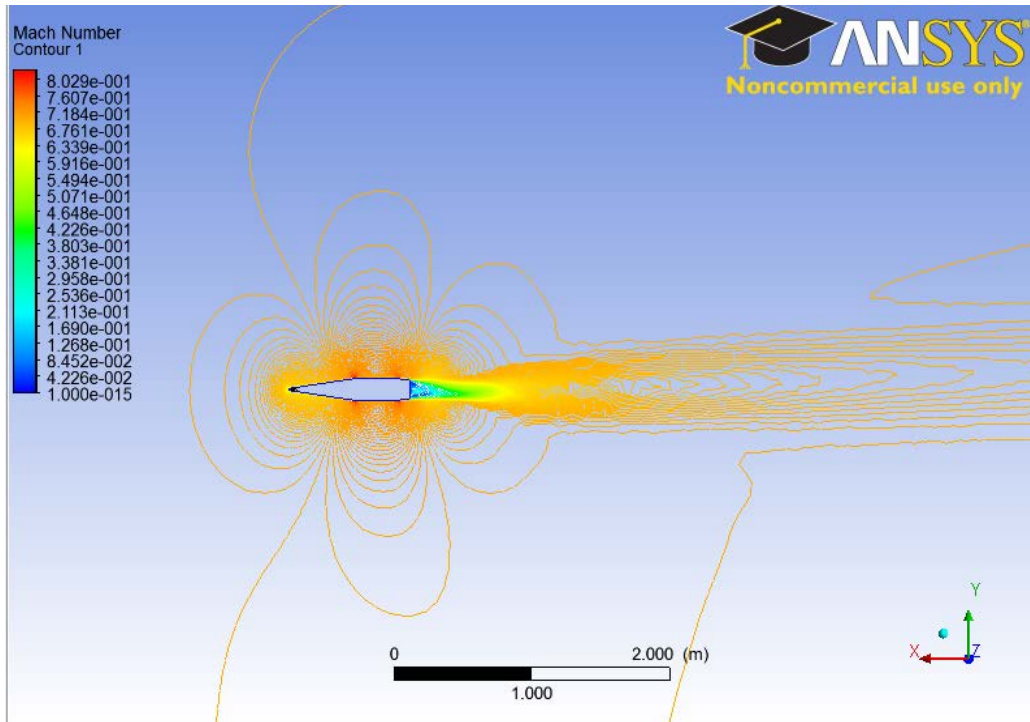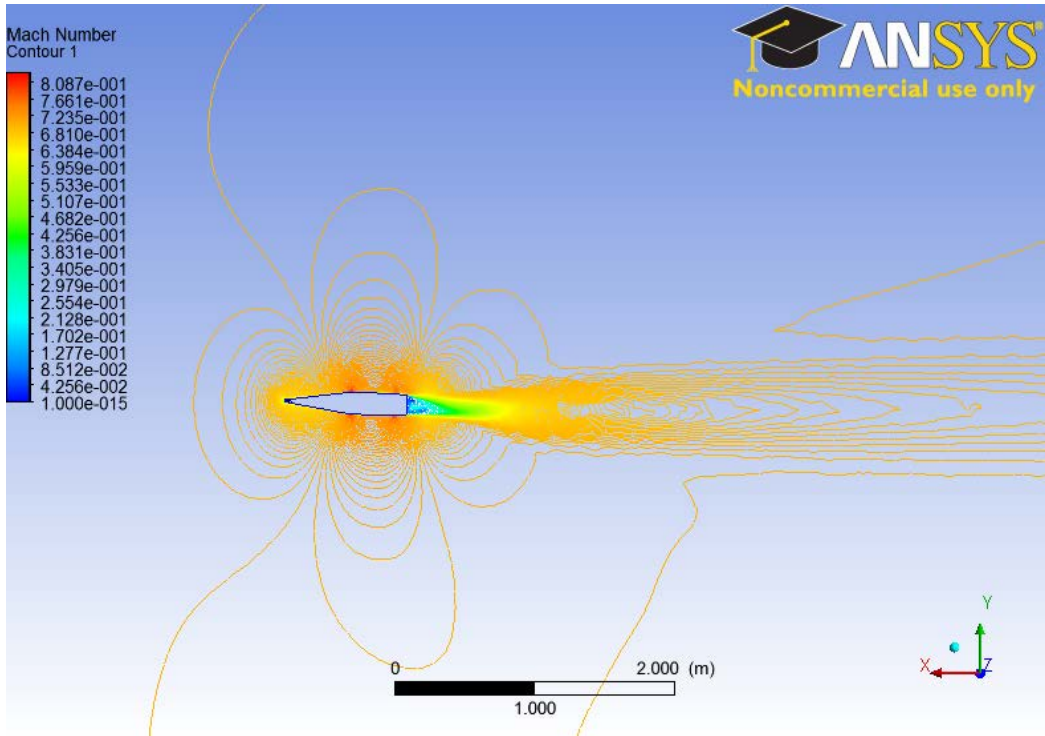

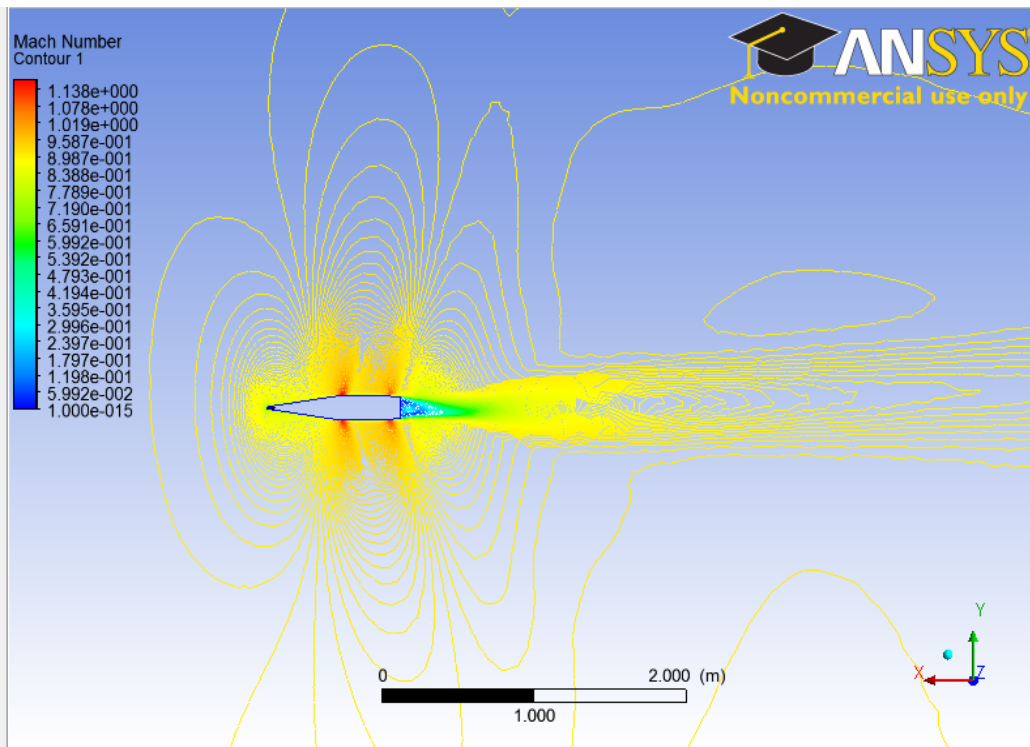Figure 49.   Mach Contour at M=0.7, AOA of 2°, BIR.
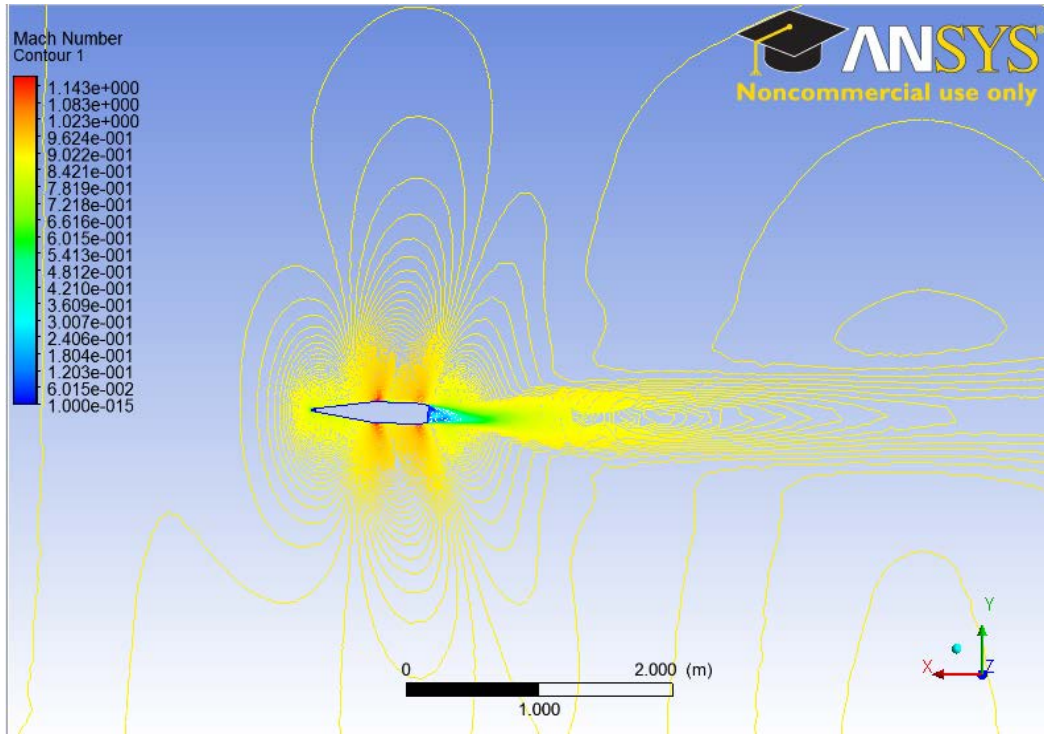
Figure 50.   Mach Contour at M=0.9, AOA of 2°, BIR.
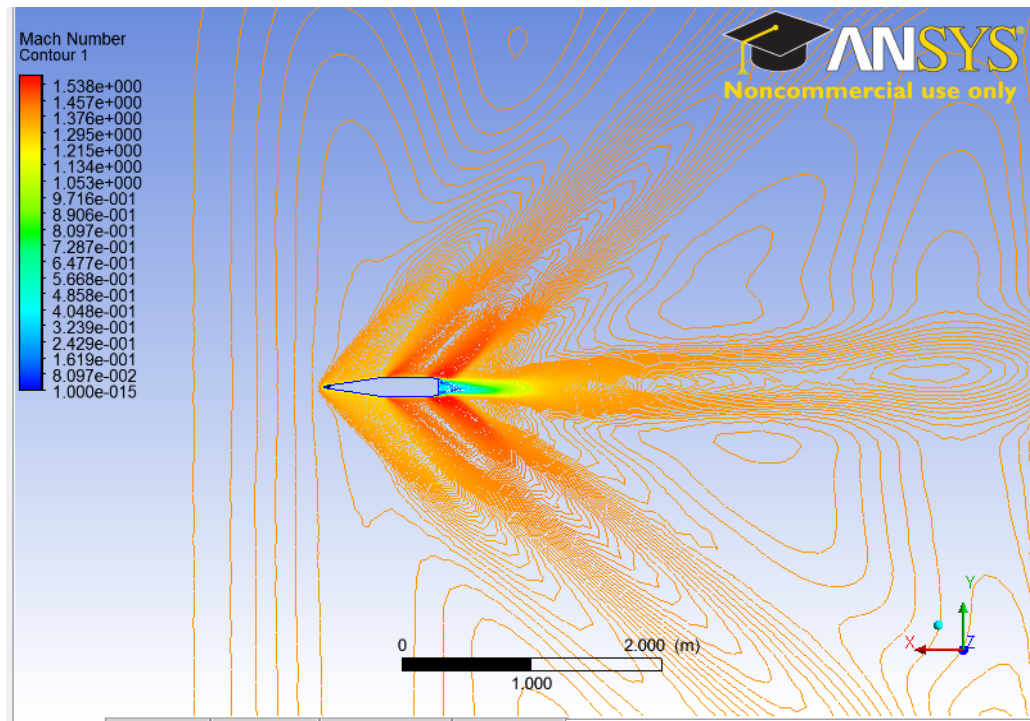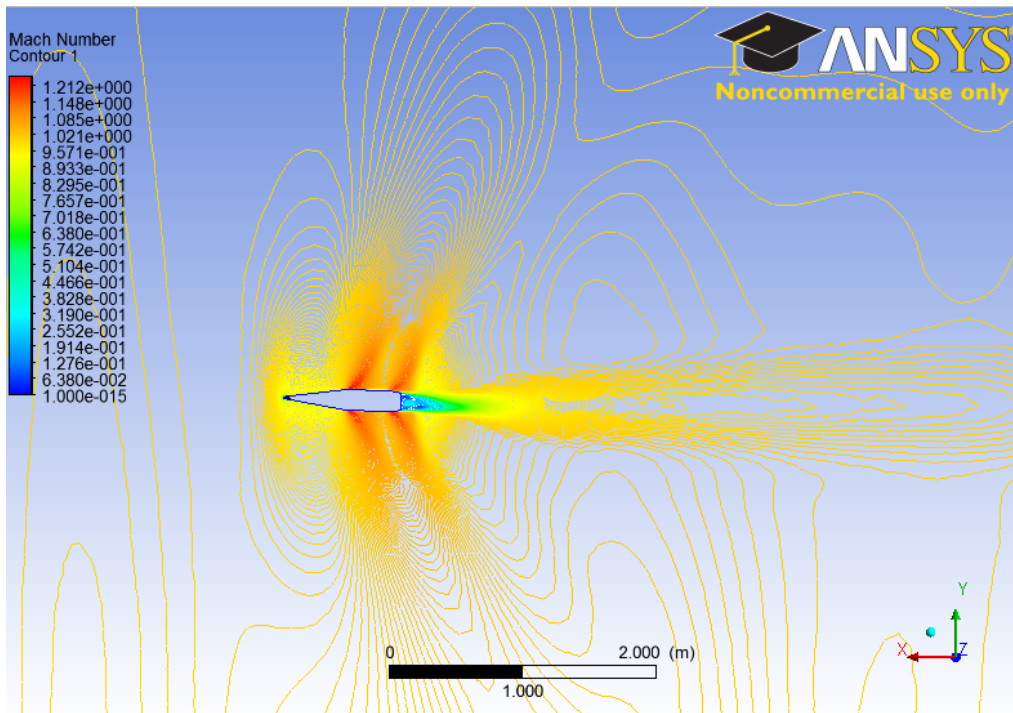

Figure 51.   Mach Contour at M=1, AOA of 2°, BIR.
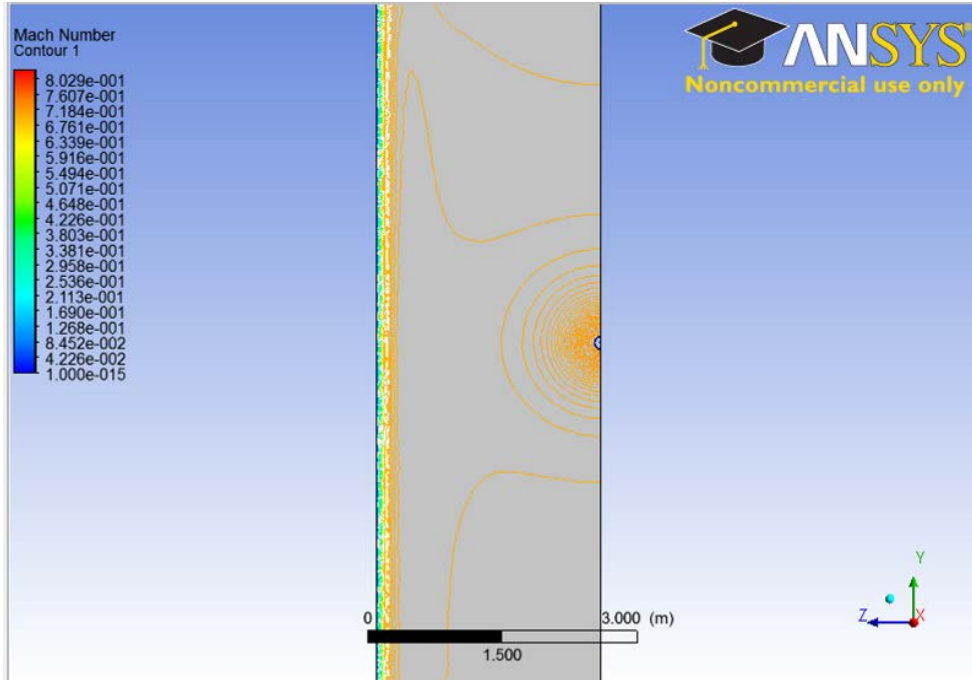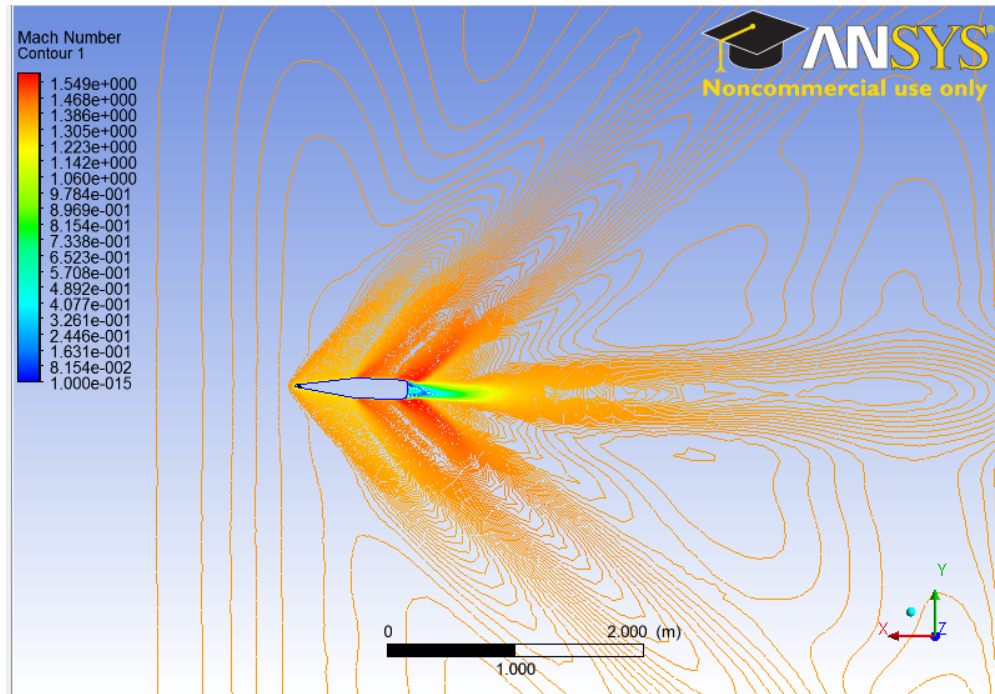
Figure 52.   Mach Contour at M=1.4, AOA of 2°, BIR.

1.   Analysis of Results

IVM is believed to provide a better prediction than BIR. In IVM, the free-stream flow direction is deliberately offset from the X axis direction. The formula stated in Equation 2.3 and 2.4 is applied so that the forces calculated are adjusted to account for the AOA. "force_y" in Function Calculator is equal to normal force on the body of interest. In BIR, the generated "force_y" is the lift force perpendicular to the free-stream velocity. Theoretically, by applying the formula in 2.3 and 2.4, the result should be the same. However, the tilted body in BIR increased the meshing complexity, evident in the increase of mesh nodes and elements as compared to IVM. The difference in mesh profile is believed to be the reason for the minor variation between the two methods.

C.   PART III–MODIFIED NOSE CONFIGURATION

Modification to the projectile body is not desirable as it will discontinue the usage of existing projectile stockpile. Thus, modification was made only on the fuze. It is proposed that a new design fuze is able to tilt at various angles to allow lift generation.

Modification to the fuze model was performed using SolidWorks as illustrated in Figure 53. In order to check whether lift is generated by tilting the nose of the projectile, the fuze is made to tilt at angles of 2°, 4°, 6°, 8° and 10°.
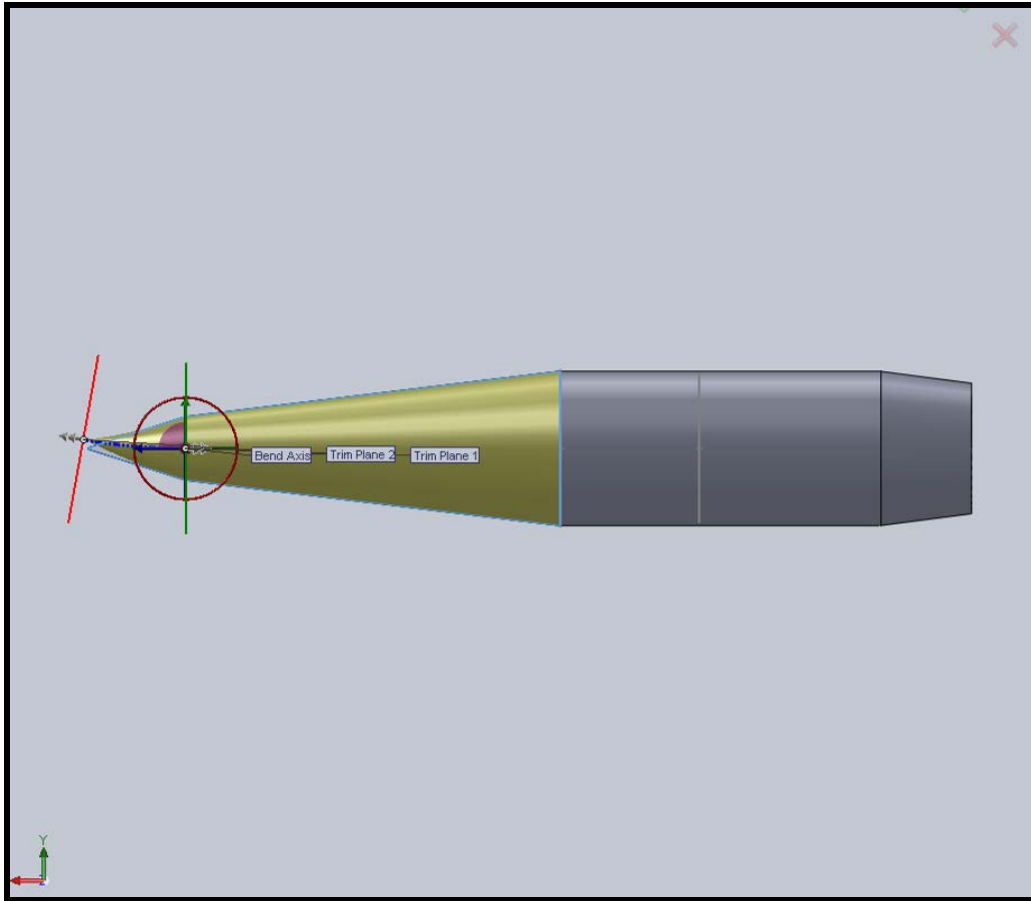
Figure 53.   Modified Fuze Model.

For the Modified Nose Configuration, ANSYS CFX and AP09 simulations were performed on a modified M549 projectile model for various AOA and Mach numbers.

1. **Lift Coefficient versus Mach Number at Nose Tilt Angles of 0°, 2°, 4°, 6°, 8° and 10°**

The computed lift coefficient versus Mach number distributions are illustrated in Figure 54. They were obtained using eight data points from Mach 0.7 to Mach 1.4 with an interval of 0.1.
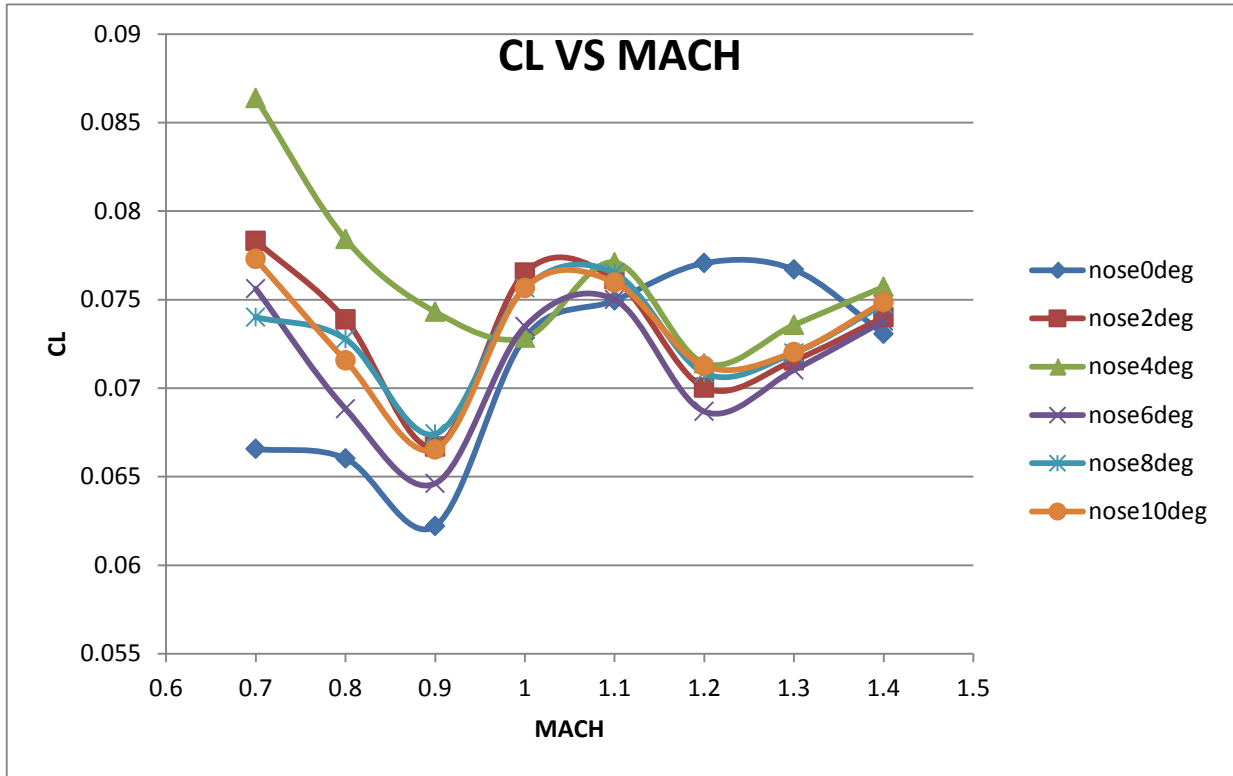
Figure 54.   Lift Coefficient versus Mach Number.

From Figure 54, it is seen that, as expected, in subsonic and transonic flight, lift increased as the nose tilt was increased to 2° and 4°, but then started to diminish with a further tilt angle increase. In contrast, in supersonic flight, the tilted nose reduced the lift. An explanation of the results shown in Figure 54 is offered in Figure 55 and 56.

2.   Analysis of Results

Velocity vector plots at nose tilt angles of 0°, 4° and 6° at Mach 0.7 are shown in Figure 55.
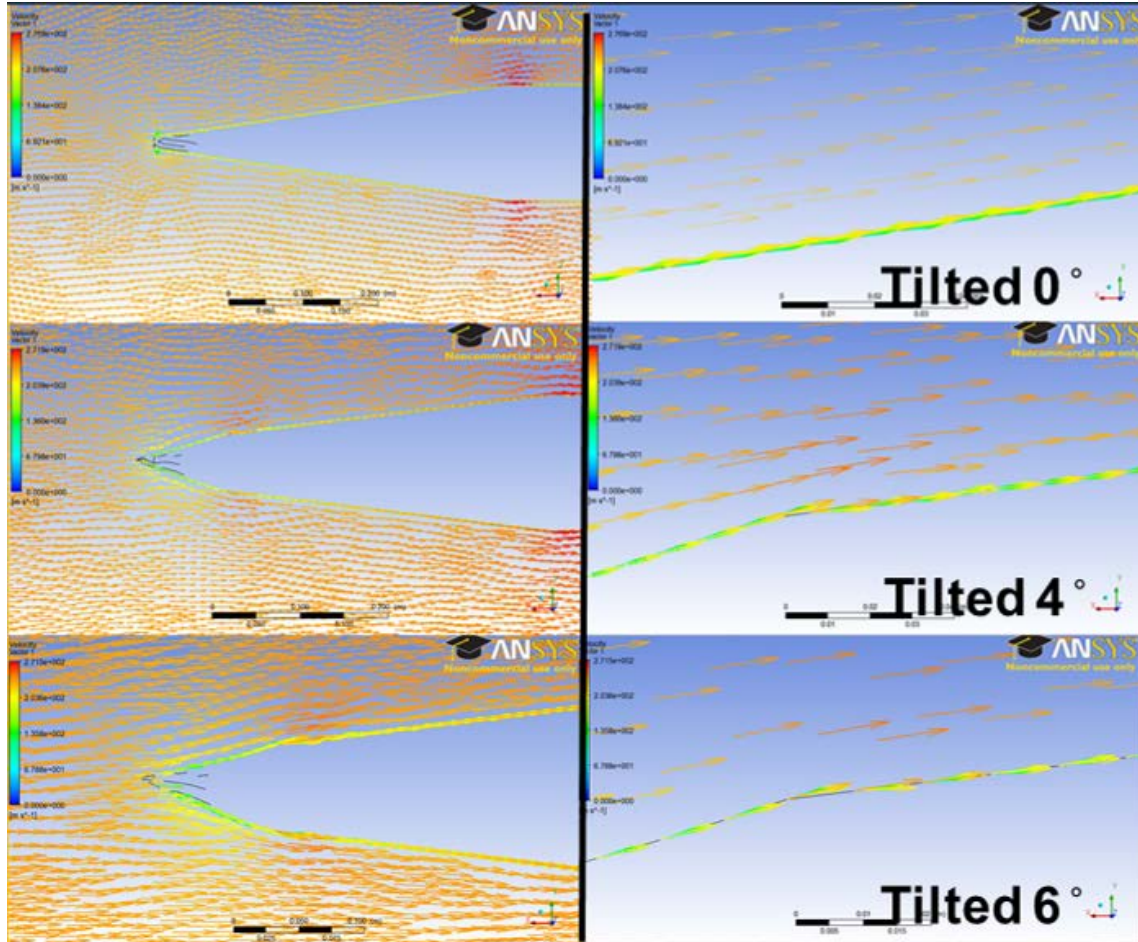
Figure 55.   Velocity Vector Plot for Nose Tilt Angles of 0°, 4° and 6° at Mach 0.7.

It is seen that the flow is attached when the nose tilt angle is 0°, 2° and 4°. However flow separation is observed at nose tilt angle of 6° and beyond. Apparently this flow separation prevented further improvement in lift as the nose tilt angles increased.
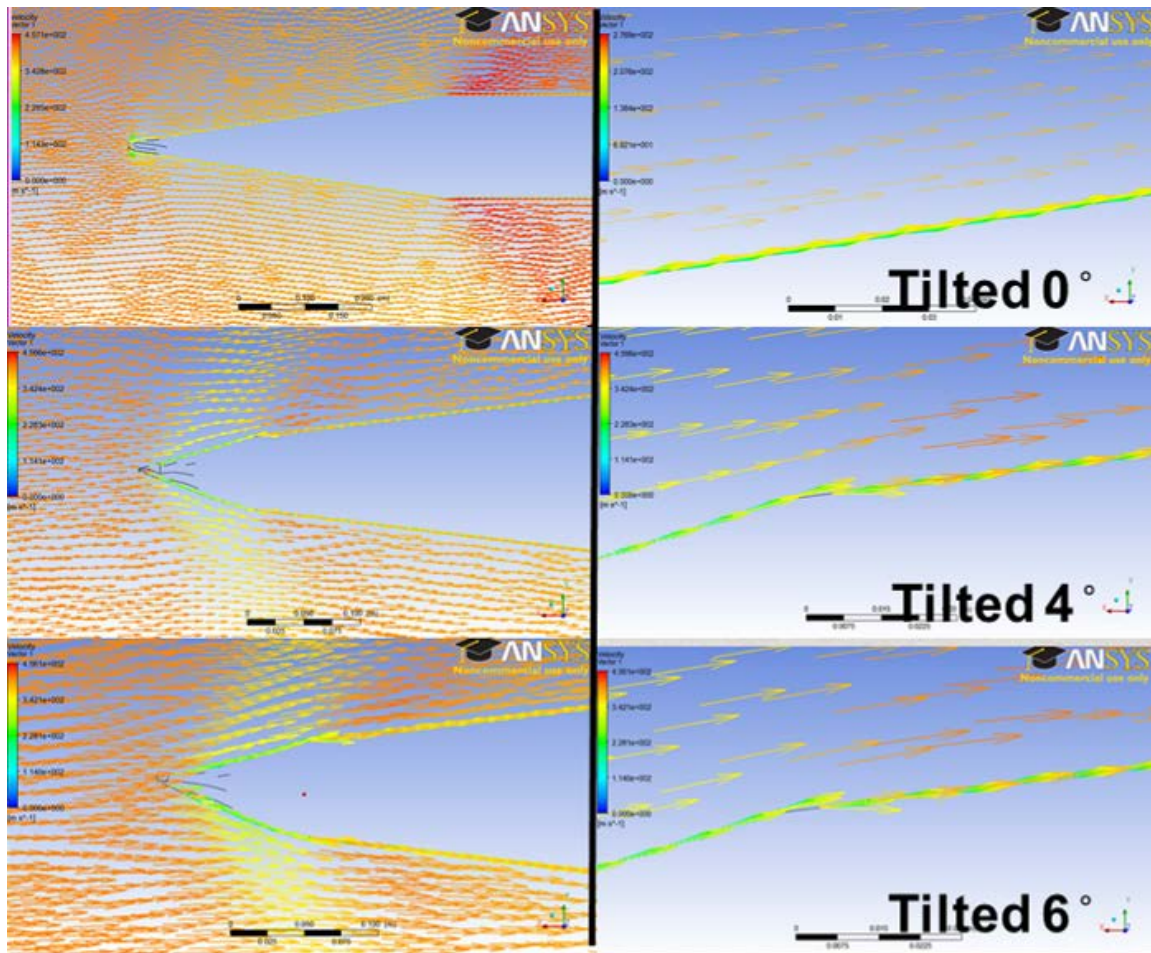
Figure 56. Velocity Vector Plot for Nose Tilt Angles of 0°, 4° and 6° at Mach 1.2.

In supersonic flow as seen from Figure 56, tilting the nose caused flow separation for all tilt angles and therefore led to a reduction of lift. However, further analysis is required to ascertain the numerical accuracy of the computations.

VI.   CONCLUSIONS AND RECOMMENDATIONS

A.   CONCLUSIONS

The key objectives of this thesis were successfully completed. The non-spinning M549 projectile's stability derivatives were successfully validated using ANSYS CFX and AP09. Comparison studies also were performed using two different AOA generation methods in ANSYS CFX. Furthermore, the feasibility of lift generation via projectile nose modification was explored using ANSYS CFX.

In general, ANSYS CFX was observed to provide better trend prediction than AP09. In this thesis, a prediction error of +/-20% was observed. This was due to restricted mesh quality imposed by computing limits. This highlighted the need to have sufficient computing power to achieve better mesh quality for accuracy. The IVM AOA generation method provided a better prediction than the BIR method. Differences in mesh profiles contributed to the minor variation between the two methods.

Lift generation via nose tilt modification was predicted for nose tilt angles of 2°, 4°, 6°, 8° and 10°. The onset of flow separation was found to impose limits on this method of lift generation.

B.   RECOMMENDATIONS

The proposed next stage of investigation is to simulate a spinning M549 projectile. This is necessary to determine the influence of the spinning motion on the aerodynamics of the projectile.

In this thesis, it was observed that both ANSYS CFX and AP09 have limitations in providing accurate prediction. Alternate prediction codes should be considered in the next stage of investigation. Commercially available prediction codes like Projectile Rocket Ordnance Design and Analysis System (PRODAS) offer more than the standard aerodynamic coefficients prediction. It allows users to conduct launch dynamic and trajectories simulation. These simulations provide essential information for the study of the aerodynamic properties of the projectile.

THIS PAGE INTENTIONALLY LEFT BLANK

LIST OF REFERENCES

[1]   J. Norris, *Artillery, A History*. Stroud, UK: Sutton Publishing Limited, 2000.

[2]   E. Sloan, *Military Transformation and Modern Warfare: a Reference Handbook*. Westport, CT: Praeger Security International, 2008.

[3]   M. D. Ilg, "Guidance, navigation, and control for munitions," Phd dissertation, Drexel University, Philadelphia, PA, 2008.

[4]   Global Security, *M549A1 Rocket Assisted Projectile*. [Online]. 2000. Available: http://www.globalsecurity.org/military/systems/munitions/m549a1.htm

[5]   J. Sahu, R. Lafarge, and C. J. Nietubicz, "Aerodynamic coefficient predictions for a projectile configuration at transonic speeds," US Army Ballistic Research Laboratory, Aberdeen Proving Ground, MD, BRL-MR-3639, Dec. 1987.

[6]   J. Sahu, "Numerical computations of transonic critical aerodynamic behavior," US Army Ballistic Research Laboratory, Aberdeen Proving Ground, MD, BRL-TR-2962, Dec. 1988.

[7]   W. J. Tan, "Aerodynamic validation of emerging projectile and missile configurations," M.S. thesis, Naval Postgraduate School, Monterey, CA, 2010.

[8]   T. V. Karman, *Aerodynamics: selected topics in the light of their historical development*. Mineola, NY: Dover Publications Limited, 2004.

[9]   J. D. Anderson, Jr, *Fundamentals of aerodynamics*. New York, NY: McGraw-Hill Companies, 2010.

[10]   M. F. Platzer, "lecture notes for missile aerodynamics," unpublished.

[11]   D. Pnueli, and C. Gutfinger, *Fluid mechanics*. Cambridge, UK: Cambridge University Press, 1992.

[12]   US Centennial of Flight Commission, *Transonic Flow*. [Online]. 2011. Available: http://www.centennialofflight.gov/essay/Theories_of_Flight/Transonic_Flow/TH 19.htm

[13]   O. Zikanov, *Essential computational fluid dynamics*. Hoboken, NJ: John Wiley & Sons, Inc, 2010.

[14]   ANSYS, *Introduction*. [Online]. 2011. Available: www.ansys.com

[15]   ANSYS Fluent, *Resources*. [Online]. 2011. Available: http://my.fit.edu/itresources/manuals/fluent6.3/help/html/ug/node487.htm

[16]   J. Sahu, "Drag predictions for projectiles at transonic and supersonic speeds," US Army Ballistics Research Laboratory, Aberdeen Proving Ground, MD, BRL-MR-3523, Jun. 1986.

[17]   SolidWorks, *Introduction*. [Online]. 2011. Available: http://www.solidworks.com

[18]   D. Planchard, and M. Planhard, *SolidWorks 2010 tutorial with multimedia CD*, KS: Schroff Development Corporation, 2010.

[19]   J. Sahu, W. Sturek, et al., "Recent application of CFD to the aerodynamics of army projectiles," Army Research Laboratory, ARL-TR-22, Dec. 1992.

[20]   CFD Online, *SST k omega*. [Online]. 2011. Available: http://www.cfd-online.com/Wiki/SST_k-omega_model

[21]   F. G. Moore, and L. Y. Moore, "The 2009 version of the aeroprediction code: the AP09,"Aeroprediction, Inc, API Report No.3, Jan. 2008.

[22]   F. G. Moore, T. C. Hymer, *et al.,* "The 2005 version of the aeroprediction code: part II- users guide," API Report no. 2, Jun. 2004.

APPENDIX A. MESH INPUT DATA

The following mesh input data is specified for this thesis. Other required input data not mentioned in the list is set as default.

Sizing	
Use Advanced	On Curvature
Relevance Center	Fine
Curvature Normal Angle	4 Deg
Min Size	1e-5m
Max Face Size	0.1m
Max Size	0.1m
Growth Rate	1.2
Min Edge	1.55e-4m
Inflation	
Inflation Option	Total Thickness
Number of Layer	40
Growth Rate	1.1
Max Thickness	1e-3m
Vertex Sizing	
Element Size	1e-2m
Sphere Radius	0.4m

Table 1.   Mesh Input Data.

THIS PAGE INTENTIONALLY LEFT BLANK

APPENDIX B. ANSYS CFX COMMAND LANGUAGE FOR RUN (LOW MACH NUMBER)

LIBRARY:

  MATERIAL: Air Ideal Gas

    Material Description = Air Ideal Gas (constant Cp)

    Material Group = Air Data, Calorically Perfect Ideal Gases

    Option = Pure Substance

    Thermodynamic State = Gas

    PROPERTIES:

     Option = General Material

     EQUATION OF STATE:

      Molar Mass = 28.96 [kg kmol^-1]

      Option = Ideal Gas

     SPECIFIC HEAT CAPACITY:

      Option = Value

      Specific Heat Capacity = 1.0044E+03 [J kg^-1 K^-1]

      Specific Heat Type = Constant Pressure

     REFERENCE STATE:

      Option = Specified Point

      Reference Pressure = 1 [atm]

      Reference Specific Enthalpy = 0. [J/kg]

      Reference Specific Entropy = 0. [J/kg/K]

      Reference Temperature = 25 [C]

     DYNAMIC VISCOSITY:

      Dynamic Viscosity = 1.831E-05 [kg m^-1 s^-1]

      Option = Value

     THERMAL CONDUCTIVITY:

      Option = Value

      Thermal Conductivity = 2.61E-2 [W m^-1 K^-1]

     ABSORPTION COEFFICIENT:

      Absorption Coefficient = 0.01 [m^-1]

      Option = Value

     SCATTERING COEFFICIENT:

      Option = Value

      Scattering Coefficient = 0.0 [m^-1]

     REFRACTIVE INDEX:

      Option = Value

      Refractive Index = 1.0 [m m^-1]

  FLOW: Flow Analysis 1

    SOLUTION UNITS:

Angle Units = [rad]

Length Units = [m]

Mass Units = [kg]

Solid Angle Units = [sr]

Temperature Units = [K]

Time Units = [s]

ANALYSIS TYPE:

  Option = Steady State

  EXTERNAL SOLVER COUPLING:

    Option = None

DOMAIN: Default Domain

  Coord Frame = Coord 0

  Domain Type = Fluid

  Location = B36

  BOUNDARY: Default Domain Default

    Boundary Type = WALL

    Location = F87.36,F88.36,F89.36,F90.36,F91.36

    BOUNDARY CONDITIONS:

      HEAT TRANSFER:

        Option = Adiabatic

      MASS AND MOMENTUM:

        Option = No Slip Wall

      WALL ROUGHNESS:

        Option = Smooth Wall

  BOUNDARY: bottom

    Boundary Type = INLET

    Location = bottom

    BOUNDARY CONDITIONS:

      FLOW REGIME:

        Option = Subsonic

      HEAT TRANSFER:

        Option = Static Temperature

        Static Temperature = 288.15 [K]

      MASS AND MOMENTUM:

        Option = Cartesian Velocity Components

        U = -238 [m s^-1]

        V = 8.33 [m s^-1]

        W = 0 [m s^-1]

      TURBULENCE:

        Option = Medium Intensity and Eddy Viscosity Ratio

  BOUNDARY: inlet

    Boundary Type = INLET

Location = inlet

BOUNDARY CONDITIONS:

FLOW REGIME:

Option = Subsonic

HEAT TRANSFER:

Option = Static Temperature

Static Temperature = 288.15 [K]

MASS AND MOMENTUM:

Option = Cartesian Velocity Components

U = -238 [m s^-1]

V = 8.33 [m s^-1]

W = 0 [m s^-1]

TURBULENCE:

Option = Medium Intensity and Eddy Viscosity Ratio

BOUNDARY: outlet

Boundary Type = OUTLET

Location = outlet

BOUNDARY CONDITIONS:

FLOW REGIME:

Option = Subsonic

MASS AND MOMENTUM:

Option = Static Pressure

Relative Pressure = 0 [Pa]

BOUNDARY: sym1

Boundary Type = SYMMETRY

Location = sym1

BOUNDARY: sym2

Boundary Type = WALL

Location = sym2

BOUNDARY CONDITIONS:

HEAT TRANSFER:

Option = Adiabatic

MASS AND MOMENTUM:

Option = No Slip Wall

WALL ROUGHNESS:

Option = Smooth Wall

BOUNDARY: top

Boundary Type = OUTLET

Location = top

BOUNDARY CONDITIONS:

FLOW REGIME:

Option = Subsonic

MASS AND MOMENTUM:

   Option = Average Static Pressure

   Pressure Profile Blend = 0.05

   Relative Pressure = 0 [Pa]

  PRESSURE AVERAGING:

   Option = Average Over Whole Outlet

DOMAIN MODELS:

 BUOYANCY MODEL:

  Option = Non Buoyant

 DOMAIN MOTION:

  Option = Stationary

 MESH DEFORMATION:

  Option = None

 REFERENCE PRESSURE:

  Reference Pressure = 1 [atm]

FLUID DEFINITION: Fluid 1

 Material = Air Ideal Gas

 Option = Material Library

 MORPHOLOGY:

  Option = Continuous Fluid

FLUID MODELS:

 COMBUSTION MODEL:

  Option = None

 HEAT TRANSFER MODEL:

  Include Viscous Work Term = On

  Option = Total Energy

 THERMAL RADIATION MODEL:

  Option = None

 TURBULENCE MODEL:

  Option = SST

  TRANSITIONAL TURBULENCE:

   Option = Gamma Theta Model

   TRANSITION ONSET CORRELATION:

    Option = Langtry Menter

 TURBULENT WALL FUNCTIONS:

  High Speed Model = Off

  Option = Automatic

INITIALISATION:

 Option = Automatic

 INITIAL CONDITIONS:

  Velocity Type = Cartesian

  CARTESIAN VELOCITY COMPONENTS:

Option = Automatic with Value

          U = -238 [m s^-1]

          V = 8.33 [m s^-1]

          W = 0 [m s^-1]

        STATIC PRESSURE:

          Option = Automatic

        TEMPERATURE:

          Option = Automatic

        TURBULENCE INITIAL CONDITIONS:

          Option = Medium Intensity and Eddy Viscosity Ratio

    OUTPUT CONTROL:

      RESULTS:

        File Compression Level = Default

        Option = Standard

    SOLVER CONTROL:

      Turbulence Numerics = High Resolution

      ADVECTION SCHEME:

        Option = High Resolution

      COMPRESSIBILITY CONTROL:

        High Speed Numerics = On

      CONVERGENCE CONTROL:

        Length Scale Option = Conservative

        Maximum Number of Iterations = 100

        Minimum Number of Iterations = 1

        Timescale Control = Auto Timescale

        Timescale Factor = 10

      CONVERGENCE CRITERIA:

        Residual Target = 1e-07

        Residual Type = RMS

      DYNAMIC MODEL CONTROL:

        Global Dynamic Model Control = On

    EXPERT PARAMETERS:

      max continuity loops = 3

      topology estimate factor = 1.1

COMMAND FILE:

  Version = 13.0

  Results Version = 13.0

SIMULATION CONTROL:

  EXECUTION CONTROL:

    EXECUTABLE SELECTION:

      Double Precision = On

    INTERPOLATOR STEP CONTROL:

Runtime Priority = Standard

PARALLEL HOST LIBRARY:

  HOST DEFINITION: skypc

    Remote Host Name = SKY-PC

    Host Architecture String = winnt-amd64

    Installation Root = C:\Program Files\ANSYS Inc\v%v\CFX

PARTITIONER STEP CONTROL:

  Multidomain Option = Independent Partitioning

  Runtime Priority = Standard

  EXECUTABLE SELECTION:

    Use Large Problem Partitioner = Off

  PARTITIONING TYPE:

    MeTiS Type = k-way

    Option = MeTiS

    Partition Size Rule = Automatic

    Partition Weight Factors = 0.50000, 0.50000

RUN DEFINITION:

  Run Mode = Full

  Solver Input File = Fluid Flow CFX.def

SOLVER STEP CONTROL:

  Runtime Priority = Standard

  PARALLEL ENVIRONMENT:

    Number of Processes = 2

    Start Method = HP MPI Local Parallel

    Parallel Host List = skypc*2

APPENDIX C. ANSYS CFX COMMAND LANGUAGE FOR RUN (HIGH MACH NUMBER)

```
LIBRARY:
  MATERIAL: Air Ideal Gas
    Material Description = Air Ideal Gas (constant Cp)
    Material Group = Air Data, Calorically Perfect Ideal Gases
    Option = Pure Substance
    Thermodynamic State = Gas
    PROPERTIES:
      Option = General Material
      EQUATION OF STATE:
        Molar Mass = 28.96 [kg kmol^-1]
        Option = Ideal Gas
      SPECIFIC HEAT CAPACITY:
        Option = Value
        Specific Heat Capacity = 1.0044E+03 [J kg^-1 K^-1]
        Specific Heat Type = Constant Pressure
      REFERENCE STATE:
        Option = Specified Point
        Reference Pressure = 1 [atm]
        Reference Specific Enthalpy = 0. [J/kg]
        Reference Specific Entropy = 0. [J/kg/K]
        Reference Temperature = 25 [C]
      DYNAMIC VISCOSITY:
        Dynamic Viscosity = 1.831E-05 [kg m^-1 s^-1]
        Option = Value
      THERMAL CONDUCTIVITY:
        Option = Value
        Thermal Conductivity = 2.61E-2 [W m^-1 K^-1]
      ABSORPTION COEFFICIENT:
        Absorption Coefficient = 0.01 [m^-1]
        Option = Value
      SCATTERING COEFFICIENT:
        Option = Value
        Scattering Coefficient = 0.0 [m^-1]
      REFRACTIVE INDEX:
        Option = Value
        Refractive Index = 1.0 [m m^-1]
FLOW: Flow Analysis 1
  SOLUTION UNITS:
```

Angle Units = [rad]

Length Units = [m]

Mass Units = [kg]

Solid Angle Units = [sr]

Temperature Units = [K]

Time Units = [s]

ANALYSIS TYPE:

  Option = Steady State

  EXTERNAL SOLVER COUPLING:

    Option = None

DOMAIN: Default Domain

  Coord Frame = Coord 0

  Domain Type = Fluid

  Location = B36

  BOUNDARY: Default Domain Default

    Boundary Type = WALL

    Location = F87.36,F88.36,F89.36,F90.36,F91.36

    BOUNDARY CONDITIONS:

      HEAT TRANSFER:

        Option = Adiabatic

      MASS AND MOMENTUM:

        Option = No Slip Wall

      WALL ROUGHNESS:

        Option = Smooth Wall

  BOUNDARY: bottom

    Boundary Type = INLET

    Location = bottom

    BOUNDARY CONDITIONS:

      FLOW REGIME:

        Option = Subsonic

      HEAT TRANSFER:

        Option = Static Temperature

        Static Temperature = 288.15 [K]

      MASS AND MOMENTUM:

        Option = Cartesian Velocity Components

        U = -476.13 [m s^-1]

        V = 16.67 [m s^-1]

        W = 0 [m s^-1]

      TURBULENCE:

        Option = Medium Intensity and Eddy Viscosity Ratio

  BOUNDARY: inlet

    Boundary Type = INLET

72

Location = inlet

BOUNDARY CONDITIONS:

FLOW REGIME:

Option = Subsonic

HEAT TRANSFER:

Option = Static Temperature

Static Temperature = 288.15 [K]

MASS AND MOMENTUM:

Option = Cartesian Velocity Components

U = -476.13 [m s^-1]

V = 16.67 [m s^-1]

W = 0 [m s^-1]

TURBULENCE:

Option = Medium Intensity and Eddy Viscosity Ratio

BOUNDARY: outlet

Boundary Type = OUTLET

Location = outlet

BOUNDARY CONDITIONS:

FLOW REGIME:

Option = Subsonic

MASS AND MOMENTUM:

Option = Static Pressure

Relative Pressure = 0 [Pa]

BOUNDARY: sym1

Boundary Type = SYMMETRY

Location = sym1

BOUNDARY: sym2

Boundary Type = WALL

Location = sym2

BOUNDARY CONDITIONS:

HEAT TRANSFER:

Option = Adiabatic

MASS AND MOMENTUM:

Option = No Slip Wall

WALL ROUGHNESS:

Option = Smooth Wall

BOUNDARY: top

Boundary Type = OUTLET

Location = top

BOUNDARY CONDITIONS:

FLOW REGIME:

Option = Subsonic

MASS AND MOMENTUM:

  Option = Average Static Pressure

  Pressure Profile Blend = 0.05

  Relative Pressure = 0 [Pa]

  PRESSURE AVERAGING:

    Option = Average Over Whole Outlet

DOMAIN MODELS:

  BUOYANCY MODEL:

    Option = Non Buoyant

  DOMAIN MOTION:

    Option = Stationary

  MESH DEFORMATION:

    Option = None

  REFERENCE PRESSURE:

    Reference Pressure = 1 [atm]

FLUID DEFINITION: Fluid 1

  Material = Air Ideal Gas

  Option = Material Library

  MORPHOLOGY:

    Option = Continuous Fluid

FLUID MODELS:

  COMBUSTION MODEL:

    Option = None

  HEAT TRANSFER MODEL:

    Include Viscous Work Term = On

    Option = Total Energy

  THERMAL RADIATION MODEL:

    Option = None

  TURBULENCE MODEL:

    Option = SST

    TRANSITIONAL TURBULENCE:

      Option = Gamma Theta Model

      TRANSITION ONSET CORRELATION:

        Option = Langtry Menter

  TURBULENT WALL FUNCTIONS:

    High Speed Model = Off

    Option = Automatic

INITIALISATION:

 Option = Automatic

 INITIAL CONDITIONS:

  Velocity Type = Cartesian

  CARTESIAN VELOCITY COMPONENTS:

Option = Automatic with Value

        U = -476.13 [m s^-1]

        V = 16.67 [m s^-1]

        W = 0 [m s^-1]

      STATIC PRESSURE:

        Option = Automatic

      TEMPERATURE:

        Option = Automatic

      TURBULENCE INITIAL CONDITIONS:

        Option = Medium Intensity and Eddy Viscosity Ratio

  OUTPUT CONTROL:

    RESULTS:

      File Compression Level = Default

      Option = Standard

  SOLVER CONTROL:

    Turbulence Numerics = High Resolution

    ADVECTION SCHEME:

      Option = High Resolution

    COMPRESSIBILITY CONTROL:

      High Speed Numerics = On

    CONVERGENCE CONTROL:

      Length Scale Option = Conservative

      Maximum Number of Iterations = 20

      Minimum Number of Iterations = 1

      Timescale Control = Auto Timescale

      Timescale Factor = 10

    CONVERGENCE CRITERIA:

      Residual Target = 1e-07

      Residual Type = RMS

    DYNAMIC MODEL CONTROL:

      Global Dynamic Model Control = On

  EXPERT PARAMETERS:

    max continuity loops = 3

    topology estimate factor = 1.1

COMMAND FILE:

  Version = 13.0

  Results Version = 13.0

SIMULATION CONTROL:

  EXECUTION CONTROL:

    EXECUTABLE SELECTION:

      Double Precision = On

    INTERPOLATOR STEP CONTROL:

Runtime Priority = Standard

PARALLEL HOST LIBRARY:

HOST DEFINITION: skypc

Remote Host Name = SKY-PC

Host Architecture String = winnt-amd64

Installation Root = C:\Program Files\ANSYS Inc\v%v\CFX

PARTITIONER STEP CONTROL:

Multidomain Option = Independent Partitioning

Runtime Priority = Standard

EXECUTABLE SELECTION:

Use Large Problem Partitioner = Off

PARTITIONING TYPE:

MeTiS Type = k-way

Option = MeTiS

Partition Size Rule = Automatic

Partition Weight Factors = 0.50000, 0.50000

RUN DEFINITION:

Run Mode = Full

Solver Input File = Fluid Flow CFX.def

SOLVER STEP CONTROL:

Runtime Priority = Standard

PARALLEL ENVIRONMENT:

Number of Processes = 2

Start Method = HP MPI Local Parallel

Parallel Host List = skypc*2

APPENDIX D. OUTPUT PLOTS FOR AOA OF 0°
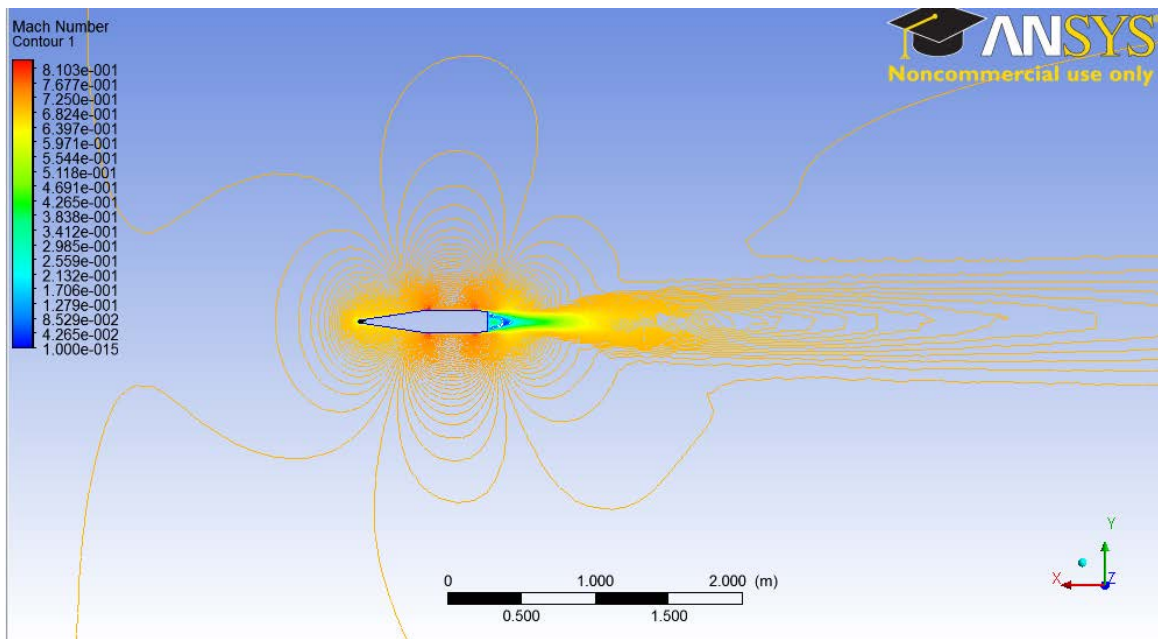
Figure 57.   Mach Contour at M=0.7, AOA of 0°, IVM.
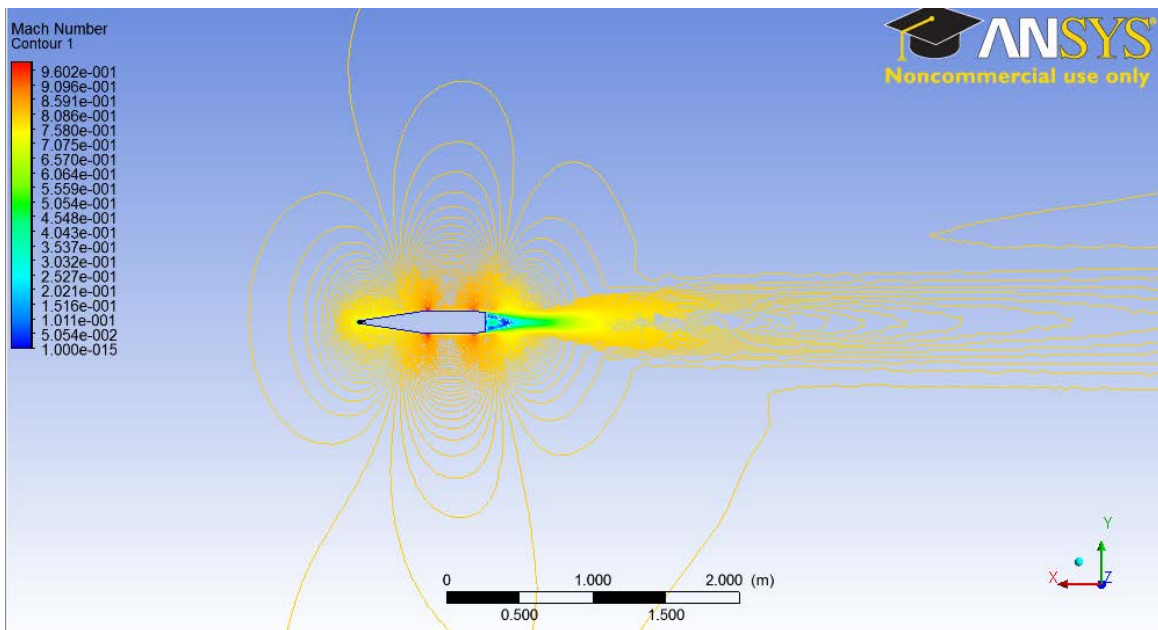
Figure 58.   Mach Contour at M=0.8, AOA of 0°, IVM.
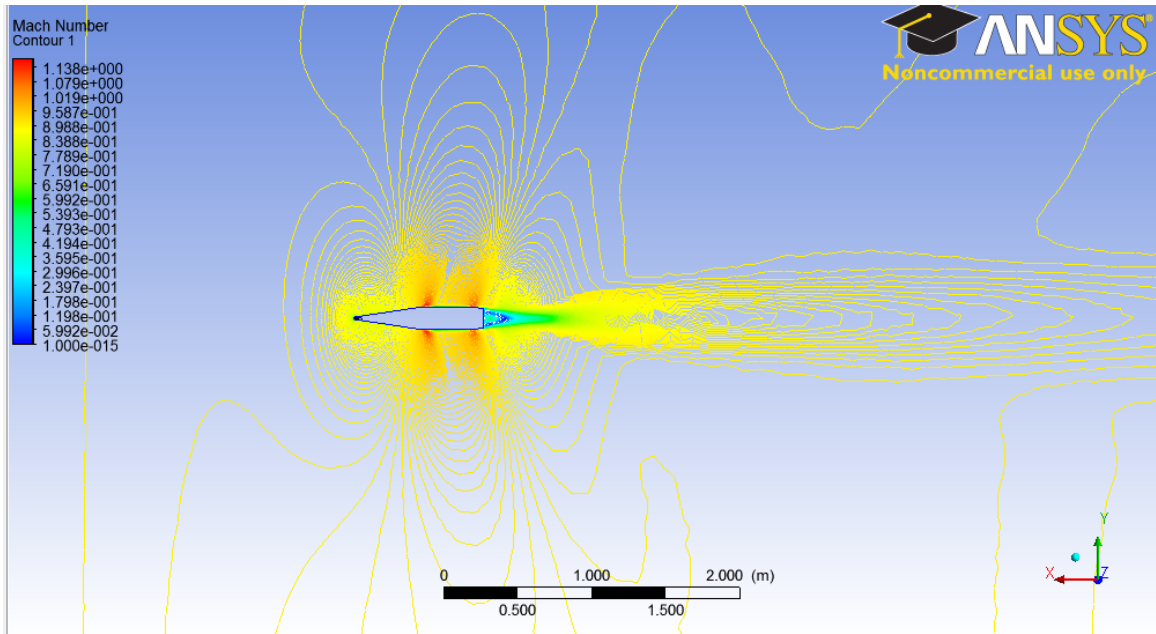
Figure 59.   Mach Contour at M=0.9, AOA of 0°, IVM.
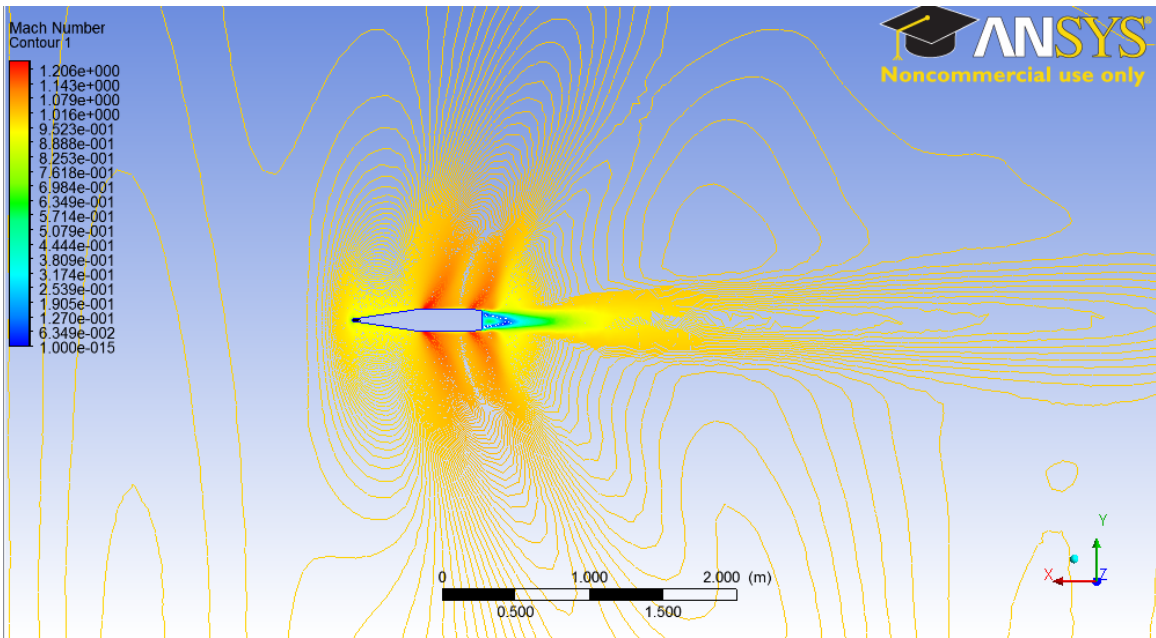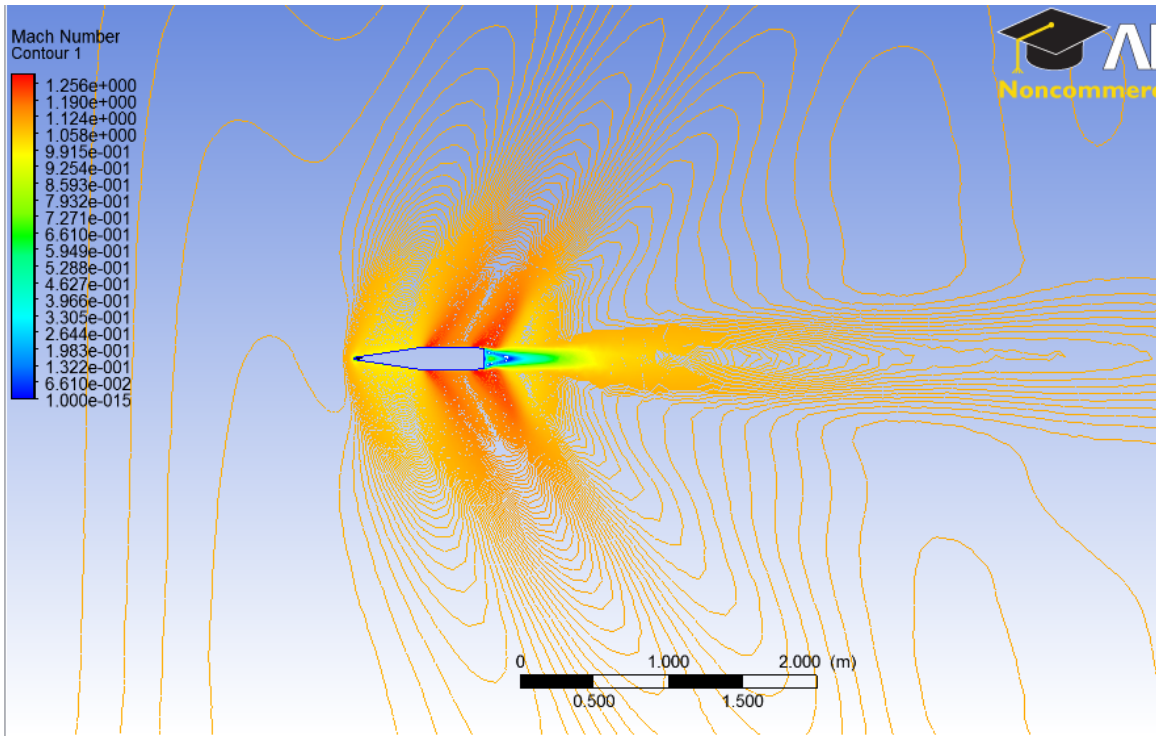

Figure 60.   Mach Contour at M=1, AOA of 0°, IVM.
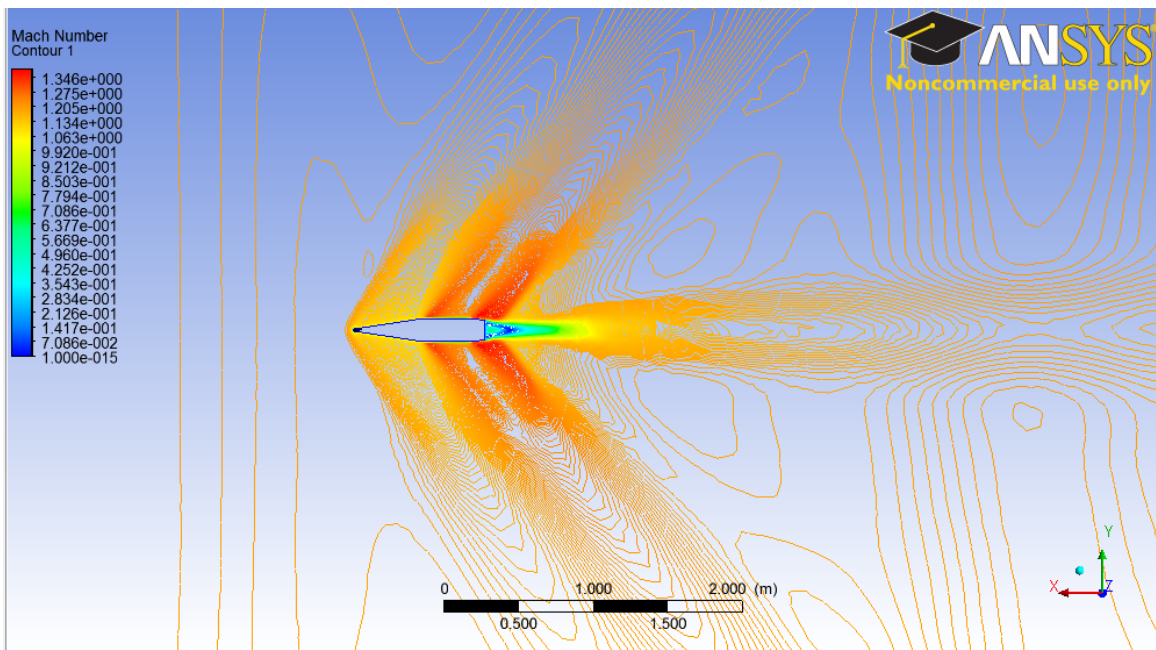
Figure 61.   Mach Contour at M=1.1, AOA of 0°, IVM.

Figure 62.   Mach Contour at M=1.2, AOA of 0°, IVM.

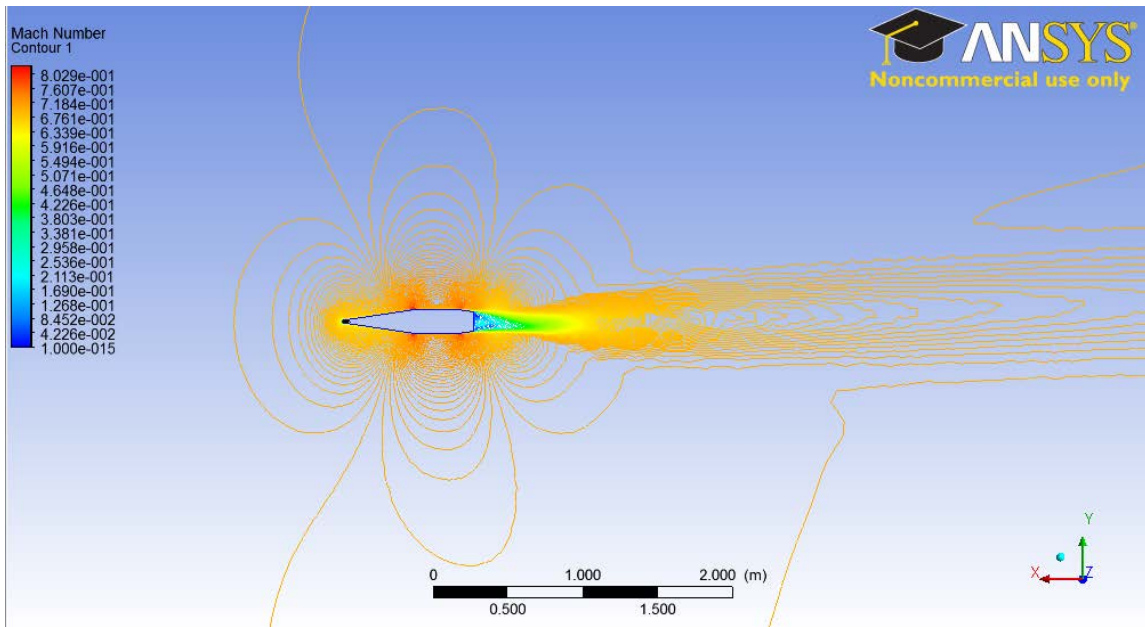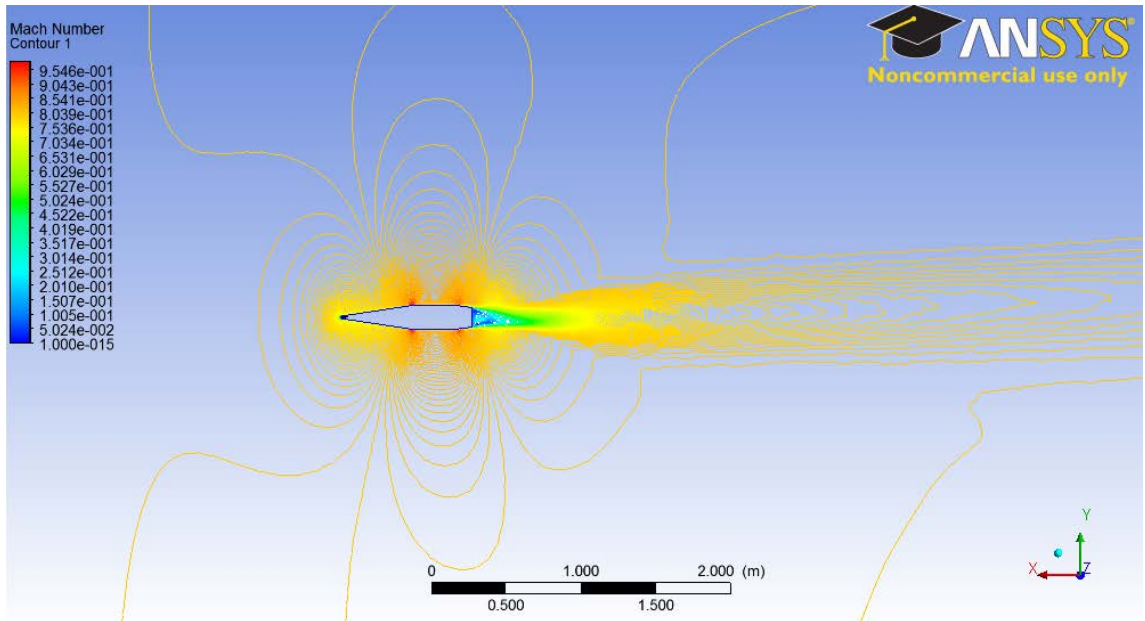THIS PAGE INTENTIONALLY LEFT BLANK

APPENDIX E. OUTPUT PLOTS FOR AOA OF 2°

Figure 63.   Mach Contour at M=0.7, AOA of 2°, IVM.
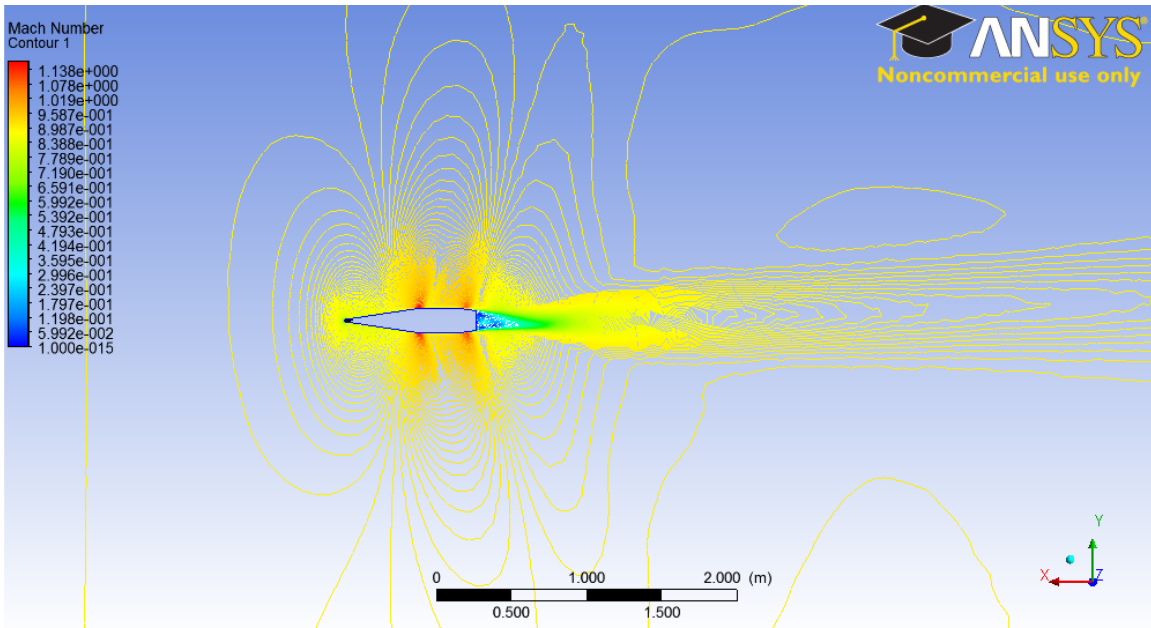

Figure 64.   Mach Contour at M=0.8, AOA of 2°, IVM.

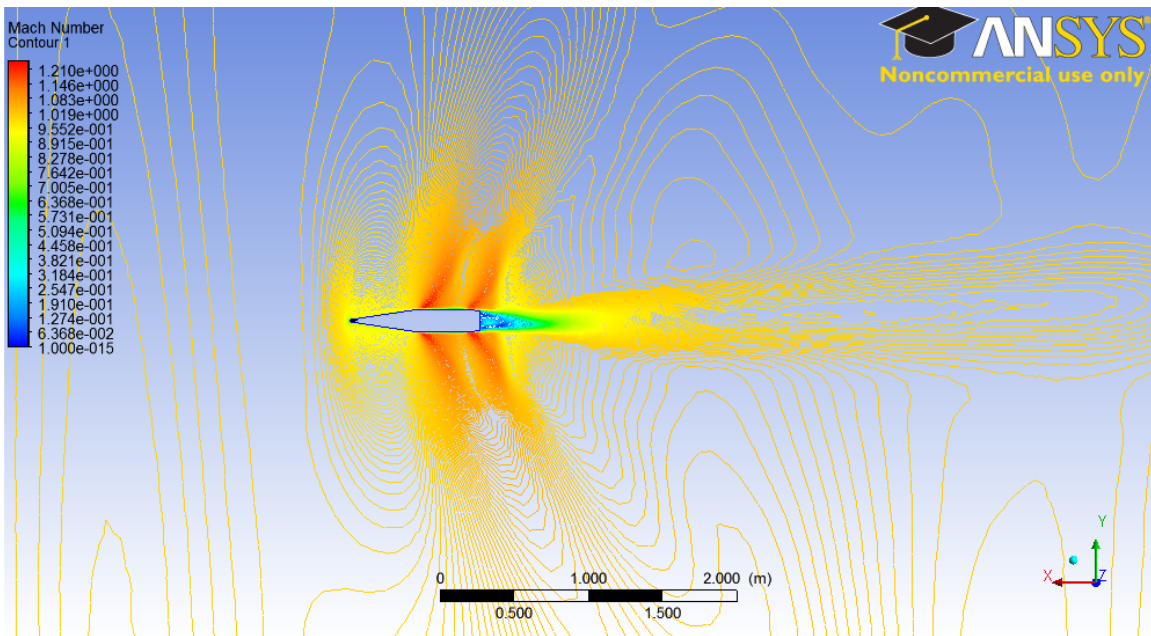Figure 65.   Mach Contour at M=0.9, AOA of 2°, IVM.
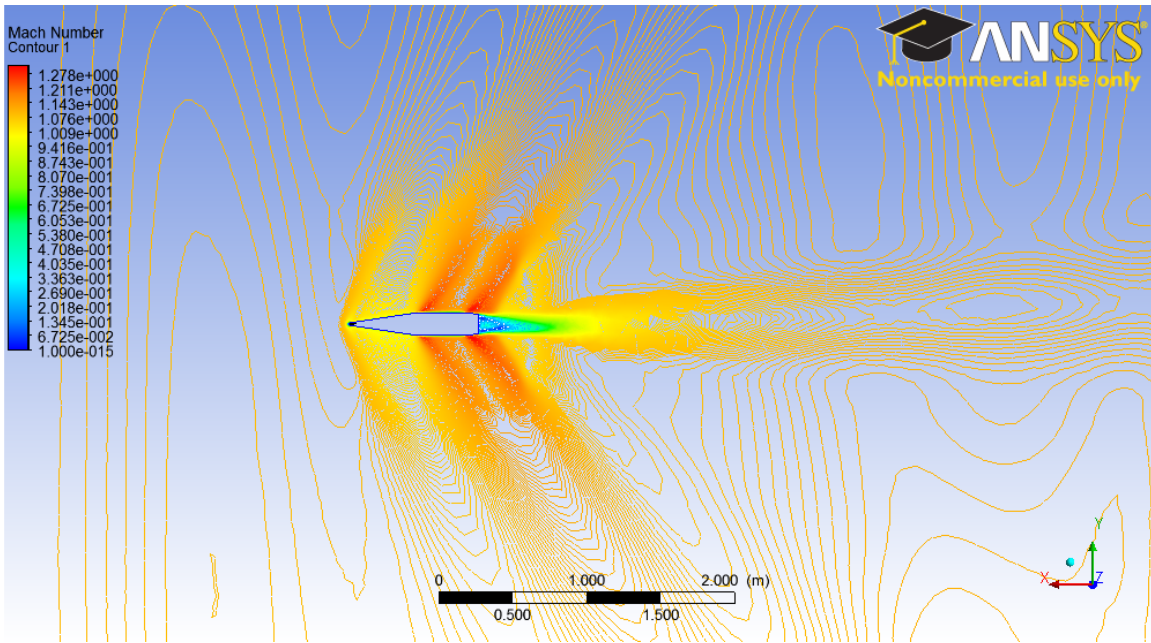

Figure 66.   Mach Contour at M=1, AOA of 2°, IVM.
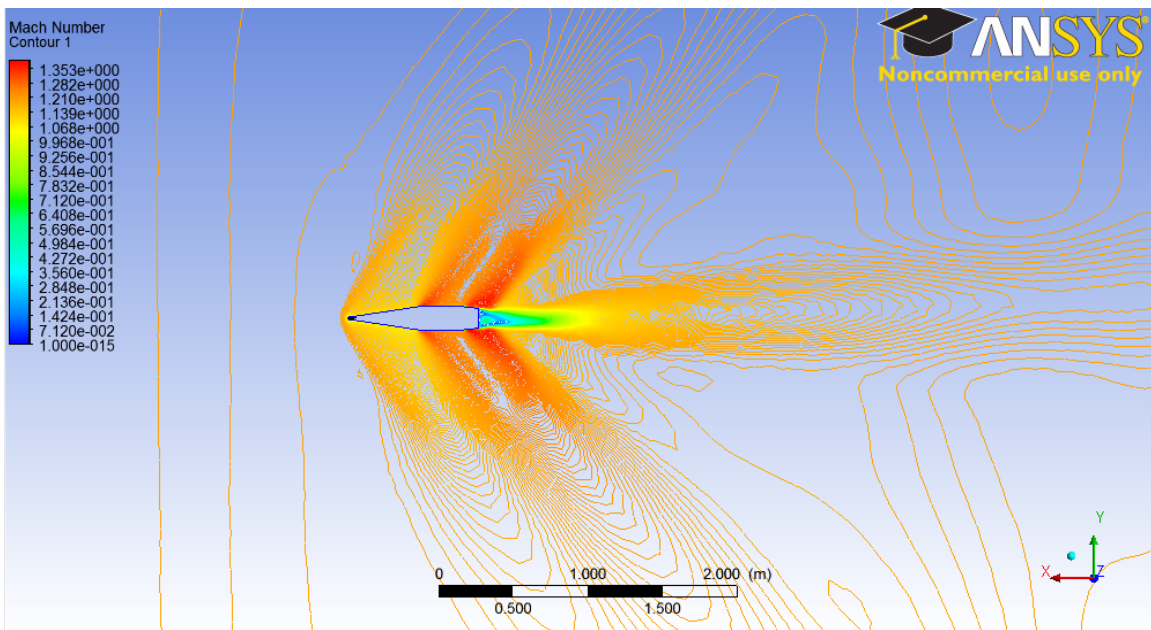
Figure 67.   Mach Contour at M=1.1, AOA of 2°, IVM.

Figure 68.   Mach Contour at M=1.2, AOA of 2°, IVM.
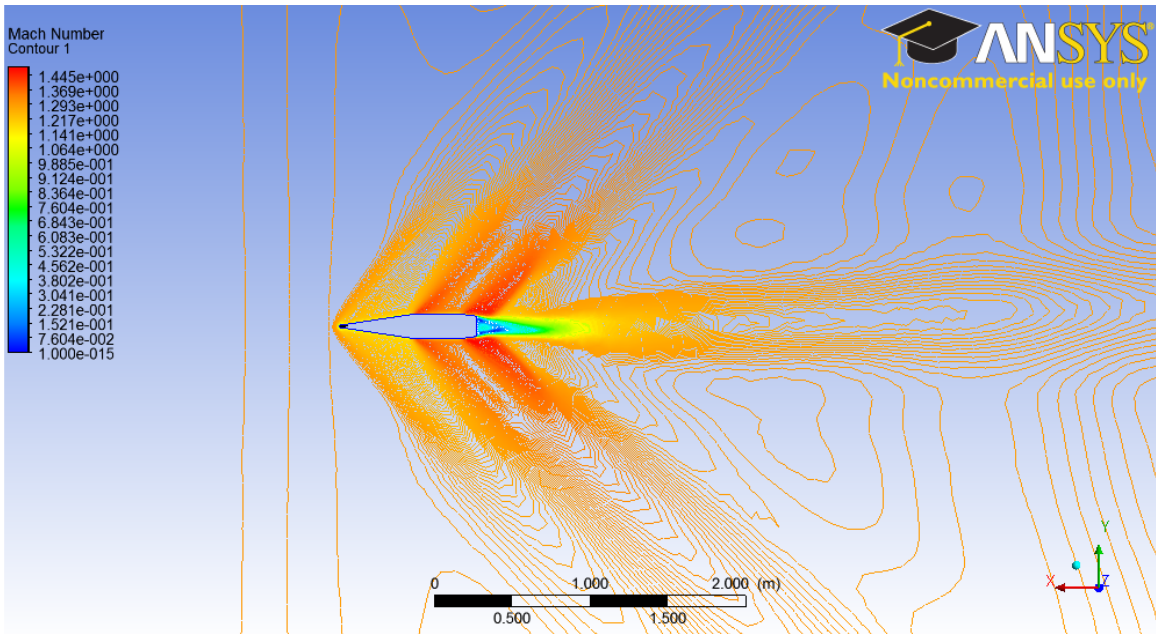
83

Figure 69.   Mach Contour at M=1.3 AOA of 2°, IVM.
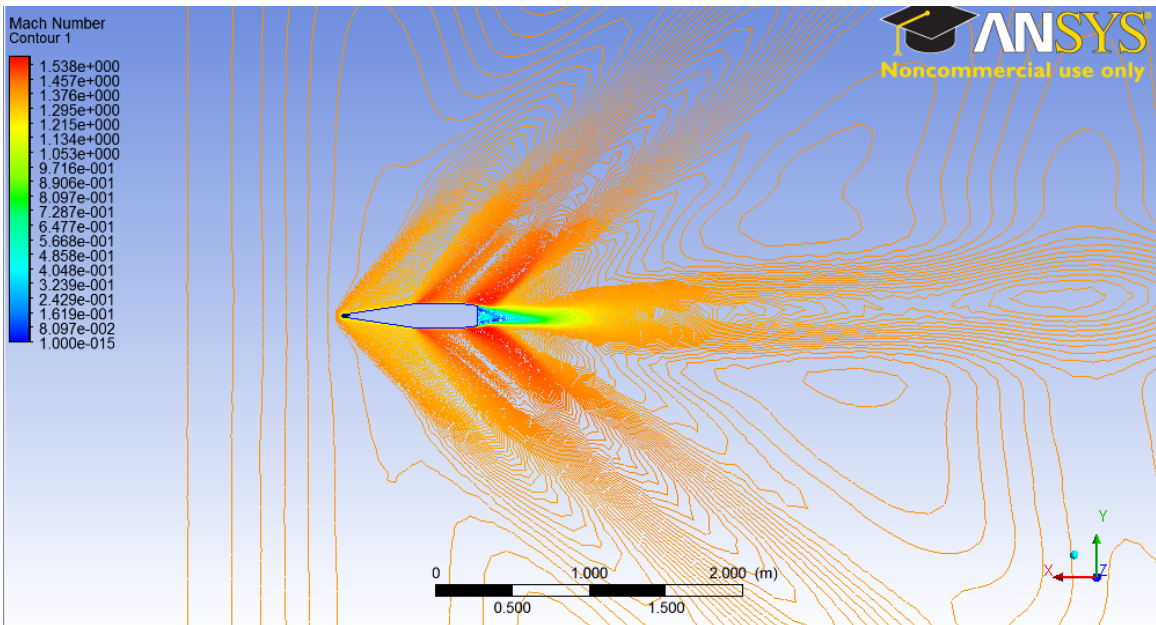

Figure 70.   Mach Contour at M=1.4 AOA of 2°, IVM.

INITIAL DISTRIBUTION LIST

1.   Defense Technical Information Center
        Ft. Belvoir, Virginia

2.   Dudley Knox Library
        Naval Postgraduate School
        Monterey, California

3.   Professor and Chairman Knox T. Millsaps
        Department of Mechanical Engineering and Aeronautical Engineering
        Naval Postgraduate School
        Monterey, California

4.   Professor Maximilian F. Platzer
        Department of Mechanical Engineering and Aeronautical Engineering
        Naval Postgraduate School
        Monterey, California

5.   Professor Anthony J. Gannon
        Department of Mechanical Engineering and Aeronautical Engineering
        Naval Postgraduate School
        Monterey, California

6.   Professor Yeo Tat Soon
        Temasek Defence Systems Institute
        National University of Singapore
        tdshead@nus.edu.sg

7.   Ms. Tan Lai Poh
        Temasek Defence Systems Institute
        National University of Singapore